Doctoral Thesis

Localization of the voltage-gated K_v10.2 potassium channel in the mouse organism

In partial fulfillment of the requirements for the degree

"Doctor rerum naturalium (Dr. rer. nat.)"

in the Molecular Medicine Study Program at the

Georg-August University Göttingen

submitted by

Gerd-Marten Kuscher

from

Neuruppin, Germany

Göttingen, April 2013

Thesis committee members

Prof. Dr. Walter Stühmer

Department of Molecular Biology of Neuronal Signals

Max Planck Institute of Experimental Medicine

Göttingen

Prof. Dr. Thomas A. Bayer

Department for Psychiatry

Division of Molecular Psychiatry

Göttingen University Medical School

Prof. Dr. Hubertus Jarrry

Deptartment of Clinical and Experimental Endocrinology

Göttingen University Medical School

Advisor

Prof. Dr. Frauke Alves

Department of Hematology and Oncology

Göttingen University Medical School

Date of the oral examination: 05/15/2013

Statement of Authorship

By this I declare that I independently authored the presented thesis:

"Localization of the voltage-gated K_v10.2 potassium channel in the mouse organism"

and that I did not use other auxiliary means than indicated. Paragraphs that are taken from other publications, by wording or by sense, are marked in every case with a specification of the literary source.

Furthermore I declare that I carried out the scientific experiments following the principles of Good Scientific Practice according to the valid "Richtlinien der Georg-August-Universität Göttingen zur Sicherung guter wissenschaftlicher Praxis".

Göttingen, 02.04.13

(Gerd-Marten Kuscher)

Table of content

Abstract

Already 100 years ago, the importance of ion channels for nerve cell conduction was described. Subsequently, an expression und function of ion channels outside of the nervous system was discovered. Approximately 20 years ago, ion channels were found to be involved in diseases, termed channelopathies. Within the K_v10 family of voltage-gated potassium channels, a functional role of $K_v10.1$ in cancer and cell proliferation has been demonstrated. Up to date, not much is known about $K_v10.2$, the second member of the K_v10 family.

Therefore, the aim of this PhD thesis was to characterize the distribution of $K_v10.2$ in mouse tissues and specifically in the brain. We generated and evaluated a novel anti-$K_v10.2$ antibody, which recognized both human and murine $K_v10.2$ and did not cross-react with $K_v10.1$. Using this antibody, we found a broad expression of the $K_v10.2$ protein in various mouse tissues and an enrichment of $K_v10.2$ in certain brain areas, such as the olfactory bulb, thalamus, amygdala and globus pallidus. Within the central nervous system, $K_v10.2$ was shown to be mainly localized to neurons.

We found $K_v10.2$ expressed during early brain development as well as in other embryonic tissues. While knockout of $K_v10.1$ resulted only in a mild phenotype, genetic ablation of $K_v10.2$ effected embryonic survival. This may indicate a function of the channel during embryonic development. With our newly generated antibody we provide a valuable tool for further investigations to unravel the biological role of $K_v10.2$ in human physiology and disease.

List of Abbreviations

A	Amnion
aa	Amino acid
ABTS	2,2'-Azinobis [3-ethylbenzothiazoline- 6-sulfonic acid]-diammonium salt
A/B block	Antibody block
AC III	adenylyl cyclase III
Amg	Amygdala
Amp	Ampecillin
AP	Alkaline phosphatase
appr	Approximatly
ATCC	American Type Culture Collection
ATP	Adenosine-5'-triphosphate
BBS	α-bungarotoxin binding site
BCA	Bicinchoninic acid
BCIP	5-bromo-4-chloro-3-indolyl phosphate
BLAST	Basic Local Alignment Search Tool
bp	Basepair
BrSt	Brainstem
BSA	Bovine serum albumin
CA	Cornu ammonis area
Cb	Cerebellum
CC	Corpus callosum
cDNA	complementory deoxyribonucleic acid
CHO	Chinese hamster ovary
cNBD	Cyclic nucleotide binding domain

CNS	Central nervous system
CPu	Caudate putamen
ct	Cycle treshold
C-terminus	Carboxyl-terminus
Cx	Cortex
DAB	3, 3'-diaminobenzidine
Dcn	Dentate cerebellar nucleus
ddH_2O	Double distilled Water
DEPC	Diethylpyrocarbonate
DG	Dentate gyrus
DIG	Digoxegenin
dil	Dilution
DMEM	Dulbecco's Modified Eagle's Medium
DMSO	Dimethylsulfoxid
DNA	Deoxyribonucleic acid
dNTP	Deoxyribonucleotide triphosphates
DPBS	Dulbecco's Phosphate-Buffered Saline
DTT	Dithiothreitol
E	Embryo
E.coli	*Escherichia coli*
eCFP	Enhanced cyan fluorescent protein
EDTA	Ethylendiamin-tetraacetat
eGFP	Enhanced green fluorescent protein
ELISA	Enzyme-linked immunosorbent assay
EMX1	Empty spiracles homeobox 1
EtOH	Ethanol
eYFP	Enhanced yellow fluorescent protein

F	Forward
FAM	Flourescin amidite
FCS	Fetal calf serum
GCL	Granular cell layer
GFAP	Glial fibrillary acidic protein
GL	Granular layer
GP	Globus pallidus
GuHCl	Guanidinium hydrochloride
h	Hour
HCl	Hydrochloric acid
HEPES	4-(2-hydroxyethyl)-1- piperazineethanesulfonic acid
HEK	Human embryonic kidney
Hip	Hippocampus
Hil	Hilus
HRP	Horseradish peroxidase
HPRT	Hypoxanthine-guanine phosphoribosyltransferase
IC	Internal capsula
IHC	Immunohistochemistry
Hpc	Hippocampus
HPRT	hypoxanthine phosphoribosyltransferase
IPTG	Isopropyl-â-D-thiogalactopyranosid
ISH	*In Situ* hybridization
kb	Kilo base pairs
kDa	Kilo Dalton
l	Liter
LB	Luria Broth
LDS	Lithium dodecyl sulfate

LG	Lateral genicular nucleus
LGC	Laboratory of Government Chemist
mAb	Monoclonal antibody
MB	Medullablastoma
MCL	Mitral cell layer
MES	2-(N-morpholino) ethanesulfonic acid
MG	Medial genicular nucleus
ML	Molecular layer
mRNA	Messanger ribonucleic acid
MtOH	Methanol
$MgCl_2$	Magnesium chloride
N-terminus	Amino-terminus
N2a	Neuro 2a
NBT	Nitro blue tetrazolium
Ni-NTA	Nickel(II)-nitrilotriacetic acid
NFR	Nuclear fast red
o/n	Over night
OB	Olfactory bulb
OCx	Olfactory cortex
Oligo dT	Deoxy-thymine nucleotides
P	Pore
PAS	Per-Arnt-Sim
PBS	phosphate-buffered saline
PC	Purkinje layer
PCR	Polymerase chain reaction
PFA	Paraformaldehyde
pH	Potentium hydrogenii

Pl	Placenta
PN	Postnatal
PMSF	Phenylmethanesulfonyl fluoride
PLL	Poly-L-lysine
PYS	Parietal yolk sac
qRT-PCR	quanitative real-time polymerase chain reaction
R	Reverse
RM	Reichert's membrane
RNA	Ribonucleic acid
rpm	Rotations per minute
RT	Room temperature
SD	Standart deviation
SDS	Sodium dodecylsulfat
SDS-PAGE	Sodium dodecyl sulfate-polyacrylamide gel electrophoresis
SSC	Saline (sodium chloride)- sodium citrate
SVZ	Subventricular zone
TBS	Tris buffered saline
TBST	Tris buffered saline containing Tween-20
TE	Tris-EDTA
TEMED	N,N,N',N'-tetramethylethylenediamine
TfR	Transferrin receptor
Th	Thalamus
TM	Transmembrane
Tris	Tris(hydroxymethyl)aminomethane hydrochloride
U	Uterus
Ubc	Ubiquitin C

UC	Umbilical cord
UPL	Universal probe library
UV	Ultraviolett
V	Ventricle
v/v	Volume/volume
VYS	Visceral yolk sac
WB	Western blot
WM	White matter
Wt	Wild type
w/v	Weight/volume
xg	Acceleration of gravity
ZI	Zona incerta

List of Amino Acids

A	Alanine
R	Arginine
N	Asparagine
D	Aspartic acir
C	Cysteine
E	Glutamic acid
Q	Glutamine
G	Glycine
H	Histidine
I	Isoleucine
L	Leucine
K	Lysine
M	Methionine

F	Phenylalanine
P	Proline
S	Serine
T	Threonine
W	Tryptophan
Y	Tyrosine
V	Valine

List of Figures

List of Tables

1 Introduction

All prokaryotic and eukaryotic cells are surrounded by a lipid layer, the cell membrane. In eukaryotic cells various cellular compartments are further separated by membranes, such as the nucleus or the Golgi apparatus. In order to transport ions across these membrane barriers cells rely on two mechanisms: facilitated diffusion or active transport. The facilitated diffusion is mainly carried out by transmembrane proteins through which ions can diffuse according to their concentration gradient without energy consumption (Stein and Lieb, 1986). Alternatively, ions can be forced to move against their concentration gradient during the process of active transport. For this purpose, the cell employs proteins embedded in the membrane, which use the energy of adenosine-5'-triphosphate (ATP). These reestablish the concentration differences of the ions on opposite sides of the cell membrane. The difference in ion concentration on both sides of the membrane leads to a difference in charge, thereby generating an electrical potential difference known as the membrane potential. The unaltered membrane potential in excitatory and non-excitatory cells is termed the resting potential. Modulation of the resting potential in cells, due to ion channel opening, can lead to an electric current. In simplified terms, once this momentary change of the electric membrane potential surpasses a certain threshold, an action potential is generated (Egri and Ruben, 2012). Amongst others, the physiological roles of ion channels include cell volume regulation by governing ion flux control and controlling signal cascades, in which especially calcium (Ca^{2+}) conducting channels are involved (Dolmetsch et al., 2001, Okada, 2004). Ion channels have a pivotal role in the stabilization of the membrane potential, as well as in the modulation of action potentials. The protein group of ion channels is very heterogeneous and classifications are typically based on the type of ion for which they are specific, such as sodium (Na^{+}), Ca^{2+} or potassium (K^{+}) channels. Subclassifications within these groups are diverse, for instance by gating behavior, i.e. ion channels that are voltage-gated or ligand-gated, or based on the pharmacological properties of an ion channel.

1.1 K^+ channels

K^+ channels are essential for setting of the membrane potential as well as for the modulation of the resting potential in excitatory and non-excitatory cells. Furthermore, in excitatory cells such as neurons and muscle cells they participate in the generation and modulation of action potentials (Coetzee and Rudy, 2006, Egri and Ruben, 2012). Moreover, K^+ channels are involved in proliferation and differentiation (DeCoursey et al., 1984, Bruggemann et al., 1997). Expression of genes encoding K^+ channels is regulated in an ontogenetic, cell or tissue dependent manner, thereby generating the most diverse group of ion channels (Rudy, 1988, Hille, 2001). The translation of a K^+ channel gene leads to the synthesis of an α-subunit of the K^+ channel (Figure 1A). A conductance pore is assembled by multiple α-subunits (Figure 1B). This further enhances the diversification of K^+ channels by not only forming homomeric ion channels, but also heteromeric channels, based on their α-subunits. Moreover, K^+ channels are often effector proteins of second messenger cascades modulating channel activity, including kinases and phosphatases (Covarrubias et al., 1994, Drain et al., 1994, Jonas and Kaczmarek, 1996), Ca^{2+} (Stansfeld et al., 1996) or G-proteins (Huang et al., 1993). These attributes make K^+ channels an interesting and important target for research, also in context of the emerging field of channelopathies.

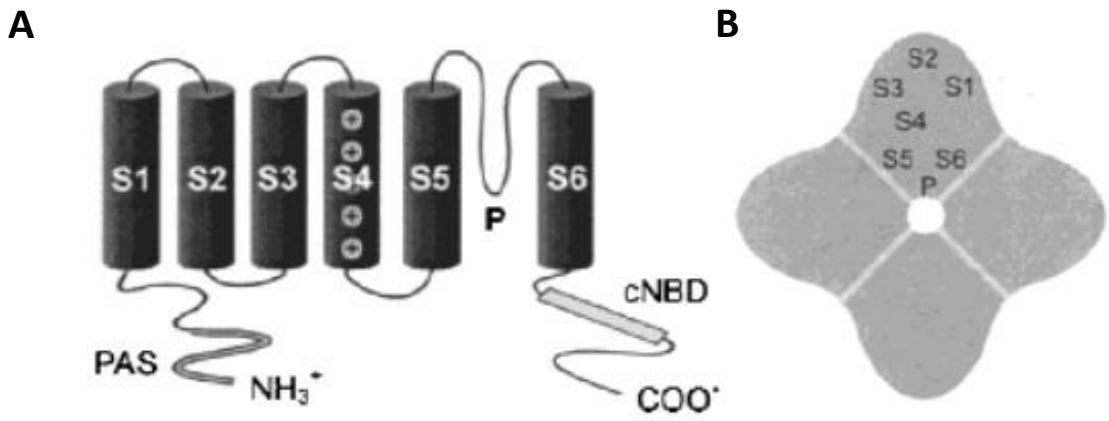

Figure 1: Overview of K_v protein channel structure
A: A schematic representation of an α-subunit of the Eag potassium ion channel family. It contains six transmembrane (TM) domains (S1-S6), a pore (P) forming domain, a N-terminal Per-Arnt-Sim (PAS) domain and a C-terminal cyclic nucleotide binding domain (cNBD). The S4 TM domain functions as the voltage sensor. **B:** Proposed structure of a functional ion channel by tetramerization of α-subunits. **A,B:** Figure from Bauer (Bauer and Schwarz, 2001).

K^+ channels are not only present in the plasma membrane but also in other cell organelle membranes, e.g. the nuclear (Mazzanti et al., 1990, Maruyama et al., 1995, Chen et al., 2011) or mitochondrial membranes (Szewczyk et al., 1996, Siemen et al., 1999, Szabo et al., 2005).

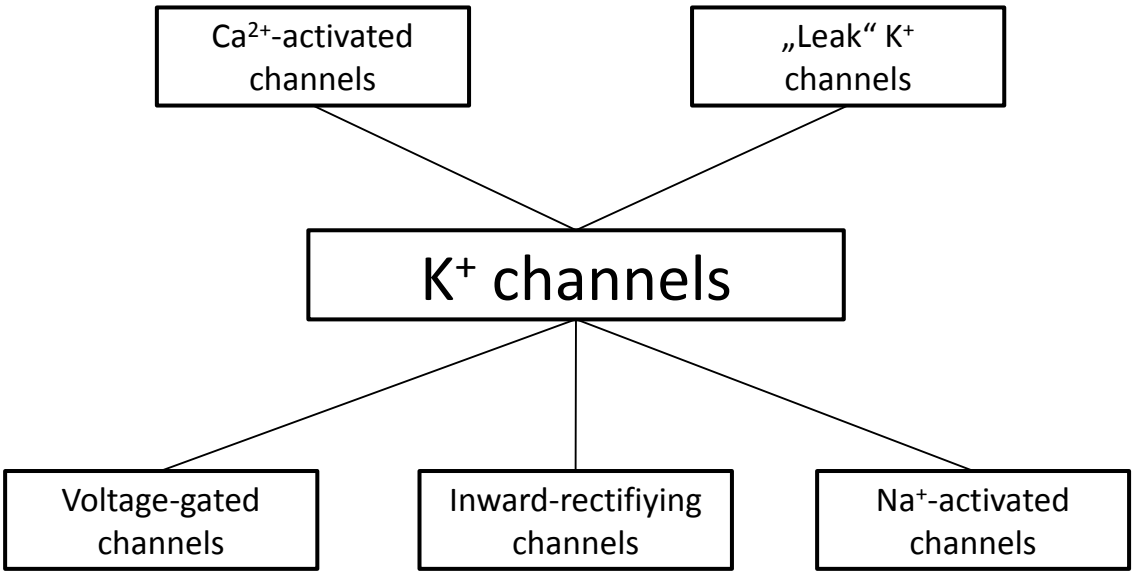

Figure 2: Classification of K^+ ion channels by gating behavior
K^+ channels can be divided into subgroups according to their gating behavior. There are Ca^{2+}-activated channels, membrane voltage-activated channels and channels that are inward-rectifying. Furthermore, K^+ channels exist that are not gated, resulting in "leak" K^+ permeabilization of the membrane and Na^+-activated K^+ channels. Figure modified from Coetzee (Coetzee and Rudy, 2006).

More than 100 different K^+ channel proteins have been identified, either by cloning from different organisms (Capel, 1974, Jan and Jan, 1997, Kim and Hoffman, 2008), by genome projects (Wei et al., 1996) or through in silico analysis (Salkoff and Jegla, 1995). K^+ channels can be grouped into five main classes according to their function (Coetzee and Rudy, 2006) (Figure 2):

1. Voltage-gated K^+ channels, activation occurs by membrane depolarization.
2. Ca^{2+}-activated K^+ channels, activation depends on the intracellular Ca^{2+} concentration.
3. Inward-rectifying K^+ channels which allow efflux of K^+ ions.
4. "Leak" K^+ channels which do not show specific control of K^+ flux.
5. Na^+-activated K^+ channels, gating properties depend on the intracellular Na^+ ion concentration (Coetzee and Rudy, 2006).

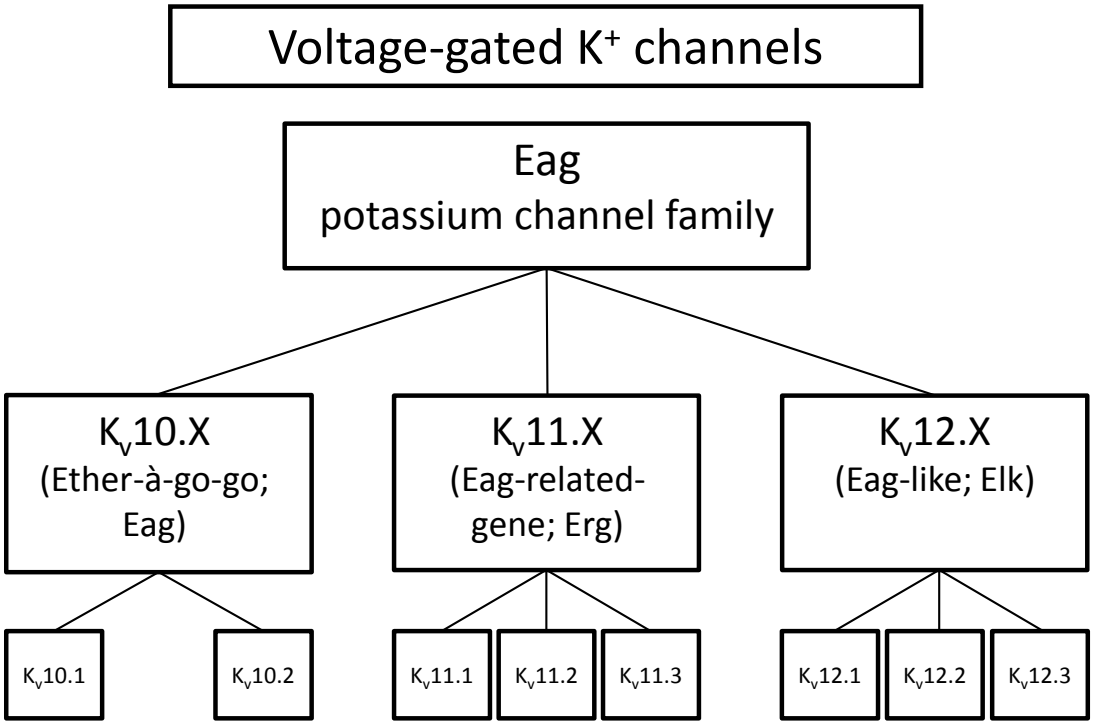

Figure 3: Overview of the mammalian K_v10 family
Schematic representation of the Eag family which belongs to the voltage-gated K^+ channels and includes three subfamilies: K_v10 (eag), K_v11 (erg) and K_v12 (elk). Figure was modified from Bauer (Bauer and Schwarz, 2001).

The Eag family belongs to the group of voltage-gated potassium channels (Warmke et al., 1991) (Figure 3). These channels have a higher selectivity for K^+ ions than for Na^+ or Ca^{2+} ions in mammals (Hille, 2001).

1.2 Eag family of ion channels

Shaker (Sh, mammalian nomenclature: K_v1.1) was discovered by investigation of a *Drosophila melanogaster* mutant which showed a phenotype of abnormal motor behavior under ether narcosis (Kaplan and Trout, 1969). Mutations resulting in this motor behavior were traced to the gene locus of Sh which was the first K^+ channel encoding gene to be genetically investigated (Kamb et al., 1987, Papazian et al., 1987, Papazian et al., 1988, Pongs et al., 1988) together with ether-à-gogo (Eag; mammalian nomenclature: K_v10.1) (Kaplan and Trout, 1969). Sequence analysis of Eag revealed that this protein contains similarities with the Shaker K^+ channel. The highest homology was reported in the voltage sensor (S4 domain) and the pore domain (Warmke et al., 1991).

Further genetic investigations in *Drosophila melanogaster* resulted in the discovery of aditional K^+ channels expanding Shaker, Eag and other potassium channels to whole gene families. The Shaker family was expanded by the finding of Shab, Shaw and Shal (Butler et al., 1989, Butler et al., 1990). Eag (mammalian nomenclature: K_v10, K_v11, K_v12) (Warmke et al., 1991, Bruggemann et al., 1997) became a family by the discovery of ether-à-gogo -like potassium channel (elk, mammalian nomenclature: K_v12) (Warmke and Ganetzky, 1994) and ether-à-gogo -related gene potassium channel (erg, mammalian nomenclature: K_v11) (Titus et al., 1997) subfamilies.

In mammals, eight genes belonging to the Eag family have been reported: *KCNH1* ($K_v10.1$), *KCNH5* ($K_v10.2$), *KCNH2* ($K_v11.1$), *KCNH6* ($K_v11.2$), *KCNH7* ($K_v11.3$), *KCNH8* ($K_v12.1$), *KCNH3* ($K_v12.2$), *KCNH4* ($K_v12.3$) (Packer et al., 2000, Bauer and Schwarz, 2001) (Figure 3). The nomenclature of these channels has been standardized by the International Union of Basic and Clinical Pharmacology (IUPHAR) (Gutman et al., 2005). For a better overview, a table with the new and outdated names according to the IUPHAR is shown in the appendix section (Appendix, Table 1). Characterization of the Eag family of ion channels lead to the observation that they all share a common constitution of four α-subunits assembling one functional ion channel (Figure 1Figure 1B). Besides the general structure, the α-subunits have a common structure of six hydrophobic membrane-spanning domains (S1-S6), a hydrophobic pore segment (P) and an intracellular amino- (N-) and carboxy- (C-) terminal domain (Yellen, 2002, Wray, 2004) (Figure 1A).

Being the founding member of the Eag family, $K_v10.1$ had novel features revealed by sequence analysis. Most notable and divergent from known members of the K_v1 family was the cyclic nucleotide-binding domain (cNBD) in the cytoplasmic C-terminus of $K_v10.1$ (Guy et al., 1991). The fourth transmembrane domain (S4) contains the voltage sensor, which senses the depolarization of the membrane (Papazian et al., 1991, Logothetis et al., 1992) (Figure 1A). Assembly or tetramerization of a functional K_v ion channel is based on protein domains located in the cytoplasmic C-terminus of the α-subunits (Li et al., 1992, Shen et al., 1993). For all three human K_v11 channels it has been shown that the α-subunits can tetramerize to form a heteromultimeric channel when expressed in Chinese hamster ovary (CHO) cells (Wimmers et al., 2001, Wimmers et al., 2002). Moreover, this has been described *in vivo* by electrophysiological measurements in the rat embryonic rhombencephalon (Hirdes et al., 2005).

The conserved domains of the Eag family include a Per-Arnt-Sim (PAS) domain at the N-terminal cytoplasmic region and at the C-terminus a cNBD and a domain required for assembly (Ludwig et al., 1997, Cui et al., 2001). Furthermore, the ion channels within one family share a high homology of the DNA and amino acid sequence. For example, the human K_v10.1 protein is 73 % identical to K_v10.2 (Ju and Wray, 2002).

In terms of electrophysiology the K_v10 family is characterized by outward rectification without inactivation. Furthermore, the activation kinetics depend on the holding potential as well as on the extracellular magnesium concentration (Ludwig et al., 1994, Stansfeld et al., 1996, Terlau et al., 1996, Saganich et al., 1999, Bauer and Schwarz, 2001).

1.3 Expression of members of the K_v10 subfamily of the Eag family

The K_v10 subfamily of the Eag family consists of two members, K_v10.1 and K_v10.2. As well as the understanding of the structure of an ion channel based on its domains and electrophysiological studies, which indicate its possible physiological function *in vivo*, it is pivotal to localize its expression. Since the K_v10 family of ion channels was discovered in *Drosophila melanogaster* neurons, a neuronal localization of K_v10.1 in the mammalian brain was speculated. In contrast to K_v10.1 for which specific expression analyses have been reported at the RNA and protein level in different mammalian samples, protein analysis data for the K_v10.2 channel is limited since distribution studies have mainly been performed at the RNA level.

1.3.1 Expression pattern of *KCNH1* (K_v10.1)

In humans and the rat, *Kcnh1* expression is limited to the brain and testes (Ludwig et al., 1994, Pardo et al., 1999). As detected by *in situ* hybridization (ISH) , *Kcnh1* has the highest mRNA expression in the olfactory bulb (ob), cerebral cortex (Cx), hippocampus (Hipp) and cerebellum (Cer) of adult rats (Ludwig et al., 2000, Saganich et al., 2001) (Figure 4A,B). Martin and co-workers performed further mRNA analysis of *Kcnh1* of regions of the rat brain by qRT-PCR (Martin et al., 2008). This study revealed a low expression of *Kcnh1* in the thalamus. In this brain region the ISH by Saganich (Saganich et al., 2001) and Ludwig (Ludwig et al., 2000) were negative for *Kcnh1*. Additionally, the distribution of this ion channel was assessed on the protein level by immunohistochemical (IHC) analysis in rat brain (Martin et al., 2008) (Figure

4C), which revealed a ubiquitious protein distribution. Comparison of the mRNA distribution detected by ISH by Ludwig (Ludwig et al., 2000) and Saganich (Saganich et al., 2001) with the protein distribution by Martin et al. (Martin et al., 2008) leads to further inconsistencies of *Kcnh1* protein and mRNA localization in the adult rat brain. Discordances in expression pattern for this gene were found, for example, in different nuclei of the thalamus, amygdale and brainstem. Furthermore, in all layers of the cortex, K_v10.1 was equally distributed (Martin et al., 2008), while mRNA was found abundantly in layers IV and VI (Saganich et al., 2001). In the cerebellum the K_v10.1 protein and mRNA of *Kcnh1* detected showed no correlation. In this brain region, mRNA levels detected were highest in the granular layer and lowest in the Purkinje layer (Ludwig et al., 2000, Saganich et al., 2001) Protein levels were vice versa, high in the Purkinje layer and low in the granular layer (Martin et al., 2008). Within the same study the expression of K_v10.1 in rat brain was compared to the expression of K_v10.1 in selected human brain regions (Martin et al., 2008). In humans the frontal cortex, the hippocampus and the cerebellum were positive for K_v10.1 as observed in the rat brain (Martin et al., 2008). Additionally, the authors claimed positive staining of the human thalamus and brainstem but did not show the data in their publication.

Furthermore, the distribution of K_v10.1 and K_v10.2 was investigated in rat retina (Jow and Jeng, 2008). K_v10.1 was ascertained in the outer and inner segments of photoreceptor cells, in the outer plexiform layer, in the inner nuclear layer and the ganglion cell layer. The strongest staining and therefore the highest K_v10.1 protein level was observed in the inner plexiform layer (Jow and Jeng, 2008). This protein was not found in the outer nuclear layer. In contrast, K_v10.2, the second K_v10 family member, was not present in the inner plexiform layer, while the outer nuclear layer was positive for K_v10.2. Strong signals were observed in the outer and inner segments of photoreceptor cells, the outer plexiform layer and the inner nuclear layer. The ganglion cell layer was also positive for K_v10.2, but to a lesser extend (Jow and Jeng, 2008).

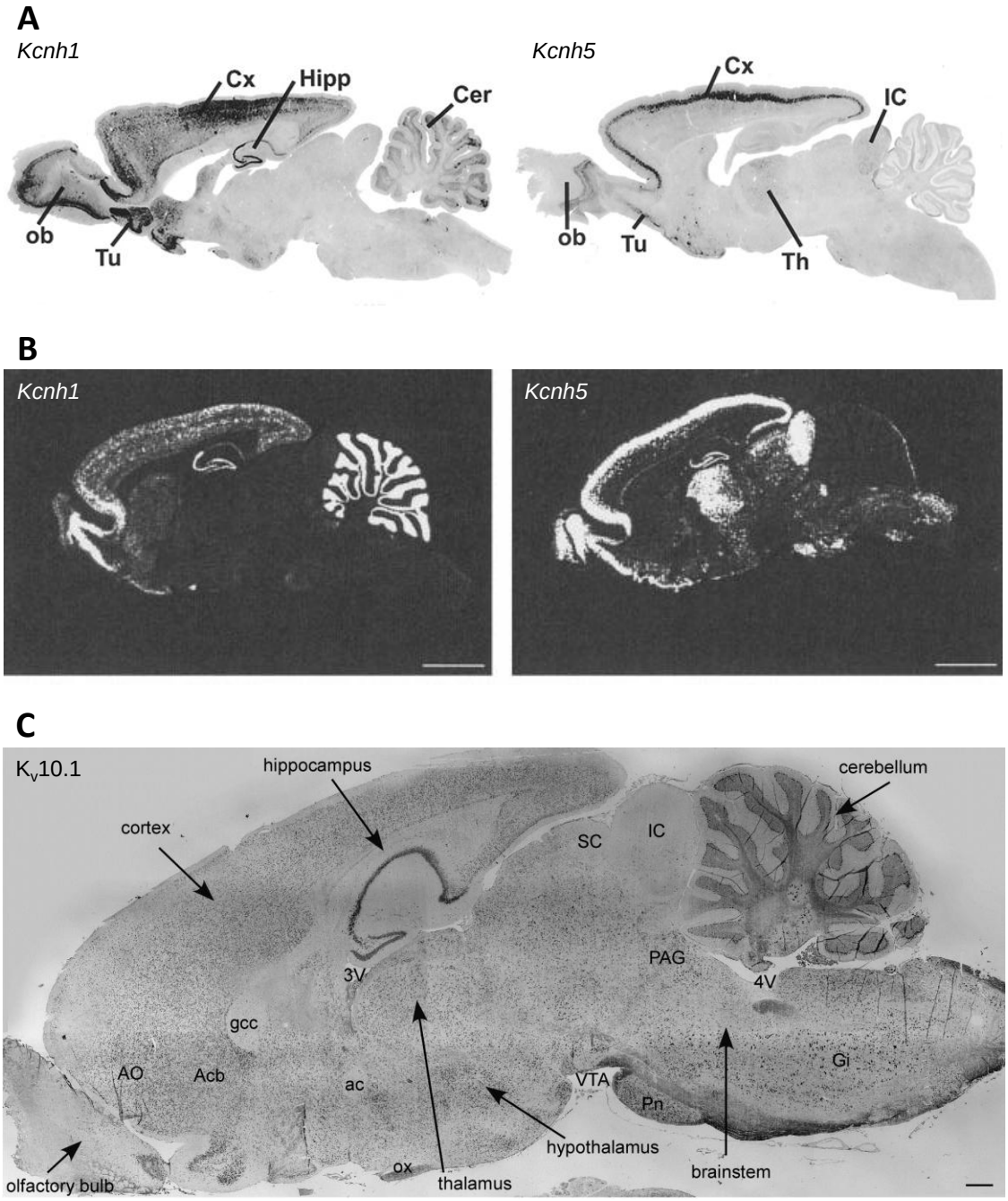

Figure 4: Expression of K_v10 ion channels mRNA determined by two *In Situ* hybridization approaches and IHC for K_v10.1 on adult rat brain sections

A: *Kcnh1* (left) and *Kcnh5* (right) mRNA distribution in adult rat brain sections with non radioactive ISH. Abbreviations used are according to FigureA. *Kcnh1* is localized to the olfactory bulb (ob), olfactory tubercle (Tu), hippocampus (Hipp) and cerebellum (Cer). The caudate putamen and several nuclei of the amygdala were also *Kcnh1* mRNA positive. *Kcnh5* was localized to the ob, Tu, cortex, inferior colliculus (IC) and thalamus (Th). Furthermore, low expression was detected in the intercalated nucleus of the amygdala and in some nuclei of the brainstem. Cryo frozen sections obtained at 40 µm. Figure from Saganich et al. (Saganich et al., 2001). **B:** *Kcnh1* (left) and *Kcnh5* (right) mRNA distribution in adult rat brain sections with radioactive ISH. *Kcnh1* transcripts were detected in the olfactory bulb, hippocampus, all cortical layers, and some nuclei of the amygdala, hypothalamus, caudate putamen and cerebellum. *Kcnh5* was detected in the olfactory bulb, hippocampus, cortical layers III and IV, some nuclei of the amygdala, hypothalamus, thalamus, inferior colliculus, superior colliculus, lateral lemniscus and nuclei of the lower brainstem. Cryo frozen sections were obtained at 10 to 16 µm. Scale bars represent 3000 µm. Figure from Ludwig et al. (Ludwig et al., 2000). **C:** Overview of an IHC for K_v10.1 on adult rat sagittal section resulting in ubiquitious K_v10.1 distribution. Abbreviations used are according to FigureC: anterior

commissure (ac), nucleus accumbens (Acb), anterior olfactory nucleus (AO), genu of corpus callosum (gcc), gigantocellular reticular nucleus (Gi), inferior colliculus (IC), optic chiasm (ox), periaqueductal gray (PAG), pontine nuclei (Pn), superior colliculus (Sc), 3rd ventricle (3V), 4th ventricle (4V). Scale bar represents 500 µm. Figure from Martin et al. (Martin et al., 2008).

1.3.2 Expression pattern of *KCNH5* (K_v10.2)

Although first evidence linking K_v10.2 to certain diseases is available, data on protein expression pattern are very limited. With the exception of the rat retina study, the knowledge regarding distribution of *Kcnh5* mRNA has been studied in the brain of rat and partially in mouse and ferret by ISH. The *Kcnh5* transcript has been consistently found in the olfactory bulb, cortex, thalamus and amygdala of rats (Saganich et al., 1999, Ludwig et al., 2000, Saganich et al., 2001) (Figure 4A,B). At the regional level, differences of *Kcnh5* mRNA distribution were found in the hippocampus and cerebellum. Data acquired by Saganich and co-workers (Saganich et al., 2001) concerning *Kcnh5* mRNA distribution in adult rat brain are partially inconsistent with the data he presented earlier (Saganich et al., 1999). In his earlier work, *Kcnh5* expression is shown to be strongest in the cortical layer IV, while no *Kcnh5* expression was found in layers II and III; in these layers the staining was estimated to be at the background level. More recent work by Saganich (Saganich et al., 2001) shows abundant *Kcnh5* expression in layer III and to a lesser degree in layer II of the rat cortex. In contrast to Saganich's (Saganich et al., 2001) findings, Ludwig (Ludwig et al., 2000) detected *Kcnh5* expression by ISH on rat brain in cortical layer VI. Further comparison of the ISH by Ludwig (Ludwig et al., 2000) and Saganich (Saganich et al., 2001) revealed discrepancies in *Kcnh5* distribution, for example in the nucleus accumbens of the basal ganglia, periglomerular cell layer of the olfactory bulb and the spinal trigeminal nucleus. Additional analysis of *Kcnh5* expression was performed with PCR by Saganich (Saganich et al., 1999). Expression of *Kcnh5* was virtually limited to the brain in the rat model organism, with the exception of the testes (Saganich et al., 1999), while heart, skeletal muscle, spleen, lung, kidney and liver were negative for *Kcnh5*.

Northern blot analysis of rat tissue revealed a shorter transcript of 3 kb compared to the 12 kb transcript of *Kcnh5* found in the brain. It was postulated by the authors that this might be an alternatively processed *Kcnh5* transcript (Saganich et al., 1999). Interestingly, in humans Ju and co-worker found K_v10.2 protein that was truncated in the C-terminal cNBD domain (Ju and Wray, 2002). This protein was only 611 amino acids long, compared to the 988 amino acids of the full length human K_v10.2. Within the same publication, *KCNH5* mRNA distribution in human tissue was analyzed by Northern blot, resulting in a *KCNH5* transcript

size of 6.8 kb. Moreover, Ju and colleague (Ju and Wray, 2002) found a transcript of 1.4 kb in size in heart and skeletal muscle, further underlining the possible existence of alternative *KCNH5* spliced transcripts.

Additionally, RNA distribution analysis was done by Rowell and co-workers in the neocortex of the ferret and mouse by ISH (Rowell et al., 2010). Although the ferret is more distantly related to rodents, the data gained indicate a possibly conserved gene expression profile of the *Kcnh5* channel between mammalian species. Similar to the expression pattern of *Kcnh5* in the rat brain, *Kcnh5* is found in the ferret brain in the cortical layers II – V and in the upper layer VI, with the strongest signal obtained in layer IV (Rowell et al., 2010). Strikingly, within the visual cortex, the layer IV can be separated in a *Kcnh5* positive upper and a *Kcnh5* negative lower layer. The ISH performed on the mouse visual cortex revealed expression in layer V neurons and a stringent labeling of layer IV, with no sub lamination as seen in the ferret brain (Rowell et al., 2010). Concerning its distribution in the cerebellum, Huang and co-worker detected *Kcnh5* expression in the granular layer, molecular and the Purkinje cell layer by ISH (Huang et al., 2012). This is in accordance with results from Western blot analysis performed by the same group that detected $K_v10.2$ protein in total cerebellar lysate.

1.4 Channelopathies of K^+ channels

Interest in ion channel research increased considerably once it was discovered that they are in fact the cause of a number of pathological conditions or disorders in man. Diseases caused by dysfunctional ion channels are termed channelopathies (Griggs and Nutt, 1995) and have been reported for some genes encoding K^+ channels (Sanguinetti and Spector, 1997, Kullmann, 2002). Different genes of the Eag family also have been described to be involved in diseases, for example $K_v10.1$ in carcinogenesis (Asher et al., 2010). Due to the conserved domains and the high homology within the Eag family, the published diseases of this ion channel family might indicate further relevance of $K_v10.2$ in the context of channelopathies.

Besides their involvement in channelopathies, research of ion channels participating in cell cycle propagation has been conducted (Blackiston et al., 2009). Uncontrolled cell cycle progression often results in carcinogenesis. An example of an ion channel involved in diseases is *KCNH2*. The human *KCNH2* ($K_v11.1$) gene encodes the α-subunit of a K^+ channel that is involved in mediating the rapid delayed rectifying potassium currents of the heart (Trudeau et al., 1995, Sanguinetti et al., 1996).

KCNH2 has been reported to be involved in the Long QT2 syndrome (Larsen et al., 2001, Sugiyama et al., 2011). Missense mutations and intragenic deletions of *KCNH2* result in alteration of repolarisation in the cardiac ventricles. The deceleration of repolarisation is linked to the long QT2 syndrome (LQT2S, Romano-Ward-syndrome), where the excitation and repolarization of the heart are desynchronized, leading to arrhythmia (Torsade de pointes) (Keating and Sanguinetti, 1996, Sanguinetti, 2010). Until December 2010, 291 mutations of *KCNH2* leading to LQT2S had been reported according to the inherited arrhythmias database (http://www.fsm.it/cardmoc/).

In human cancer cell lines enhanced expression of *KCNH2* has been reported, while its expression is also found in primary tumors of the endometrium and colon (Bianchi et al., 1998, Arcangeli et al., 1999, Cherubini et al., 2000, Lastraioli et al., 2004).

Other ion channels, which have been reported to be involvement in cancer, are the members of the K_v10 family. Although in humans and rodents the expression of *KCNH1* is limited to the brain (Pardo et al., 1999, Ludwig et al., 2000, Saganich et al., 2001), Pardo and co-workers found protein of this ion channel expressed in human cancer (Pardo et al., 1999, Pardo et al., 2005). In non-CNS cancerous tissue derived from patients, $K_v10.1$ expression is found in >75% of all samples investigated (Hemmerlein et al., 2006). Its oncogenic potential is further supported by the fact, that CHO transfected cells expressing human *KCNH1* resulted in increased proliferation *in vitro* (Pardo et al., 1999) and injection of these cells into immune-suppressed mice resulted in tumor formation *in vivo* (Pardo et al., 1999).

In the context of cancer, the involvement of *KCNH5* is controversial because of the following reasons. In non-small cell lung cancer *KCNH5* was found to be highly methylated in comparison to controls (Feng et al., 2008), indicating a downregulation of gene expression. Recent findings indicate a role of $K_v10.2$ in facilitating medulloblastoma (MB) growth (Huang et al., 2012), by the fact that overexpression of $K_v10.2$ was found in MB subgroups of mouse and human while knockdown of *Kcnh5* resulted in late G2 phase arrest. Concerning diseases of the CNS, *Kcnh5* expression was significantly downregulated in the brain of adult rats on the 7^{th} day after transient global brain ischemia in rats (de Oliveira et al., 2012), indicating a role of *Kcnh5* in stroke recovery. Furthermore, Martin and co-workers analyzed *Kcnh5* expression in isolated reared rats (Martin et al., 2010). *Kcnh5* was found to be downregulated in all brain regions except the cerebellum in isolated reared rats compared to controls. This is indicative of a possible role of *Kcnh5* in psychological disorders. So far, *Kcnh5*-caused channelopathies were mainly based on genetic alterations or RNA expression studies. The detection of $K_v10.2$ on the

protein level may give insights of $K_v10.2$ function and may lead to further discoveries of the involvement of this ion channel in diseases.

1.5 Primary cilium

Cilia are membrane-bounded cell organelles that derive from the centrioles of cells, which can be separated into two groups based on their structure (Murray and Larson, 2010). Both types of cilia consist of a cytoskeleton that is formed by microtubule projections (axoneme). The first group, the motile cilia, consists of nine microtubule doublets which surround a central pair of singlet microtubules (9 + 2 axoneme) (Sorokin, 1962). These cilia can generate a physical flow (Guirao and Joanny, 2007). However, few examples of immotile 9 + 2 cilia have been reported (Menco, 1994). The second group of cilia contains of nodal and primary cilia (Figure 5A). These cilia also contain the outer ring of microtubule doublets but not the central pair of singlet microtubules (9 + 0 axoneme) (Figure 5B). Nodal cilia are motile and present on the mouse embryonic node (Sulik et al., 1994). The primary cilium is an immotile, solitary cellular protrusion that is present on virtually all vertebrate cell types

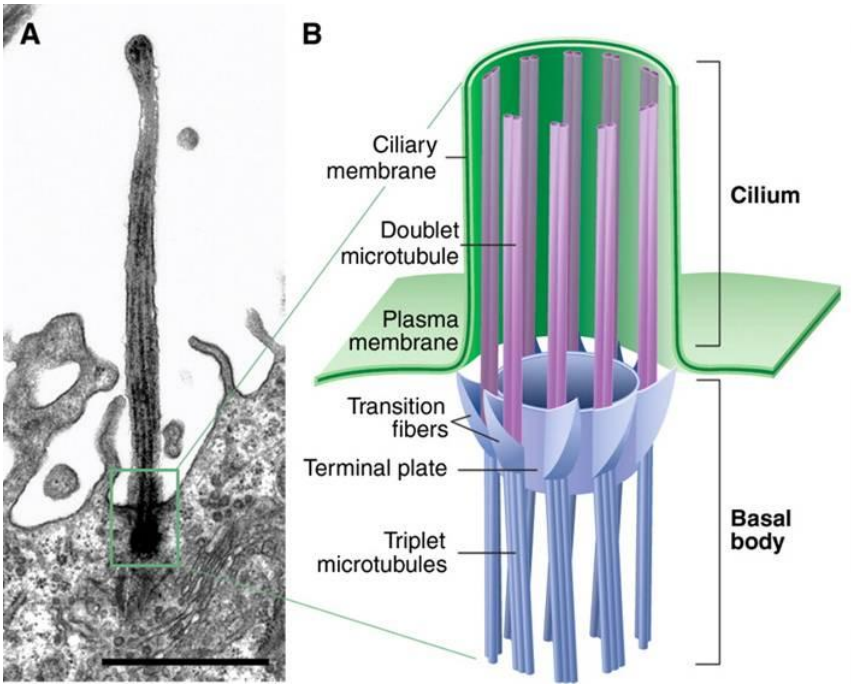

Figure 5: Overview of the structure and the appearance of the primary cilium
A: Electron micrograph of the primary cilium of a canary brain radial glia. Scale bar represents 10 µm. **B**: Schematic representation of the primary cilium and its basal body. The basal body, derived from a centriole, contains triplet microtubules. The 9 + 0 axoneme is extended into the cilium. Figure from Singla (Singla and Reiter, 2006).

(http://www.bowserlab.org/primarycilia/cilialist.html). Ciliogenesis of the primary cilium is co-ordinately regulated with the cell cycle (Quarmby and Parker, 2005). Briefly, the formation of cilium starts in the interphase of the cell cycle (Yoshimura et al., 2011) is present during the G_1 or G_0 phase and reabsorbed when the cell re-enters the cell cycle (Kim and Tsiokas, 2011). At the cytoplasmatic end of the primary cilium lays the basal body, from which it originates. The basal body itself is derived from a centriole, yet, this process is reversible (Hoyer-Fender, 2010). Due to the role of centrioles in cell cycle progression (Doxsey et al., 2005), it remains unclear, if the formation and resumption of the primary cilium controls the cell cycle progression or vice versa.

The role of the primary cilium is diverse. Besides others, it is involved in signaling pathways, such as Hedgehog (Rohatgi and Scott, 2008, Kim et al., 2009), Wnt (Corbit et al., 2008, Lienkamp et al., 2012), platelet-derived growth factor-αα (Christensen et al., 2008, Schneider et al., 2010) as well as mechano sensing (Praetorius and Spring, 2001, 2003).

2 Aim of the study

The major goal of this thesis was to explore the K_v10.2 distribution in the whole mouse organism, since investigations on the protein level are virtually missing and the function of K_v10.2 is still unknown. K_v10.2 could be localized in neurons on mRNA level; however, expression on protein level is virtually missing. One reason is probably a lack of specific antibodies that can distinguish between K_v10.2 and the highly related channel K_v10.1. Therefore, we aimed to:

1) Obtain an antibody that specifically recognizes K_v10.2

K_v10.2 and K_v10.1 are highly similar proteins, therefore we need an antibody that can specifically distinguish both channels. To fulfill this aim, various commercially antibodies will be evaluated. If none of the antibodies is specific, we will generate a novel antibody.

2) Investigate the expression of K_v10.2 in mouse tissues

Using the antibody obtained from aim 1, we will study the expression of K_v10.2 in different tissues of the mouse. Since K_v10.2 is known to be expressed in the brain, we further want to determine the localization in different brain regions. These experiments will be complemented with an expression analysis on an mRNA level. K_v10.1 knockout mouse exhibits only a mild phenotype. A possible explanation would be an upregulation of K_v10.2 in these animals. Therefore the aim is to study the expression of K_v10.2 in K_v10.1 total knockout mouse.

3) Get first insights into the physiological role of K_v10.2

To investigate its physiological function *in vivo*, we wanted to analyze a conditional K_v10.2 knockout mouse. As an alternative approach, we planned knockdown experiments in cell cultures.

3 Materials and Methods

Unless stated otherwise, standard protocols were followed (Green and Sambrook, 2012). Likewise, standard buffers and solutions were prepared and used as described (Green and Sambrook, 2012).

3.1 Instrument and equipment

Instrument	Producer
Agarose gel documentation Duo Store	Intas, Goettingen
Analytical balance, Competence CP64	Sartorius, Goettingen
Apparatus for tissue processing, TP 1020	Leica, Bensheim
Autoclave Vakulab S3000	Systec, Giessen
Axiocam Color	Carl Zeiss, Goettingen
Barcode printer Ebar II	Ventana (Roche), Mannheim
Centrifuge Biofuge 28RS	Heraeus Laboratory products, Hanau
Chemi-Doc luminescence detection system	Bio-Rad, Munich
Centrifuge 5424	Eppendorf, Hamburg
Centrifuge 5402	Eppendorf, Hamburg
Centrifuge 5804R	Eppendorf, Hamburg
Desinfector G7736	Miele, Gütersloh
Digital monochrome printer P93D	INTAS, Goettingen
Electro-Luter 422	BioRad, Munich
Heating plate 14801	Medax, Regensburg
Hybridization incubator OV 3	Biometra, Goettingen
Incubator B5042 E	Heraeus Laboratory products, Hanau
Incubator BB6220	Heraeus Laboratory products, Hanau

Incubater shaker, Innova 4330	New Brunswick scientific (Eppendorf), Hamburg
Incubator UT 6060 (200°C)	Heraeus Laboratory products, Hanau
LaminAir TL 2472 cell culture hood	Heraeus Laboratory products, Hanau
LaminAir HBB 2472 cell culture hood	Heraeus Laboratory products, Hanau
Light microscope, Telaval 31	Carl Zeiss, Goettingen
LightCycler 480	Roche, Mannheim
Light microscope, Axioscope 2	Carl Zeiss, Goettingen
Magnetic stirrer/heater, IKAMAG RCT	Janke und Kunkel, Staufen i. Br.
Microwave R-937	Sharp, Hamburg
Microscope Stemi SV6	Carl Zeiss, Goettingen
Microtome RM2255	Leica, Bensheim
Nano photometer, Pearl	Implen, Munich
Neubauer chamber	Schütt Labortechnik, Goettingen
NuPAGE Bis-Tris Electrophoresis System	BioRad, Munich
PCR cycler, labcycler	Sensoquest, Goettingen
Perfusor Compact S	Braun, Melsungen
pH-meter, SevenEasy	Mettler-Toledo, Giessen
Pipetting robot epMotion 5075	Eppendorf, Hamburg
Power Pack P25	Biometra, Goettingen
Purewater Arium 611	Sartorius, Goettingen
Rollmixer	Fröbel Labortechnik, Lindau
SP5 confocal laser scanning microscope	Leica, Mannheim
Steamer, MultiGourmet	Braun, Kronberg
Thermomixer 5436	Eppendorf, Hamburg
Thermomixer compact	Eppendorf, Hamburg
Tissue lyzer	Qiagen, Hilden

Ultrasonic Desintigrator Sonopuls GM70/UW70	Janke und Kunkel, Staufen i. Br.
UV Stratalinker 1800	Stratagene (Agilent), Waldbronn
UV-table 3-3102	Fotodyne, New Berlin (USA)
Ventana Discovery XT	Ventana (Roche), Mannheim
Vibratome VT1000S	Leica, Bensheim
Vortexer, Vortex Genie 2	Bender & Hobein,Zurich, Switzerland
Wallac 1420 Victor 2 multilabel counter	American Instrument Exchange, Haverhill, MA, USA
Waterbath 25900	Medax, Regensburg

3.2 Chemicals and reagents

Chemicals	**Producer**
100 bp DNA Ladder	Invitrogen, Darmstadt
1 Kb DNA Ladder	Invitrogen, Darmstadt
ABTS single solution (2,2'-Azinobis [3-ethylbenzothiazoline- 6-sulfonic acid]-diammonium salt)	Invitrogen, Darmstadt
Acetic acid	Merck, Darmstadt
Acrolein	Sigma-Aldrich, Seelze
Agar	Gibco (Invitrogen), Darmstadt
Agarose	Gibco (Invitrogen), Darmstadt
Aminopterin	Sigma-Aldrich, Seelze
Ampicillin	Roche, Mannheim
Antibody diluent	Roche, Mannheim
B-27 supplement	Gibco (Invitrogen), Darmstadt
Bacto-Trypton	Carl Roth GmbH, Karlsruhe
Boric acid	Merck, Darmstadt

Chemiluminescent HRP substrate	Millipore, Billerica, MA, USA
Chloroform	Merck, Darmstadt
Coomassie Brilliant Blue R250	Biomol, Hamburg
Cytoseal 60	Roche, Mannheim
Dimethylsulfoxid (DMSO)	Carl Roth GmbH, Karlsruhe
Dithiothreitol (DTT)	Biomol, Hamburg
dNTPs (deoxyribonucleotide triphosphates) (100 mM)	New England Biolabs, Frankfurt am Main
DEPC (diethylpyrocarbonate)	Sigma-Aldrich, Seelze
DIG (digoxigenin) RNA labelig mix	Roche, Mannheim
DMEM (Dulbecco's Modified Eagle's Medium)	Gibco (Invitrogen), Darmstadt
DMSO (Dimethyl sulfoxide)	Sigma-Aldrich, Seelze
DPBS (Dulbecco's Phosphate-Buffered Saline)	Gibco (Invitrogen), Darmstadt
Ethidiumbromid	Sigma-Aldrich, Seelze
Ethylendiamin-tetraacetat (EDTA)	Sigma-Aldrich, Seelze
Ethanol	Merck, Darmstadt
Ethidiumbromide	Sigma-Aldrich, Seelze
Ficoll 400	Sigma-Aldrich, Seelze
FCS (Fetal Calf Serum)	PAN Systems, Aidenbach
Formaldehyde	Merck, Darmstadt
Formamid	Sigma-Aldrich, Seelze
Geniticin (G418)	Invitrogen, Darmstadt
Gentamycin	Invitrogen, Darmstadt
Glutamax	Gibco (Invitrogen), Darmstadt
Guanidine Hydrochlorate	Sigma-Aldrich, Seelze
Haematoxylin	Merck, Darmstadt
HEPES (4-(2-hydroxyethyl)-1-	Carl Roth, Karlsruhe

piperazineethanesulfonic acid)	
Hydrochloric acid, 37%	Merck, Darmstadt
Hydrogen peroxid	Sigma-Aldrich, Seelze
Hypoxanthine	Sigma-Aldrich, Seelze
Imidazol	Fluka (Sigma-Aldrich), Seelze
Insulin- Transferin- Selenium- A 100x	Invitrogen, Darmstadt
Isopropyl-â-D-thiogalactopyranosid (IPTG)	Biomol, Hamburg
Isopropanol	Merck, Darmstadt
Ketamine 10%	Medistar, Holzwickede
L-Thyroxine	Sigma-Aldrich, Seelze
LDS (lithium dodecyl sulfate) sample buffer	Invitrogen, Darmstadt
Luria Broth	Invitrogen, Darmstadt
β-Mercaptoethanol	Fluka (Sigma-Aldrich), Seelze
Methanol	Merck, Darmstadt
Monopotassium phosphate (KH_2PO_4)	Merck, Darmstadt
Ni-NTA (nickel(II)-nitrilotriacetic acid) agarose	Qiagen, Hilden
Nitro blue tetrazolium (NBT)/	Roche, Mannheim
5-bromo-4-chloro-3-indolyl phosphate (BCIP)	
NuPAGE MES Running buffer (20x)	Invitrogen, Karlsruhe
NuPAGE LDS Sample buffer (4x)	Invitrogen, Karlsruhe
NuPAGE Antioxidant	Invitrogen, Darmstadt
OligoFectamine	Invitrogen, Karlsruhe
Orange-G	Sigma-Aldrich, Deisenhofen
Paraffin (melting temperature: 60 °C)	Leica, Bensheim
Paraformaldehyde (PFA)	Serva, Heidelberg
PBS tablets	Gibco, Invitrogen, Darmstadt
Permount	Fischer Scientific, Schwerte

Penicillin/Streptamycin	Gibco, Invitrogen
Phenylmethanesulfonyl fluoride (PMSF)	Sigma-Aldrich, Deisenhofen
PMSF (phenylmethanesulfonylfluoride)	Sigma-Aldrich, Deisenhofen
Poly-L-lysine (PLL)	Sigma-Aldrich, Seelze
Potassium chloride (KCl)	Invitrogen, Darmstadt
Precision Plus protein standard 7710	Bio-Rad, Munich
ProLong Gold antifade reagent with DAPI	Invitrogen, Darmstadt
Putrescine	Sigma-Aldrich, Seelze
QIAzol lysis reagent	Qiagen, Hilden
Reducing agent	Invitrogen, Darmstadt
Sodium azide (NaN_3)	Merck, Darmstadt
Sodium chloride (NaCl)	Sigma-Aldrich, Seelze
Sodium citrate ($C_6H_6Na_2O_7$)	Sigma-Aldrich, Seelze
Sodium dihydrogen phosphate (NaH_2PO_4)	Merck, Darmstadt
Sodium dodecylsulfat (SDS)	Sigma-Aldrich, Seelze
Sodium flouride (NaF)	Sigma-Aldrich, Seelze
Sodium hydroxide (NaOH)	Merck, Darmstadt
Sodium pyrophosphate dibasic ($Na_2H_2P_2O_7$)	Sigma-Aldrich, Seelze
Sodium orthovanadate (Na_3VO_4)	Sigma-Aldrich, Seelze
Dynabeads MyOne Streptavidin T1	Invitrogen, Darmstadt
Thymidine	Sigma-Aldrich, Seelze
Tris-Base	Sigma-Aldrich, Seelze
Tris-HCL	Merck, Darmstadt
Tris-acetate SDS running buffer	Invitrogen, Darmstadt
Tri-Iodo-Thyrodine (TIT)	Fluka (Sigma-Aldrich), Seelze
Triton X-100	Sigma-Aldrich, Seelze
Tween-20	Sigma-Aldrich, Seelze

Urea	MP Biomedicals, Ohio, USA
Western blot stripping buffer	Thermo Scientific, Bonn
Whatman filter paper	GE Healthcare, Munich
Xylazine 2%	Riemser, Greifswald
Xylol	Merck, Darmstadt
Zeocin	Invitrogen, Darmstadt

3.3 Biochemical solutions und Enzymes

Biochemicals	**Producer**
Biotherm polymerase	Genecraft, Cologne
Bovine serum albumin (BSA)	Sigma-Aldrich, Seelze
Casein	Roche, Mannheim
DNase (anti-Deoxyribonuclease) I	Qiagen, Hilden
Fetal calb serum (FCS)	PAN, Aidenbach
Goat serum	Gibco (Invitrogen), Darmstadt
Ni-NTA Agarose	Qiagen, Hilde
Progesteron	Sigma-Aldrich, Seelze
Protease 3	Roche, Mannheim
Protease inhibitor cocktail	Roche, Mannheim
Proteinase K	Carl Roth GmbH, Karlsruhe
RNase H	Invitrogen, Darmstadt
Reverse Transkriptase SuperScript II	Invitrogen, Karlsruhe
T7 RNA polymerase	Roche, Mannheim
Trypsine-EDTA (0.25 %)	PAA Laboratories, Pasching, Austria
Uracil-DNA-glycosylase	New England BioLabs, Frankfurt am Main
Yeast extract	Carl Roth GmbH, Karlsruhe

3.4 Commercial kits

Kits	Producer
A/B Block	Roche, Mannheim
Antibody diulent	Roche, Mannheim
BCA protein assay kit	Thermo Scientific, Bonn
BlueMap Kit	Roche, Mannheim
CC1	Roche, Mannheim
CC2	Roche, Mannheim
DAB Map Kit	Roche, Mannheim
EndoFree Plasmid Maxi Kit	Qiagen, Hilden
ECL Developing Kit	Millipore (Merck), Darmstadt
FastStart High Fidelity PCR System	Roche, Mannheim
NucleoSpin Plasmid Kit	Macherey-Nagel, Düren
NucleoSpin Spin Kit	Macherey-Nagel, Düren
NFR	Roche, Mannheim
OneStep RT-PCR-Kit	Qiagen, Hilden
Pellet Paint	Novagen, Darmstadt
RiboFix Kit	Roche, Mannheim
Ready-to-use hot-start PCR master mix	Roche, Mannheim
RNase-free DNase set	Qiagen, Hilden
RNeasy mini kit	Qiagen, Hilden
SuperScript first-strand synthesis system for RT-PCR	Invitrogen, Darmstadt
TaqMan PCR Reagent Kit	Applied Biosystems, Darmstadt
Tri-Reagent	Sigma-Aldrich, Deisenhofen

3.5 Solutions

Commonly used solutions were prepared after Sambrook (Green and Sambrook, 2012) and are listed below. Depending on their usage, chemicals were dissolved in double distilled or 1% (v/v) DEPC treated water and autoclaved or sterile filtered. Application specific solutions are listed in the appropriate sections.

Phosphate buffered saline (PBS)

1 PBS tablet dissolved in 500 ml ddH_2O

Saline-sodium citrate buffer (SSC) 20x

3 M NaCl

0.3 M Sodiumcitrate

adjust to pH 7.0 mit NaOH

Tris-buffered saline (TBS) 10x

1.37 M NaCl

100 mM Tris-HCl, pH 7.6

add ddH_2O to 1000 ml

Tris-EDTA buffer

10 mM Tris-HCl, pH 8.0

1 mM EDTA

dissolved in ddH_2O

3.6 Media, antibiotics and agar plates

3.6.1 Media for bacteria

LB (Luria-Bertani)-Medium

1% (w/v) Trypton

0,5% (w/v) Yeast extract

1 % (w/v) NaCl

adjust to pH 7.0

Media for cultivation of bacteria were dissolved in ddH_2O, autoclaved and stored at 4°C. According to the required resistance, ampicillin (final concentration: 100 µg/ml) or kanamycin (final concentration: 50 µg/ml) was added.

3.6.2 Agar plates

LB- medium was supplemented with 1.5 % (w/v) agar prior to autoclaving. After autoclaving, solution was cooled to 55°C, supplemented with ampicillin (final concentration: 50 µg/ml) and poured into petri dishes. After solidification, agar plates were stored at 4°C.

3.6.3 Media for eukaryotic cell culture

The culture media composition with all additives are listed below. FCS was inactivated at 56°C for 30 min. Media additives sterility was assured by manufactorers or achieved by sterile filtration if possible. Genectin (G418) or Zeocin was added to the media for selection of transgenic cell lines.

Medium for HEK293 cells

500 ml Dulbecco's Modified Eagle's Medium (DMEM, 4.5 g/l glucose and L-glutamine)

10 % (v/v) fetal calf serum (FCS)

Medium for 108CC05 and 108CC15 cells

900 ml DMEM (4.5g Glucose/l)

10% (v/v) FCS

10 ml 10 mM hypoxanthine in approx. 0.1 mM NaOH

2 ml 0.5 mM aminopterin in ddH_20

1 ml 16 mM thymidine in ddH_20

Medium for Oli-Neu cells

96 ml DMEM (4.5g Glucose/L)

1 ml Insulin- Transferin- Selenium- A 100x

1 ml Horse Serum

1 ml 10 mM Putrecine in ddH_20

100 µl 500 µM Tri-iodo-Thyrodine (TiT)

50 µl Gentamycin Solution

13 µl 4mM L-Thyroxin

10 µl 2mM Progersteron in Ethanol

3.7 Sterilisation of consumable supplies, solutions and media

Consumable supplies, solutions and media for cultures were autoclaved overnight at 121°C and 1.5 bar or sterilized at 220°C overnight. Solutions sensitive to heat were sterile filtered. Aqueous solutions for RNA preparation or analysis were treated with 1% (v/v) DEPC, incubated for 12 – 24 h at RT und autoclaved.

3.8 Biological material

3.8.1 Bacterial strains

For cloning procedures and plasmid preparation the chemo-competent *Escherichia coli* DH5α (Hanahan, 1983) (Invitrogen, Darmstadt) with the following genotype was used:

***E. Coli* strain**	**Genotype**
DH5α	80*lac*ZΔM15, *rec*A1, *end*A1, *gyr*A96, *thi*-1, *hsd*R17 (rK-,mK+), *sup*E44, *rel*A1, *deo*R, Δ(*lac*ZYA-*arg*F)U169
BL21	*E.coli* B, F-, *dcm*, *omp*T, *hsd*S(rB- mB-), galλ (DE3)

3.9.2 Eukaryotic cell lines

If not stated otherwise, cell lines were obtained from ATCC and LGC (LGC Standards GmbH, Wesel) and listed below:

Name	**Description**
HEK293	Human embryonic kidney cells. Established from a human primary embryonal kidney transformed by adenovirus type 5; from ATCC.
Neuro-2a (N2a)	Established from a neuroblastoma of a strain A albino mouse; gift from Sebastian Schmidt (Max Planck Institute of Experimental Medicine, Goettingen).
Oli-neu	Established from mouse oligodendrocyte precursor cells transformed by retroviral transfection with neu tyrosine kinase; gift from Dr. Celia Kassmann (Max Planck Institute of Experimental Medicine, Goettingen).
108CC05 & 108CC15	Fused neuroblastoma cells (N18TG2) with gliomacells (C6-BU-1); gift from Prof. Hamprecht (University of Tübingen, Tübingen).

3.8.3 Animals

Strain C57BL6/N, animal house of the Max Planck Institute of Experimental Medicine, Goettingen.

K_v10.1 deficient mice, strain C57BL6/N: K_v10.1 deficient mice were generated by homologous recombination in embryonic stem (ES) cells to disrupt part of the K_v10.1 gene. The "3 Lox P strategy" was used to generate total and conditional knockout mice. In order to produce non-functional K_v10.1 proteins, Exon 7, which encodes the voltage sensors and pore regions of K_v10.1 protein, was deleted. This work was done previous in our department. Mice were described in Ufartes et al. (2013).

K_v10.2 deficient mice, strain C57BL6/N: K_v10.2 deficient mice were generated by homologous recombination in embryonic stem (ES) cells to disrupt part of the K_v10.2 gene. The "3 Lox P strategy" was used to generate total and conditional knockout mice. In order to produce non-functional K_v10.2 proteins, exon 7, which encodes the voltage sensors and pore regions of K_v10.2 protein, was deleted. This work was done previous in our department.

TYFF (Thy1-EYFP, yellow neurons), strain FVB/N, mice were described in Hirrlinger et al. (Hirrlinger et al., 2005).

GFEA (GFAP-EGFP, green Bergmann glia/astrocytes), strain FVB/N, mice were described in Nolte et al. (Nolte et al., 2001).

CXCR1 (CX3CR1-EGFP, green microglia), strain C57BL6/N mice were described in Jung et al. (Jung et al., 2000).

EMX1-Cre mice, strain C57BL6/N were gifted from the Cortical Development Group (Max Planck Institute of Experimental Medicine) and were described in Gorski et al. (Gorski et al., 2002).

Wistar rats, animal house of the Max Planck Institute of Experimental Medicine, Goettingen.

Mice were housed in a 12 h light-dark cycle facility with free access to food and water.

3.9 Synthetic oligonucleotides

3.9.1 Synthetic oligonucleotides for In Situ hybridization

Oligonucleotides were obtained from Metabion (Martinsried, Germany), underlined sequences are the T7 RNA polymerase promoter for *In vitro* transcription.

Oligonucleotide name	**Sequence 5' – 3'**
Kcnh5 exon 7 ISH forward	GCT CTAC CAG TTG GCC TTG A
Kcnh5 exon 7 ISH reversed	TAC AAT ACG AGT GCA GGG ATC TG
Kcnh1 exon 7 ISH forward	GCT CTA CCA ACT GGC ATT GG
Kcnh1 exon 7 ISH reversed	GGG TCT GGT TCA GGG AAG TG
Kcnh5 exon 7 T7 ISH forward	<u>TAA TAC GAC TCA CTA TAG GG</u>G CTC TAC CAG TTG GCC TTG A
Kcnh5 exon 7 T7 ISH reversed	<u>TAA TAC GAC TCA CTA TAG GG</u>C AGA TCC CTG CAC TCG TAT TGT A
Kcnh1 Exon7 T7 ISH forward	<u>TAA TAC GAC TCA CTA TAG GG</u>G CTC TAC CAA CTG GCA TTG G
Kcnh1 exon 7 T7 ISH reversed	<u>TAA TAC GAC TCA CTA TAG GG</u>C ACT TCC CTG AAC CAG ACC C
Kcnh1 exon 7 forward	GCATCAGCAGCCTGTTCAGT
Kcnh1 exon 7 reversed	ATCTTCGCAGTGGCCATCAT
Kcnh5 exon 7 forward	GGAATCAGCAGTCTCTTCAGC
Kcnh5 exon 7 reversed	AGATGTTCTCAGTGGCCATGA
Calbindin forward	ATC AGG ATG GCA ACG GAT AC
Calbindin reversed	TGG CCT AAG CAT GGT CTT TC

Kcnh5 exon 6-8 forward	CAGCTGGGATCAGACATCCT
Kcnh5 exon 6-8 reversed	TAACGGTTGGTGTTGGCATA
HPRT forward	GAC CGG TCC CGT CAT GCC GA
HPRT reversed	GGC ATA ATG ATT AGG TAT AC

3.9.2 Synthetic oligonucleotides for genotyping of mouse strains

Kcnh1 (K_v10.1) total knockout mice

Oligonucleotide name	**Sequence 5' – 3'**
5'F forward	TGC GTA CAT GGT GCT TGA TTT C
NeoR reversed	CGC GAA GGG GCC ACC AAA G
ExF forward	CAT GAT GAT TGG CTG TGA GTA TG
3'R reversed	CCC TCT TTC CAC TAA CAG CAT C

Kcnh5 (K_v10.2) conditional and total knockout mice

Oligonucleotide name	**Sequence 5' – 3'**
E2-KO-geno-BamH forward	ACAGGGTCCCCTACCAGAGA
E2-KO-geno-Ex forward	CACCATGACGAGCCTTACAAC
E2-Null reversed	TCCCCACACACAGTTTTTCA
E2-LoxP1 forward	GGAATTGCTCCTCTTCAAACAC
E2-LoxP1 reversed	TCAGGAGACAACTCAGCCTACA

Cre-recombinase mice

Oligonucleotide name	**Sequence 5’ – 3’**
Cre forward	TCG ATG CAA CGA GTG ATG AG
Cre reversed	TTC GGC TAT ACG TAA CAG

TYFF mice

Oligonucleotide name	**Sequence 5’ – 3’**
TYFF forward	CGC TGA ACT TGT GGC CGT TTA CG
TYFF reversed	TCT GAG TGG CAA AGG ACC TTA GG

GFEA mice

Oligonucleotide name	**Sequence 5’ – 3’**
GFEA forward	CAGGTTGGAGAGGAGACGCATCA
GFEA reversed	CCAGCTTGTGCCCCAGGATGT

Wildtype control for TYFF and GFEA mice

Oligonucleotide name	**Sequence 5’ – 3’**
Wildtype control forward	GAGGCACTTGGCTAGGCTCTGAGGA
Wildtype control reversed	GAGGAGATCCTGACCGATCAGTTGG

CXCR mice

Oligonucleotide name	Sequence 5’ – 3’
CXCR forward	TCAGTGTTTTCTCCCGCTTGC
CXCR wt reversed	CAGTGATGCTCTTGGGCTTCC
CXCR ki reversed	GTAGTGGTTGTCGGGCAGCAG

3.9.3 Synthetic oligonucleotides for quantitative real-time PCR

UPL synthetic oligonucleotides obtained from Roche Diagnostics and Taqman synthetic oligonucleotides obtained from Sigma-Aldrich for samples analysis by Lightcycler 480.

Oligonucleotide name	Sequence 5’ – 3’
hKcnh1 forward	TCT GTC CTG TTT GCC ATA TGA TGT
hKcnh1 reversed	CGG AGC AGC CGG ACA A
hKcnh1 Taq	(6-FAM) AAC GTG GAT GAG GGC ATC AGC AGC CT (6-Tamra)
hKcnh5 forward	CCC TCT GCT TTG TGG TGT CAG
hKcnh5 reversed	CGG ACG TTC GCA CAT GC
hKcnh5 Taq	(6-FAM) CCC TTC CCT AAA ATA GCC ACC ACC TCA (6-Tamra)
hTfR forward	GAC TTT GGA TCG GTT GGT GC
hTfR reversed	CCA AGA ACC GCT TTA TCC AGA T
hTfR Taq	(JOE) TGA ATG GCT AGA GGG ATA CCT TTC GTC CC (6-Tamra)
mKcnh5 forward	TTG TCT CAA CAT GGT CAA TGT CA
mKcnh5 reversed	CGG TTC AGA TGA ACA CAG ATG TC

mKcnh5 TaqMan probe # 3158	(6-FAM) AGA TGG AGA GGA CCT TCT CTG TGT CG (6-Tamra)
mKcnh1 forward	TCT GTC CTG TTT GCC GTA TGA CG
mKcnh1 reversed	GAG ACG GAG CAG CCG CAC
TaqMan Probe	(6-FAM) AAC AGG CTG CTG ATG CCC TCA TCC AC (6-Tamra)

3.10 Antibodies

Description	**Supplier**
Mouse anti-tetra-His antibody, IgG	Qiagen, Hilden
Rabbit anti-goat IgG, HRP-labeled: 172-1034	Bio-Rad Laboratories, Munich
Anti-digoxigenin fab fragment, AP-labeled	Roche, Mannheim
αBungerotoxin, biotin-labeled	Invitrogen, Darmstadt
Rabbit anti-K_v10.2: APC-053	Alomone Labs, Jerusalem, Israel
Donkey anti-rabbit IgG, HRP-labeled: NA934	GE Healthcare, Munich
Mouse anti-Tubulin IgG: T 6074	Sigma, Seelze
Goat anti-rat IgG, HRP labeled: AP136P	Merck, Millipore, Schwalbach
Rabbit anti-K_v10.2 (C-20) IgG: sc-69290	Santa Cruz Biotechnology, Heidelberg
Rabbit anti-K_v10.2 N-terminal IgG: ab32975	Abcam, Cambridge, UK
Rabbit anti-K_v10.2 C-terminal IgG: ab86216	Abcam, Cambridge, UK
Rabbit anti-K_v10.2 IgG: HPA030487	Sigma, Seelze
Rabbit anti-adenylyl cyclase III (C-20) IgG: sc-588	Santa Cruz Biotechnology, Seelze
Goat anti-actin IgG, (C-11): sc-1615	Santa Cruz Biotechnology, Seelze
Mouse anti-acetylated tubulin IgG2b: 6-11B-1	Sigma, Seelze
Goat anti-rabbit IgG, Alexa-633 labeled (A-21071)	Invitrogen, Darmstadt
Rabbit anti-K_v10.2 IgG	Aldevron/own work

3.11 Plasmids and constructs

Plasmid	Supplier
pET16b	Novagen, Darmstadt
pTracer	Invitrogen, Karlsruhe
pCDNA3.1	Invitrogen, Karlsruhe

Construct

K_v10.1-BBS in pTracer

A minimal bungarotoxin binding site (BBS) was inserted at the extracellular loop between transmembrane segments 3 and 4 of full length human K_v10.1 (Figure 6). This location was chosen because there exists a natural splice variant with additional 27 amino acid residues at this location that shows no functional differences with the major form; detailed characterization of this construct did not detect functional differences with the wild type channel. This construct was made and described by Kohl et al. (Kohl et al., 2011).

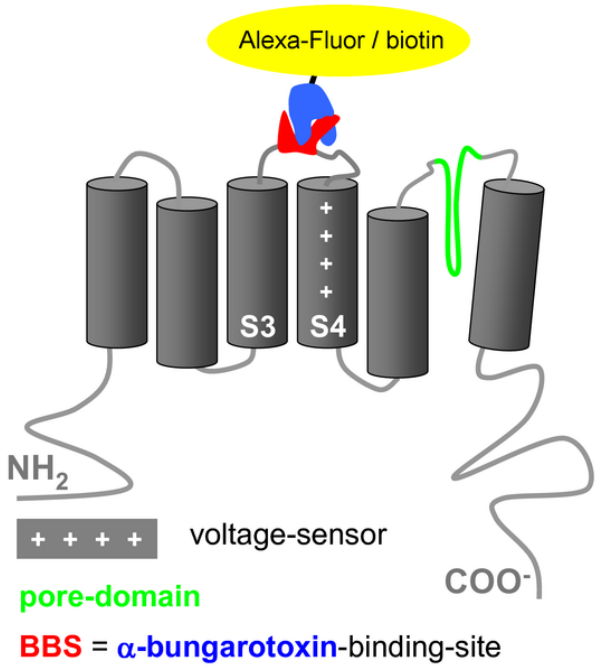

Figure 6: schematic representation of BBS insertion in human K_v10.1
Schematic representation of BBS (red) insertion in human K_v10.1 in the extracellular domain between the 3rd and 4th transmembrane domain. Figure from Kohl et al. (Kohl et al., 2011).

K_v10.2-BBS in pcDNA3

A minimal bungarotoxin binding site (BBS) was inserted at the extracellular loop between transmembrane segments 3 and 4 of full length human K_v10.2. This was previous work of the department.

3.12 Proteins

H1X:

MSDKIIHLTDDSFDTDVLKADGAILVDFWAEWCGPCKMIAPILDEIADEYQGKLTVAKLNIDQNPGTAPKYG
IRGIPTLLLFKNGEVAATKVGALSKGQLKEFLDANLAGSGSGHMHHHHHHSSGLVPRGSGMKETAAAKFER
QHMDSPDLGTDDDDKAMGDYEIFDEDTKTIPTTAGCPTSDGHWPPYQFNGSGSRKWEGGPSKNSVYISSL
DFTMTSLTSV

The peptide H1X consists of two amino acid chains, the sequence of the pore region and C-terminal part of K_v10.1, linked by a peptide linker containing a 6xHis-tag. This was previous work of the department.

C-terminus of hK_v10.2:

HHHHHHHHHHSSGHIEGRHMLELRQKNEVTLSIPVDHPVRKLFQKFKQQKELRNQGSTQGDPERNQLQV
ESRSLQNGTSITGTSVVTVSQITPIQTSLAYVKTSESLKQNNRDAMELKPNGGADQKCLKVNSPIRMKNGNG
KGWLRLKNNMGAHEEKKEDWNNVTKAESMGLLSEDPKSSDSENSVTKNPLRKTDSCDSGITKSDLRLDKA
GEARSPLEHSPIQADAKHPFYPIPEQALQTTLQEVKHELKEDIQLLSCRMTALEKQVAEILKILSEKSVPQASSP
KSQMPLQVPPQIPCQDIFSVSRPESPESDKDEIHF.

The peptide hK_v10.2 consists of the C-terminal cytoplasmatic domain of the human K_v10.2 sequence with a C-terminal 10xHis-tag linked by a peptide linker.

UBC-H5

MALKRIQKELSDLQRDPPAHCSAGPVGDDLFHWQATIMGPPDSAYQGGVFFLTVHFPTDYPFKPPKIAFTT
KIYHPNINSNGSICLDILRSQWSPALTVSKVLLSICSLLCDPNPDDPLVPDIAQIYKSDKEKYNRHAREWTQKY
AMSSGHIEGRHMLEHHHHHH.

The peptide UBC-H5 consists of a sequence of the human ubiquitin-conjugating enzyme E2D 1, with a C-terminal 6xHis-tag linked by a peptide linker. This peptide was gifted by Dr. Hiroshi

Kawabe (Department of Molecular Neurobiology, Max Planck Institute of Experimental Medicine).

3.13 Isolation of nucleic acids

3.13.1 Plasmid mini preparation

For plasmid mini preparations the MACHEREY-NAGEL NucleoSpin Plasmid Kit was used. One *E.coli* colony was picked and inoculated in 5 ml LB medium containing the appropriate antibiotic. Incubation was performed for 10-16 h at 37°C with 225 rpms agitation. Cultures were harvested by centrifugation for 5 min at 5000xg and the pellet was treated according to manufacturer's instructions. DNA was eluted with 50 µl of ddH_2O.

P1 buffer (minipreparation of plasmid DNA)

50 mM Tris- HCl pH 8.0

10 mM EDTA

100 µg/ml RNase A

P2 buffer (minipreparation of plasmid DNA)

200 mM NaOH,

1% (w/v) SDS

P3 buffer (minipreparation of plasmid DNA)

3 M potassiumacetat pH 5.5

10x PBS 1.37 M NaCl

81 mM Na_2HPO_4

27 mM KCl

14.7 mM KH_2PO_4

3.13.2 Plasmid endotoxin free Maxi preperation

For transfection of HEK293 cells endotoxin free DNA was prepared with EndoFree Plasmid Maxi Kit according to manufacturer's instructions (Qiagen, Hilden). For this purpose 5 ml LB-medium containing the appropriate antibiotic was inoculated with a single colony of transformed BL21 bacterial strain and incubated overnight at 37°C with 225rpms agitaion. The preculture was inoculated in 100 ml LB- medium containing the appropriate antibiotic and incubated overnight as described previously.

3.13.3 DNA isolation from mouse tails

To isolate genomic DNA from mouse tails, tail samples were incubated at 56°C with 1000 rpms on a heating block between 2 h and overnight in lysis buffer II followed by isopropanol precipitation. The DNA was precipitated by centrifugation, washed with 70% ethanol and resuspended with 80-100 µl of ddH_2O.

Lysis buffer II (mouse tail)

100 mM Tris pH 8.5

5 mM EDTA pH 8.0

200 mM NaCl

0.2% (w/v) SDS

0.1 mg/ml proteinase K

dissolved in ddH_20

3.13.4 Ethanol precipitation of DNA

Prior to *in vitro* transcription, template DNA was ethanol precipitated in order purify DNA. Ethanol precipitation was performed with the Novagen Pellet Paint co-precipitant according to manufacturers manual. Briefly, 2 µl Pellet Paint and 0.1% (v/v) 3 M natrium acetate were added to the sample and vortexed. 2 volumes of ethanol was added and incubated for 2 min. The sample was centrifuged at 16,000 x g for 5 min. Precipitated DNA together with the Pellet Paint formed a pink pellet. The supernatant was discarded, the pellet rinsed twice with 700 µl 70% ethanol diluted in DEPC-water and centrifuged. After a final wash step with 100% ethanol

the supernatant was removed. Residual ethanol was removed by air drying. Pellet was resuspended in 30 µl DEPC-water until the pellet paint was in solution. Afterwards the concentration was determined.

3.13.5 Purification of RNA from cells

RNA from cells was extracted via the QiaShredder columns prior to the Qiagen RNeasy mini kit. Cells (2-3 x 10^6) were disrupted in 600 µl RLT Buffer supplemented with 1% (v/v) ß-mercaptoethanol and filtered through QiaShredder columns by centrifuging for 2 min at 14000xg. Ethanol was added to the lysates, vortexed, loaded on a Qiagen RNeasy mini column and manufacturer's instructions were followed. To eliminate genomic DNA, DNAse treatment was performed according to manufacturer's instructions. RNA was eluted in 30 µl RNase-free DEPC treated ddH_2O.

3.13.6 Purification of RNA from tissue

RNA from tissue was extracted via phenol-chloroform extraction followed by the use of Qiagen RNeasy mini kit. Tissue (< 100 mg) was homogenized in 1 ml QIA-zol lysis reagent with a tissue lyzer. 200 µl chloroform was supplemented to the samples, vortexed and incubated for 5 min at room temperature (RT). Samples were centrifuged for 15 min at 12000xg at 4°C. The aqueous phase was transferred to a new cup, 600 µl 70% ethanol was added and vortexed. The suspension was transferred to a RNeasy mini spin column and treated according to manufacturer's instructions. DNAse treatment and elution of RNA was performed as described above.

3.13.7 Concentration determination of DNA and RNA

DNA concentration as well as DNA purity was measured spectrometrically by NanoDrop at 260nm. The quotient of extinction at 260nm and 280nm determines purity and should have a value between 1.8 and 2.

For Pellet Paint precipitated samples, the manufacturer's protocol (Novagen) was followed.

3.14 Agarose gel electrophoresis

Agarose gel electrophoresis was used to separate DNA or RNA fragments obtained by PCR or *In Vitro* transcription. 1x Turbo buffer cotaining 1 – 4 % (w/v) agarose was heated in a microwave until the agarose was completely dissolved. After cooling to 60°C, Ethidium bromide (5 µl/100 ml) was added and poured in a horizontal gel chamber. After solidification of the gel it was placed in an electrophoresis chamber filled with 1x Turbo buffer. The PCR product was mixed with Stop-Mix I, applied on the gel and run at 200 Volt for 20 to 45 min. Ethidium bromide labeled DNA was visualized by UV light.

20x Turbo-Puffer

0.2 M NaOH

Adjust to pH 8.0 with Boric acid

in ddH_2O

Stop-Mix I

15% Ficoll 400

200 mM EDTA

0.1% (w/v) Orange G

Dissolved in ddH_2O and DEPC treated

3.15 Transformation of bacteria

Chemically competent bacteria are able to uptake plasmids after a heat shock at 42°C. Competent bacteria was thawed on ice and incubated with up to 100 ng plasmid DNA or 10 µl ligation reaction. Cells were incubated on ice for 30 min and permeabilized with a heat shock at 42°C for 45 sec followed by 2 min incubation on ice. 500 µl LB-medium was added and incubated for 45 min at 37°C with gentle agitation. Transformed bacteria were plated on LB-agar plates containing the appropriate antibiotics and grown overnight at 37°C.

3.16 Polymerase chain reaction (PCR)

3.16.1 PCR from genomic DNA or plasmid

The polymerase chain reaction (PCR) is a molecular technique to specifically amplify DNA fragments with specific oligonucleotides (primer). A PCR reaction consists of denaturation, annealing and elongation steps. These steps are repeated for 20-40 cycles. For a PCR reaction the following compounds are required: template DNA, specific primers, desoxynucleoside triphosphates (dNTPs), divalent ions ($MgCl_2$), and a heat-stable DNA polymerase. PCRs were performed in 25 µl - 50 µl reactions in the following composition:

10-100 ng cDNA

2.5 - 5 µl 10xPCR buffer with $MgCl_2$ to a final concentration of 1x

10 pmol forward primer

10 pmol reverse primer

1 µl nucleotide mix (200 µM of each dNTP)

1 unit DNA polymerase/25 µl reaction

add ddH_2O to a final volume of 25 µl or 50 µl

Initial denaturation was achieved by incubating 5 min at 98°C followed by 30-40 cycles. PCR reaction had the following steps:

Temperature	**Time**	**Cycles**
98°C	5 min	1
98°C	30 sec	30 – 40
50°C – 60°C	30 sec	30 – 40
68°C – 72°C	30 sec – 120 sec	30 – 40
68°C – 72°C	10 min	1

A last elongation step was performed for 10 min at 72°C and afterwards the sample was maintained a 4°C.

Genotyping of K_v10.1 and K_v10.2 deficient mice

For genotyping of K_v10.1 and K_v10.2 deficient mice a touchdown cycle was applied before the above mentioned PCR protocol:

5 × Touchdown cycle

Temperature	**Time**	**Cycles**
95°C	30 sec	5
64°C – 60°C	30 sec	5
(decreasing each cycle by 1°C)		
72°C	30 sec	5

Genotyping of Emx-Cre mice

Temperature	**Time**	**Cycles**
95°C	3 min	1
95°C	10 sec	30
55°C	30 sec	30
72°C	30 sec	30
72°C	5 min	1

Genotyping of TYFF, CXCR and GFEA mice

Temperature	**Time**	**Cycles**
94°C	3 min	1
94°C	30 sec	35
60°C	30 sec	35
72°C	1 min	35
72°C	10 min	1

Amplification of *In Situ* hybridization templates

For amplification of DNA template for In Situ hybridization probes, one primer, either forward or reversed, directly linked to the T7 promoter, in combination with a non-linked primer was used. Amplification was performed with the FastStart High Fidelity PCR System (Roche) in 50 µL reaction with the following composition:

100 ng cDNA

5 µl 10xFastStart High Fidelity reaction buffer with 18 mM $MgCl_2$

10 pmol forward primer

10 pmol reverse primer

1 µl nucleotide mix (200 µM of each dNTP)

2.5 units FastStart High Fidelity Enzyme Blend (5 U/µL)

add DEPC-treated ddH_2O to a final volume of 50 µl

Amplification of *In Situ* hybridization probes

Temperature	**Time**	**Cycles**
94°C	3 min	1
94°C	40 sec	50
62°C	30 sec	50
72°C	30 sec	50
72°C	5 min	1

3.16.2 Reverse transcriptase PCR

cDNA synthesis for reverse transcriptase-polymerase chain reaction (RT-PCR) was performed with the SuperScript first-strand synthesis system. For synthesis of cDNA 2.5 µg or 5 µg total RNA was used. For each reaction a negative sample was used, to validate qRT-PCR for genomic DNA contamination. Into each sample 0.5 µg oligo (dT) was added and DEPC-water to achieve a 12 µl volume. After each step the samples were mixed by vortexing and centrifuged. Samples were incubated at 70°C for 10 min and rapidly cooled on ice for 1 min. 7 µl reaction buffer was

added to the reaction mixture and incubated at 42°C for 5 min. Samples were supplemented with 1 µl reverse transcriptase enzyme (200 units), while to negative control samples 1 µl DEPC-water was added. Reaction mixtures were incubated for 50 min at 42°C. Subsequently reverse transcriptase enzyme was inactivated by heating the samples at 70°C for 15 min. To digest RNA in the samples, 2 units of RNAse H was added and incubated for 20 min at 37°C. Finally, reaction volume was adjusted with DEPC- water to a cDNA concentration of 0.1 µg/µl.

Reaction buffer

2 µl 10x reverse transcriptase buffer

2 µl $MgCl_2$ 25 mM

6 µl of dNTPs 10 mM

2 µl of dithiothreitol (DTT) 0.1 M

3.16.3 *In vitro* transcription

For *in vitro* transcription of digoxigenin labeled RNA In Situ hybridization (ISH) probes 100 ng template was used. The template was amplified as described in 3.16.1 and ethanol precipitated with Pellet Paint (Novagen) as described in 3.13.4. The reaction was set up with labeling mix I and incubated for 90 min at 37°C. To increase the reaction efficiency 10 µl labeling mix II was added and incubated for 60 min at 37°C. To remove cDNA from the reaction, 4 µl RDD buffer, 2 µl DNase and 4 µl DEPC-water was added and incubated for 8 min at 37°C. 10 µl stop buffer was added. The sample was loaded on a Microspin column and centrifuged for 1 min at 500xg. The elution was loaded on a second Microspin column and centrifuged for 2 min at 500xg. 2 µl of the elution was loaded on a 3.5% agarose gel and run at 200 Volt for 45 min. The reaction was adjusted to 100 µl with DEPC-ddH_20, 100 µl formamid was added, aliquoted and stored at -80°C.

Labeling mix I

2 µl 10x DIG RNA labeling mix

2 µl 10x transcription buffer

2 µl 100mM DTT

1 µl T7 RNA polymerase

X µl DNA template (100 ng)

add DEPC-ddH_20 to a final volume of 20 µl

Labeling mix II

1 µl 10x DIG RNA labeling mix

1 µl 10x transcription buffer

1 µl 100mM DTT

1 µl T7 RNA polymerase

6 µl DEPC-ddH_20

Stop buffer

1% (w/v) SDS

0.1 M Tris- HCl pH 8.0

10 mM EDTA pH 8.0

Dissolved in ddH_2O and DEPC treated

3.16.4 Quantitative real-time PCR

Quantitative real-time PCR (qRT-PCR) was performed utilizing the TaqMan system in the LightCycler 480 (Roche). Primers and probes were chosen from the Universal Probe Library (UPL) from Roche or designed with Primer3 software. TaqMan probes are labeled at the 5' end of the probe with the reporter dye 6-carboxyfluorescein (FAM) or 2,7,-dimethoxy-4,5-dichloro-6-carboxyfluorescein (JOE) and a Dark Quencher Dye (Tamra) at the 3' end of the probe. During PCR, exonuclease activity of the DNA polymerase cleaves the reporter and quencher dye of the probe. When separated, the reporter emits a fluorescence signal detected by the LightCycler 480.

For analyzing the mRNA expression of the desired target gene, qRT-PCR with housekeeping gene TaqMan primers and probes on the same template was used to control for RNA integrity and quantification.

Real-time PCR was performed with 100 ng cDNA, 200 nM forward and reverse primer, 100 nM TaqMan probe, 0.2 units Uracil-DNA-glycosylase, and a ready-to-use hot-start PCR mix containing Taq DNA polymerase, dNTP mix, as well as buffer and $MgCl_2$.

PCR conditions were:

Temperature	Time	Cycles
50°C	2 min	1
95°C	10 min	1
95°C	10 sec	45
60°C	30 sec	45
40°C	10 sec	45

Afterwards the sample was maintained at 4°C.

The relative mRNA expression was determined by the number of PCR cycles to reach the cycle threshold (Ct). The results were standardized to the amount of the housekeeping gene in the respective probe and to the amount of mRNA expression in the calibrator (mouse brain RNA or human brain RNA).

For this purpose the ΔΔCt-Method as described in Livak et al. (Livak and Schmittgen, 2001) was applied:

Normalized ratio: $2^{\Delta Ct1} / 2^{\Delta Ct2}$

$\Delta Ct1 = Ct\ target_{(calibrator)} - Ct\ target_{(sample)}$

$\Delta Ct2 = Ct\ housekeeping\ gene_{(calibrator)} - Ct\ housekeeping\ gene_{(sample)}$

3.17 DNA sequencing analysis

16 µl of DNA (100 ng/µl) diluted in ddH_2O was submitted to the sequence facility (AGCT Lab) of the Max Planck Institute of Experimental Medicine. The obtained sequencing data was analyzed using DNAStar (SeqManII) software package. Sequences were also verified on public domain databases such as ENSEMBL (http://www.ensembl.org) and BLAST at 'National Centre for Biotechnology Information' (NCBI). If not stated otherwise, standard primers of the sequencing facility were used.

Oligonucleotide name	Sequence 5’ – 3’
C-Terminus $hK_v10.2$ forward	TAATACGACTCACTATAGGG
C-Terminus $hK_v10.2$ reversed	GACCCGTTTAGAGGCCCCAAGG

3.18 RNA assays

3.18.1 Dot blot assay

PCR amplified target sequences of the digoxigenin labeled RNA antisense probes were diluted 1:1, 1:10, 1:100 and 1:1000. PCR amplifications of *Kcnh1* and *Kcnh5* target sequences, total brain cDNA and calbindin PCR product were dropped on a nylon membrane. Total brain cDNA served as a positive sample, while calbindin DNA served as a negative sample. Membranes were air dried, crosslinked in a UV-oven (stratalink) and rehydrated with TBS. Blocking of membranes was performed in 3% (w/v) BSA in TBST for 30 min. 3 µl Antisense probe was diluted in 100 µl 3% (w/v) BSA in TBST and denaturated at 70°C for 10 min. The membrane was hybridized with the digoxigenin labeled RNA antisense probes. Hybridization temperature was 51°C for the antisense probe targeted against *Kcnh1* and 55°C for the antisense probe targeted against *Kcnh5*. The incubation time was 30 min for both probes. Membrane was washed at 47°C in 2x SSC for 15 min, 0.1% SDS in 2x SSC for 15 min, 0.2x SSC for 15 min and in TBS. Membrane was blocked in 3% BSA in TBST for 30 min at RT. Anti-digoxigenin antibody in 0.1% Casein in TBST was incubated for 30 min at RT. Membrane was washed in TBS and AP-buffer at RT. Enzymatic reaction was performed in 20 ml substrate buffer (0.02% NBT/BCIP in AP-buffer). Rinsing of membrane with water stopped the reaction.

Alkaline phosphatase staining solution

100 µl NBT/BCIP

dissolved in 5 ml AP-Puffer

Alkaline phosphatase buffer (AP)

100 mM NaCl

50 mM $MgCl_2$

100 mM Tris- HCl pH 9.5

3.18.2 *In Situ* Hybridization

In Situ Hybridization was performed on a Ventana Discovery XT with the Research ISH Blue Map XT procedure according to manufacturer's instructions. The BlueMap Kit utilizes the nitro blue tetrazolium (NBT) and 5-Bromo-4-chloro-3-indolyl phosphate (BCIP) chemicals. In

combination with an alkaline phosphatase (AP) labeled antibody, the NBT serves as an oxidant and the BCIP as the AP substrate, resulting in a blue staining. Briefly, paraffin embedded mouse sections were deparaffinized and incubated for 12 min in Riboclear solution (Ribo Fix Kit). Tissue was conditioned in mild CC2 (Citrat Buffer pH 6) setting and for 4 min incubated with Protease 3 (0.02 units/ml alkaline protease) at 37°C. 2.5 µl antisense probe and 2.5 µl sense probe were each diluted in 100µl RiboHybe buffer and titrated on the slide. The slides were incubated at 70°C for 8 min for RNA denaturation. Hybridization was performed at 50°C for 6 h. Washing steps were performed with 0.1% SSC at 55°C. Post fixation was performed with RiboFix solution for 20 min. HRP-labeled anti-digoxegenin antibody diluted 1:500 in antibody diluent was titrated on the slide and incubated for 32 min. BlueMap detection solution was incubated for 6 h on the slide. Slide cleaning was performed.

For the *Kcnh5* probe, different condititions were applied in order to gain specificity of the ISH probe: Increased temperature of hybridization and washing steps to 57°C, shortened hybridization time (3 h) and titration of probe (0.5 µl, 1 µl, 1.5 µl and 2 µl).

3.19 Biochemistry

3.19.1 Protein extraction from cells

Cell lysates were derived from cells treated as described in 3.16. Cells were transferred to a reaction cup and washed twice with PBS, followed by centrifugation. Lysis was performed by adding 300 µl lysis buffer I and homogenized using an Insulin Needle. Lysat was incubated for 30 min at RT. Subsequently the sample was centrifuged for 15 min at 18,000xg at 4°C to remove cell debris. Supernatant containing the total cell proteins was stored at -80°C.

Lysis buffer I (cell and tissue protein)

25 mM Tris- HCl pH 7.4

150 mM NaCl

2.5 mM EDTA

0.5% Triton X-100

2.5 mM Na_2- Pyrophosphate

0.25 mM Na- Orthovanadate

0.25 mM PMSF

0.25 mM DTT

5 mM NaF

Protease inhibitor cocktail

3.19.2 Protein extraction from tissue

Extracted organs were supplemented with 100 µl – 1 ml lysis buffer I (see 3.20.1) and homogenized with the tissue lyser (Qiagen). Sample was centrifuged at 18,000xg at 4°C for 30 min to remove cell debris. Supernatant containing total protein extract was transferred to a new reaction cup and centrifuged again. Supernatant was removed and stored at -80°C.

3.19.3 BCA protein assay

To determine protein concentration the bicinchoninic acid (BCA) protein assay kit was used. To quantify protein concentration in the sample bovine serum-albumin (BSA) in different concentrations served as a standard curve. The samples along with the BSA standard were treated in triplicates and were incubated in a 96-well plate in a volume of 25 µl together with the BCA reagent. BCA reagent was composed by solution A (sodium carbonate, sodium bicarbonate, bicinchoninic acid and sodium tartrate in 0.1 M sodium hydroxide) and solution B (4 % cupric sulfate) in a ratio of 50:1. Following incubation for 30 min at 37°C the absorbance was measured in Victor Wallac plate reader at 550 nm.

3.19.4 SDS-PAGE

30 µg (cells) or 50 µg (tissues) of total protein extract per sample were diluted with Running Buffer and heated for 10 min at 70°C. Sample was loaded and separated on a gradient 3-8% TRIS-acetate SDS-PAGE (sodium dodecyl sulfate-polyacrylamide gel electrophoresis) NuPAGE Novex gel. SDS-gels were either used for Western blot analysis or stained with Comassie for protein detection and quantification.

Running buffer (10 µl)

2.5 µl 4x LDS

1 µl 10x Reducing agent

X µl protein extract

add ddH_20 to 10 µl

3.19.5 Western blot analysis

For Western blot (WB) analysis proteins were transferred from a SDS-gel to nitrocellulose hybridization membranes. Subsequently membranes were blocked for 1 h with 0.1% (w/v) casein diluted in TBST. Primary antibody was incubated overnight at 4°C diluted in 0.1% (w/v) casein TBST. Membrane was washed with 1000 ml deionized water for 7 times and incubated in TBST for 5min. Secondary antibody coupled to horseradish peroxidase (HRP) was incubated for 1 h followed by washing with 1000 ml deionized water for 7 times. To detect bound antibody chemiluminescent HRP substrate was used and signals visualized in a Chemi-Doc luminescence detection system using no illumination for chemilumiscence acquisition and epi-white light for acquisition of protein molecular weight standard. Afterwards membranes were stripped by incubation in stripping solution for 20 min at 37°C. To verify proper loading of samples and to control equal amounts of protein loaded in each sample, membranes were stained with an anti-α-tubulin antibody. The procedure is described above.

Aquired images were processed using Quantity One (Biorad) software to linear brightness and contrast adjusting. Images obtained from chemilumiscence and epi-white acquisition were superimposed. Protein standart was replaced with drawn bars to indicate the migration distance of the molecular weight standard. Furthermore, images of Western blots were cropped to the required molecular weight range.

50x Transferbuffer

0.5 M $NaHCO_3$

0.15 M Na_2CO_3

in ddH_2O

Transferbuffer

20 ml 50x Transferbuffer

20% (v/v) Methanol

0.01% (v/v) SDS

add ddH_2O to 1000 ml

TBST

10% (v/v) 10x TBS

0.05% (v/v) Tween-20

89.95% (v/v) ddH_2O

Blocking buffer (Western Blot)

TBST

0.1% (w/v) casein

Antibody	**Dilution**
Anti-α-tubulin	1:10000
Anti-actin	1:400
Anti-Eag2 (Aldevron/own work)	1:400
Anti-Eag2-Abcam-N-terminal	1:1000
Anti-Eag2-Abcam-C-Terminal	1:300
Anti-Eag2-Alomone-Biolabs	1:200
Anti-Eag2-Sigma-Aldrich	1:500
Anti-Eag2-St.Cruz-Biotechnology	1:200
Anti-Eag1-9391	1:1500

Anti-goat-HRP	1:8000
Anti-mouse-HRP	1:8000
Anti-rabbit-HRP	1:8000
Anti-tetra-His	1:800

3.19.6 Protein Staining with Coomassie

Besides visualization of proteins separated by SDS-PAGE by SybroRuby, Coomassie staining was used. SDS-gels were stained in 10 ml Coomassie staining solution for 5 min und washed overnight in ddH_2O to remove excess of Coomassie. Coomassie stained SDS-gels were documented by light in a Chemi-Doc luminescence detection system.

Coomassie staining solution

30% (v/v) Methanol

10% (v/v) acetic acid

0.05% (w/v) Coomassie Brilliant Blue R250

in DEPC ddH_20

3.19.7 Densitometrical calculation

Densitometrical calculation was performed with Quantitiy One software (BioRad) verifying for non-saturation. Values are expressed as the integrals (area * mean density) of each band and normalized to α-tubulin.

3.19.8 Purification of BBS-tagged K_v10.1 and K_v10.2

For purification of BBS-tagged K_v10.1 and K_v10.2 full-length proteins, 800µg protein lysate from HEK293 wildtype, HEK293 Kv10.1-BBS and HEK293 K_v10.2-BBS overexpressing cells was used. The volume of each sample was adjusted to 500 µl with protein lysis buffer III. 15 µl BTX-Biotin (11.5 µM) was added and sample was incubated on ice with occasional vortexing. 20 µl T1-dynabeads were washed in a reaction cup with PBS to remove any detergents. Dynabeads were recovered by magnetic separation on a magnetic rack. Protein lysates were added to the Dynabeads and rotated at 4°C for 60 min. The protein BTX-biotin complex was recovered by

magnetic separation. Supernatant was removed and pellet was washed with 500 µl lysis buffer for 10 minutes at 4°C rotating 3 times. Following magnatic separation, pellet was washed with 500 µl TBS at 4°C rotating. After magnetic separation, the beads were eluted in following buffers:

SDS-PAGE buffer

16.25 µl TBS

6.25 µl 4x Novex-LDS-buffer

2.5 µl 10x reducing agent

3.20 Generation of novel anti-K_v10.2 antibody

3.20.1 Heterologous protein expression

A colony of *E.coli* BL21 cells containing the plasmid K_v10.2-pET16b was picked and inoculated in 50 ml LB- Amp medium and incubated overnight on an orbital shaker at 37°C. 5 ml of overnight culture was inoculated in 6 x 2 liter flasks filled with 500 ml LB-Amp medium. Cultures were incubated at 37°C with 180rpms until the OD 600 of 0.6. Each flask was treated with IPTG to a final concentration of 0.7 mM. The cultures were incubated for 5 h at 37°C and 180rpms. Cells were harvested by centrifugation and resuspended in 7 ml resuspension buffer. Cells were lysed by sonification (80% power, 10% cycle) and centrifuged at 10.000xg for 30 min at 4°C. Soluble fraction was transferred to a new tube and pellet was resuspended in 50ml lysis buffer III. 5 ml Ni-NTA agarose was added and incubated overnight under constant agitation. After centrifugation for 10 min at 500xg at 4°C, beads were washed with wash buffer I. The same step was applied with wash buffer II. Bound protein was eluted from the Ni-NTA agarose with elution buffer or elution buffer urea under constant agitation at 4°C. The solution was transferred to a dialysis column (1 kDa MWCO) and dialyzed starting with either dialyses solution I till dialysis solution III or by dialysis solution Urea I till dialysis solution Urea IV by changing solutions every 12 h. After dialysis, the expressed C-terminus of K_v10.2 preparation was stored at 4°C.

Resuspension buffer

50 mM Tris- HCl

200 mM NaCl

pH 8

Lysis buffer III

6M Guanidiniumhydrochloride

20 mM $NaH_2PO_4*H_20$

500 mM NaCl

adjust to pH 7.8

Wash buffer I

8 M Urea

20 mM $NaH_2PO_4*H_20$

500 mM NaCl

in PBS

pH 7.8

Wash buffer II

8 M Urea

20 mM $NaH_2PO_4*H_20$

500 mM NaCl

in PBS

pH 6.9

Elution buffer

6 M Guanidiniumhydrochloride

20 mM $NaH_2PO_4*H_20$

500 mM NaCl

500 mM Imidazol

adjust to pH 4.0

Elution buffer urea

8 M Urea

20 mM $NaH_2PO_4*H_20$

500 mM NaCl

500 mM Imidazol

adjust to pH 6.8

Dialysis solution I

6 M Guanidiniumhydrochloride

50mM Tris- HCl pH 8.0

200mM NaCl

pH 8.0

Dialysis solution II

4 M Guanidiniumhydrochloride

50 mM Tris- HCl pH 8.0

200 mM NaCl

pH 8.0

Dialysis solution III

2 M Guanidiniumhydrochloride

50 mM Tris- HCl pH 8.0

200 mM NaCl

pH 8.0

Dialysis solution Urea I

8 M Urea

50mM Tris- HCl pH 8.0

200mM NaCl

pH 8.0

Dialysis solution Urea II

6 M Urea

50 mM Tris- HCl pH 8.0

200 mM NaCl

pH 8.0

Dialysis solution Urea III

4 M Urea

50 mM Tris- HCl pH 8.0

200 mM NaCl

pH 8.0

Dialysis solution Urea IV

2 M Urea

50 mM Tris- HCl pH 8.0

200 mM NaCl

pH 8.0

3.20.2 Generating of novel K_v10.2 antibody

The C-terminus of K_v10.2 expressed as described in 3.20.1 was sent to Aldevron (Freiburg, Germany) for vaccination of two rabbits and antibody generation. ELISA was performed by Aldevron to indicate antibody specificity. Antibody was delivered in PBS in a final concentration of 8.7 mg/ml.

The anti-K_v10.2 antibody was aliquoted and frozen at -80°C. Working dilutions were adjusted to 1 mg/ml with PBS and stored at 4°C.

3.20.3 Indirect ELISA

The enzyme-linked immunoabsorbant assay (ELISA) is a biochemical method used to detect an antigen in a sample. 96-well plate was coated with 500 ng protein in 100 µl TBS buffer and incubated at 4°C overnight. Unspecific binding sites were blocked with 3% (w/v) BSA in TBS for 1 h at RT. Antibody diluted in 3% (w/v) BSA in TBS was added and incubated for 2 h at RT.

Subsequently the well was washed 3 times and the appropriate HRP conjugated secondary antibody was added and incubated for 1 h at RT. Well plates were washed 3 times with TBS and 100 µl ABTS substrate was added. The developed reaction was measured in the Victor Wallac plate reader at 405 nm and 490 nm.

3.21 Cell culture methods

3.21.1 Cell culture of commercial cell lines

HEK293 cells were cultivated under standard cell culture conditions at 37°C in a humidified atmosphere with 5% CO_2 in an incubator.

108CC05 and 108CC15 cells were propagated as described in Hamprecht et al. (Hamprecht et al., 1985). Cells were cultivated at 37°C in a humidified atmosphere with 10% CO_2 in an incubator.

Oli-Neu cells were propagated as described in Jung et al. (Jung et al., 1995). Cells were cultivated at 37°C in a humidified atmosphere with 10% CO_2 in an incubator.

3.21.2 Sub-cultivation of cell lines

For sub-cultivation of eukaryotic cells medium was removed and cells washed twice with Dulbecco's Phosphate Buffered Saline (DPBS). 0.05% trypsine- ethylene-diamine-tetraacetic acid (EDTA) solution was added to the cells and incubated for 5 min at 37°C. 10% FCS containing medium was added to stop the enzymatic reaction. Cells were resuspended, if necessary counted in a Neubauer chamber and plated in desired cell numbers.

3.21.3 Cryoconservation

To cryoconserve eukaryotic cells were detached as described. 1-5 x 10^6 cells per ml were resuspended in cryoconservation medium and transferred to storage vials. Vials were frozen in an insulated box at -80°C overnight and stored in liquid nitrogen.

Cryoconservation medium

90% FCS

10% (v/v) dimethyl sulfoxide (DMSO)

3.21.4 Revitalization

Cryconserved cells were removed from liquid nitrogen and were thawed quickly at 37°C in a water bath. Pre-warmed supplemented medium was added and suspension was centrifuged for 2 min at 300xg. Supernatant was discarded and the pellet resuspended in the appropriate medium. Cells were transferred to a new cell culture flask and medium changed after 24 h. The revitalization procedure was performed as quickly as possible to reduce toxic side effects of DSMO.

3.21.5 Stable transfection of HEK293 cells transfection

HEK293 cells were transfected with pTracer-K_v10.1-BBS as described in Kohl et al. (Kohl et al., 2011). The same protocol was applied for transfection with pcDNA3-K_v10.2-BBS. Cells were transfected by Lipofectamine 2000 according to the manufacturer's description. Briefly, cells were seeded in a 6 well plate. After incubation of 6 µg DNA with Lipofectamine 2000 400 µl transfection solution was added to the cells, incubated for 18 h and replaced with fresh medium. To produce stable cell lines Zeocin (300 µg/ml) or G418 (500 µg/ml) was added after 48 h to the culture medium for selection. The minimal working concentration was estimated in kill curve assays.

3.21.6 Preparation of glass coverslips and PLL- coating

Glass coverslips were washed with subsequently with acetone, ethanol and 70% ethanol and sterilized in an oven for 4 h at 200°C.

Sterilized glass coverslips were placed in the appropriate well-plates and coated with 0.01% PLL overnight. Before use coverslips were washed with PBS.

T75 cell culture flasks were coated with 10 ml PLL solution (0.01% PLL in PBS).

3.22 Histological procedures

3.22.1 Fixation of cells

For immunocytochemistry cells grown on cover slides were washed twice with ice cold PBS and fixed in 4% (v/v) PFA in PBS for 20 min at RT. Fixed cells were washed twice with PBS and cover slides were glued on a Superfrost Plus slide for staining.

3.22.2 Fixation of organs

For dissection of organs mice were anesthetized using ketamine (75 mg/kg) and xylazine (15 mg/kg) and were consequently transcardially perfused with:

Paraformaldehyd fixation: PBS followed immediately by 4% (v/v) paraformaldehyd and processed as described.

Paraformaldehyd- acrolein fixation: 2% (w/v) sodium nitrate in PBS followed by acrolein solution and processed as described.

Acrolein solution

4% paraformaldehyde pH 6.8

2.5% acrolein

In 0.1 M PBS

3.22.3 Generation of paraffin sections from tissue

Paraformaldehyde fixed tissue was placed in Tissue Tek cassettes, rinsed with water for 30 min and dehydrated in a graded ethanol series and paraffinized in the apparatus for tissue processing as follows:

Applied substance	time	cycles
75% ethanol	1 h	three
96% ethanol	1 h 30 min	two
100% ethanol	1 h 15 min	three

xylol	2 h	two
paraffin	1 h	two

Acrolein fixed mouse brains were placed in Tissue Tek cassettes and dehydrated in a graded ethanol series and paraffin embedded as follows:

Applied substance	**time**	**cycles**
50% ethanol	1 h	one
70% ethanol	2 h	twice
96% ethanol	1 h	twice
100% ethanol	1 h	twice
isopropanol	1 h	once
xylol	2 h	twice
paraffin	2 h	twice

Paraffin embedded tissue was cut on a microtome in 5 µm sections, transferred on a Super Frost Plus slide and baked for 2 h at 60°C in an incubator.

3.22.4 Generation of vibratome sections from tissue

Paraformaldehyd fixed mouse brains were mounted in 5 % (w/v) agarose and cut into 25 µm sections on a vibratome. Sections were stored in PBS containing 0.04 % (w/v) NaN_3 until processing.

Vibratome cut mouse brain sections were mounted on a Superfrost Plus slide and air- dried until adherence.

3.23 Immunological protein detection

3.23.1 Immunocytochemistry

Immunocytochemistry with cells fixed as described 3.22.1 on Superfrost Plus slides was performed in the Ventana Discovery XT staining robot. DAB Map XT procedure, which utilizes 3,3'-Diaminobenzidine (DAB) as substrate in combination with a HRP-coupled antibody, was used. The HRP oxidizes DAB resulting in a brown staining.

The samples were covered with Reaction buffer and incubated with avidin and biotin (A/B block) for 4 min each to block endogenous biotin. The K_v10.2 antibody was diluted 1:100 in antibody diluent and 100 µl titrated on the slide. Incubation was performed at 37°C for 60 min. After washing steps, the biotinylated secondary antibody was dissolved 1:500 in antibody diluent and incubated on the tissue at 37°C for 32 min. Following washing steps the DAB substrate was dispensed on the slide and incubated for 8 min. Finally, slide cleaning was performed.

Antibody	**Dilution**
Anti-K_v10.2 (Aldevron/ own work)	1:100
Anti-rabbit-HRP	1:500

3.23.2 Immunohistochemistry on paraffin tissue sections

Immunohistochemistry on sectioned paraffin embedded tissue was performed with the Research IHC BlueMap XT procedure in the Ventana Discovery XT staining robot. The BlueMap procedure utilizes nitro blue tetrazolium (NBT) and 5-bromo-4-chloro-3-indolyl phosphate (BCIP) together with alkaline phosphatase resulting in a blue staining. Tissue was conditioned in CC1 buffer (EDTA Buffer pH 9) with mild settings and A/B block was applied for 4 min each. The anti-Kv10.2 antibody was incubated as described above. After washing steps, the biotinylated secondary antibody was dissolved 1:500 in antibody diluent and incubated on the tissue at 37°C for 28 min. Following washing steps the BlueMap substrate was dispensed on the slide and incubated for 48 min. Finally slide cleaning was performed.

Antibody	Dilution
Anti-K_v10.2 (Aldevron/ own work)	1:100
Anti-adenylyl cyclase III	1:200
anti-acetylated tubulin	1:2000
Anti-mouse-Biotin	1:400
Anti-rabbit-Biotin	1:400

3.23.3 Immunohistochemistry on vibratome tissue sections

Vibratom cut sections were washed with Buffer A for 5 minutes three times and incubated with the primary antibody in Buffer A overnight at 4 °C with constant agitation. Afterwards sections were washed for 5 minutes three times with Buffer A. Subsequentally the secondary antibody was applied in Buffer A for 2 h at RT. Sections were washed with PBS containing 0.15% (v/v) Triton-X100 for 5 min three times. The stained sections were placed on Super frost plus glass slides by using Montage solution, left to dry and cover-slipped in Prolong antifade with DAPI for microscopic observations.

Buffer A

2% (w/v) BSA

1% (v/v) goat serum

0.15% (v/v) Triton X-100

dissolved in PBS

Montage solution

0.2 % gelatin

0.15 % Triton X-100

dissolved in PBS

(heat 100 ml with gelatin in microwave, then fill up with 392.5 ml PBS and add 7.5 ml 10 % Triton X-100)

Antibody	Dilution
Anti-K_v10.2 (Aldevron/own work)	1:100
Goat anti-rabbit Alexa-633 conjugated	1:400

3.23.3 Embedding of samples

Microscope slides stained as described in 3.22.5 were subsequently dehydrated in a graded ethanol series. Following settings were used:

Applied substance	time
50% ethanol	5 min
70% ethanol	5 min
90% ethanol	5 min
96% ethanol	5 min
100% ethanol	5 min
xylol	10 min
xylol	10 min

Finally, cover glass was mounted on microscope slides with Permount mounting solution.

3.24 Image acquisition and processing

Images of fluorescently stained samples were acquired with a Leica SP5 (Leica, Mannheim) confocal laser scanning microscope (CLSM) equipped with hybrid detectors that were used in "photon-counting mode" in order to acquire low-noise fluorescence from representative fields-of-view with a 40x (1.25NA) oil immersion objective. Depending on sample labeling, eGFP, eYFP and Alexa Fluor (c)-633 were excited sequentially with either 488, 514 or 633nm wavelengths, respectively. The emission maximum for each flourophore was collected. Optical section was 1 µm.

Chromogenic images were acquired using the Zeiss (Jena) Axiovert microscope together with the Zeiss (Jena) Axiocam using standard brightfield settings. Shading correction was performed prior to image acquisition.

All image processing was limited to linear brightness and contrast adjusting using FIJI (Schindelin et al., 2012).

3.25 Statistical analysis

Statistical analyses were performed using unpaired, two-tailed Student's T-test.

Variance is expressed as standard error of the mean.

For evaluation of indirect ELISA, one-way analysis of variance (one way ANOVA) with posthoc test of Tamhame was performed.

3.26 Application specific computer programs

Program:	**Used for:**
AxioVision Rel.4.6	Axiovert 200M fluorescence microscope
LAS AF 2.6.0	Leica SP5 confocal laser scanning microscope
LightCycler 480 Software 1.5	LightCycler 480
Quantity One 4.6.2	Chemi-doc luminescence detection system
Wallac 1420 Manager, Version 2.0	Victor 2 multilabel counter
INTAS GDS Version 3.34.04.02.2011	Agarose gel documentation
NexEX Version 10.4	Ventana Discovery XT device software

3.27 Computer programs

Program:	Used for:
DNA Lasergene 9 suite	Sequence analysis
BLAST (NCBI)	Sequence analysis
Primer3	Primer design, Reference: Rozen and Skaletsky (Rozen and Skaletsky, 2000)
Microsoft Excel 2003	ELISA und qRT-PCR evaluation
EndNote X	Bibliography/ Citatition Manager
SPSS	Statistical analysis
Biorad Quantity One	Western blot analysis and densitometric calculation
Fiji	Image analysis, Reference: Schindelin et al. (Schindelin et al., 2012)

4 Results

4.1 Commercially available antibodies are not sensitive or specific to detect K_v10.2 in Western blot analysis

For our aim to assess the protein distribution of K_v10.2 in mouse, we first evaluated five commercially available antibodies for their sensitivity and specificity to recognize K_v10.2 in lysates of human embryonic kidney cells (HEK293) Wild type (Wt), HEK293 BBS-K_v10.1 and HEK293 BBS-K_v10.2 by Western blot analysis. HEK293 cells overexpressing full-length human K_v10.1 or K_v10.2 fused to a α-bungarotoxin binding site (BBS), as well as mouse brain lysates and HEK293 Wt cells were used as positive and negative controls, respectively. Before analyzing the overexpressing cells by Western blot, we evaluated the expression levels of *KCNH1* and *KCNH5* in the different HEK293 cells in comparison to endogenous K_v10.1 and K_v10.2 mRNA levels of HEK293 Wt cells by qRT-PCR (Figure 7A).

We detected no transcripts of *KCNH1* and *KCNH5* in HEK293 Wt cells. HEK293 BBS-K_v10.1 cells had an approximately 260 fold higher mRNA expression of *KCNH1* as compared to the human total brain calibrator, and were negative for *KCNH5*. HEK293 BBS-K_v10.2 cells were negative for *KCNH1* and had an approximately 310 fold higher *KCNH5* mRNA expression in comparison to the total human brain calibrator. Furthermore, as shown in Figure 7B, the presence of K_v10.1 protein was confirmed by a pull-down assay with a biotin-conjugated α-bungarotoxin antibody and subsequent Western blot analysis using the anti-K_v10.1 antibody 9391. This antibody has already been shown to specifically detect K_v10.1 (Chen et al., 2011). The use of the anti-K_v10.1 antibody detected a protein band of approximately 115 kDa, the predicted molecular weight of BBS-K_v10.1. The expected molecular weight of the full-length channel is 111 kDa; the BBS-tag, inserted into the second extracellular loop of the channels, increases the molecular weight by approximately 4 kDa. The same applies to K_v10.2, which has the predicted molecular weight of 112 kDa. The inserted BBS-tag increases the molecular weight to 116 kDa.

We verified by qRT-PCR and Western blot analysis that HEK293 BBS-K_v10.1 cells overexpress BBS-K_v10.1. For K_v10.2 we demonstrated mRNA expression in HEK293 BBS-K_v10.2

cells and expected that similar to HEK293 BBS-K_v10.1, HEK293 BBS-K_v10.2 cells also synthesize the BBS-K_v10.2 protein.

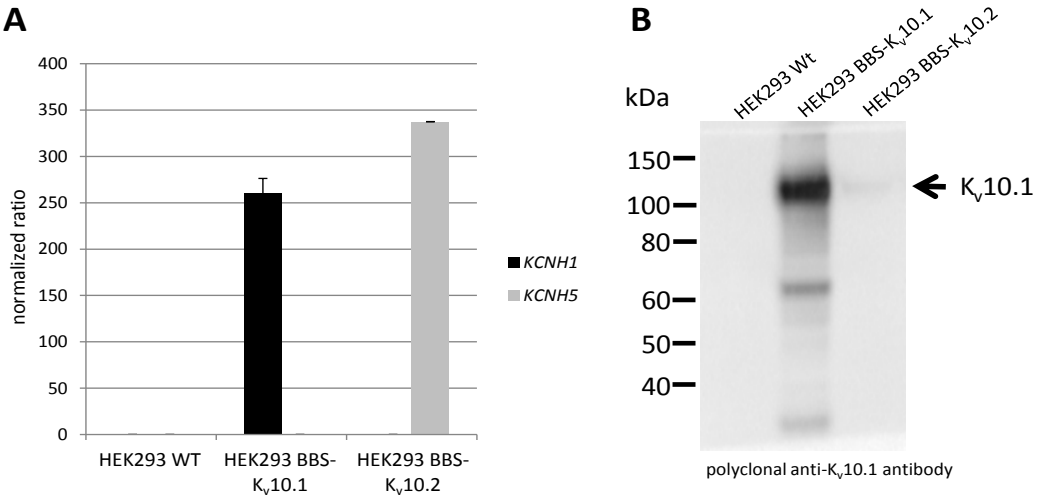

Figure 7: Validation of *KCNH1* and *KCNH5* RNA expression in HEK293 cells determined by qRT-PCR and of protein translation by pull-down assay and Western blot analysis
A: In HEK293 Wt cells no *KCNH1* (black columns) and *KCNH5* (grey columns) transcripts were detected. HEK293 BBS-K_v10.1 cells were only positive for *KCNH1*. HEK293 BBS-K_v10.2 cells only expressed *KCNH5*. All values were normalized to the human total brain calibrator (expression =1, data not shown). **B:** Validation of protein synthesis of BBS-K_v10.1 in HEK293 BBS-K_v10.1 overexpressing cells. Pull-down with biotin conjugated α-bungarotoxin was performed and subsequently analyzed by Western blot with polyclonal anti-K_v10.1 9391 antibody. Detection of an approximately 115 KDa protein, representing K_v10.1, was shown in the K_v10.1 overexpressing cells only.

To evaluate the commercially available antibodies directed against K_v10.2, whole protein lysates from HEK293 Wt, HEK293 cells overexpressing BBS-K_v10.1, HEK293 cells overexpressing BBS-K_v10.2 and mouse total brain lysates were used in Western blot analysis. Detection of a protein of approximately 116 kDa in the lysates of BBS-K_v10.2 overexpressing HEK293 cells and a protein of approximately 112 kDa in mouse brain by the use of the K_v10.2 antibody would indicate specificity to K_v10.2, whereas, a band of approximately 115 kDa in HEK293 BBS-K_v10.1 overexpressing cells would indicate cross-reactivity with K_v10.1. In control cells, the amino-terminal (N-terminal) anti-K_v10.2 antibody from *Abcam* did not react with any protein at the molecular weight of 115 kDA representing either K_v10.1 or K_v10.2 (Figure 8A). Therefore, this antibody did not show sensitivity towards K_v10.2. Instead, a protein of lower molecular weight, approximately 105 kDa, was detected in all samples derived from HEK293 cells. No protein of the predicted molecular weight of K_v10.2 was recognized in the whole brain lysate. Protein loading determined by anti-α-tubulin antibody of the HEK293 Wt and HEK293 BBS-K_v10.1 cells was lower compared to the BBS-K_v10.2 overexpressing cells. Even though

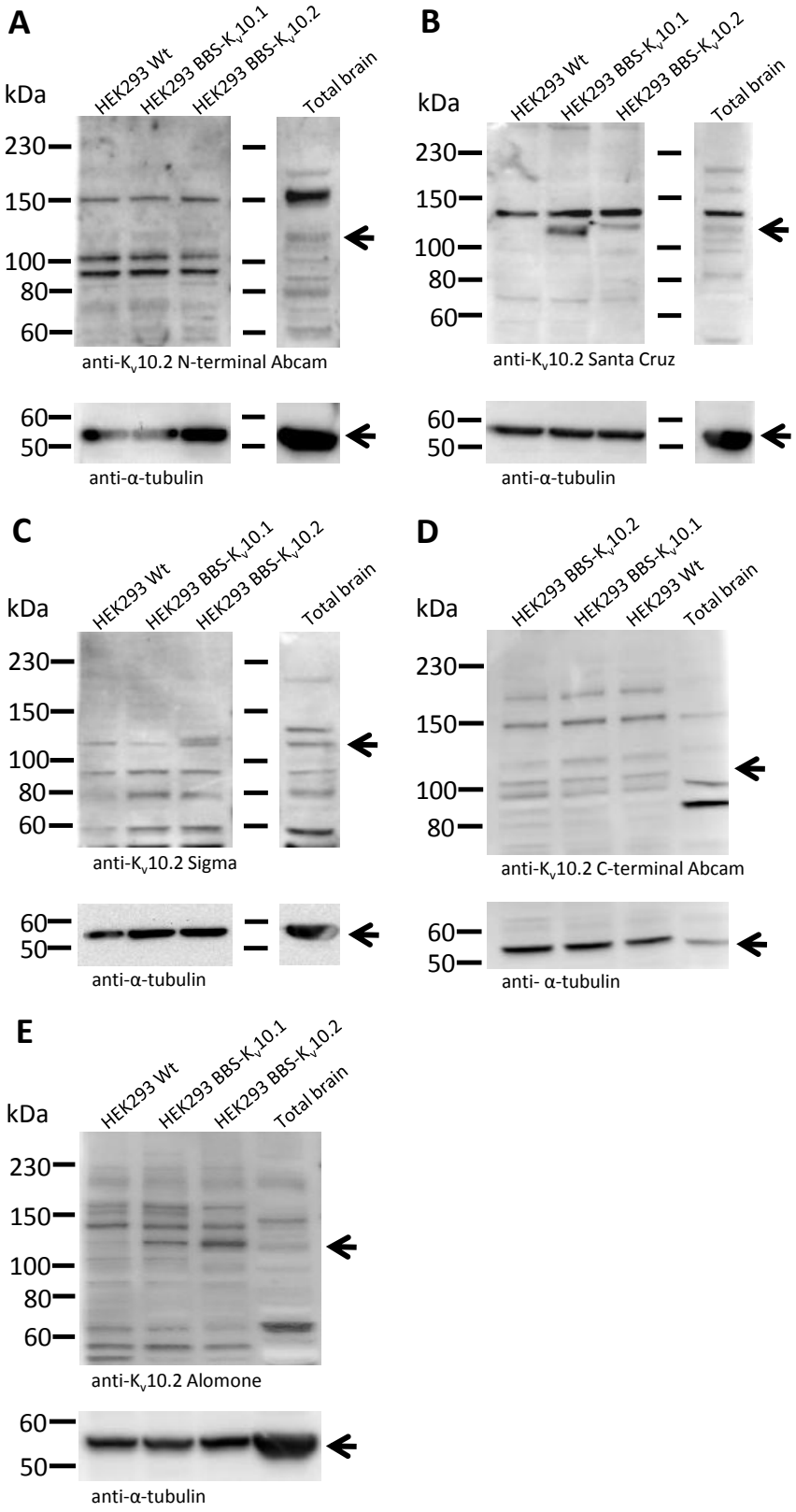

Figure 8: Evaluation of 5 commercially available anti-K_v10.2 antibodies by Western blot analysis
Immunoblotting of cell lysates of HEK293 Wt, HEK293 BBS-K_v10.1, HEK293 BBS-K_v10.2 and mouse total brain performed with commercially available anti-K_v10.2 antibodies. **A:** N-terminal anti-K_v10.2 antibody, *Abcam*: No protein was detected at the molecular weight of 116 kDa of BBS-K_v10.2 in HEK293 BBS-K_v10.2 cell lysate. **B:** Anti-K_v10.2 antibody, *Santa Cruz Biotechnology*: A protein of approximately 116 kDa

was detected in the HEK293 BBS-K_v10.2. In HEK293 BBS-K_v10.1. cell lysates, indicating cross-reactivity. **C:** Anti-K_v10.2 antibody, *Sigma-Aldrich*: The antibody detected K_v10.2 in HEK293 BBS-K_v10.2 cell lysate. Due to a non-specific band at approximately 116 kDa, an analysis of K_v10.2 protein level in total brain lysate was not possible. **D:** C-terminal anti-K_v10.2 antibody, *Abcam*: No specific protein was detected in the HEK293 BBS-K_v10.2 cell lysate. At approximately 116 kDa a protein was detected in all three HEK293 cell samples, even in those negative for K_v10.2. **E:** Anti-K_v10.2 antibody, *Alomone Biolabs*: A protein of the molecular weight of K_v10.2 was detected in HEK293 BBS-K_v10.2 overexpressing cells. A protein of the molecular weight of K_v10.1 was detected in HEK293 BBS-K_v10.1 overexpressing cells. **A-E:** Equal protein loading was determined by anti-α-tubulin (arrows). Arrows indicate the predicted molecular weight of BBS-K_v10.2 (=116 kDa).

more HEK293 BBS-K_v10.2 protein was loaded, the antibody did not bind to K_v10.2. Therefore, we can conclude that the antibody is not sensitive enough for K_v10.2 recognition in Western blot analysis.

The *Santa Cruz Biotechnology* anti-K_v10.2 antibody, directed against the human carboxyl-terminus (C-terminus), recognized in Western Blot analysis a protein with a size compatible to the molecular weight of BBS-K_v10.1 in lysates of BBS-K_v10.1 overexpressing HEK293 cells (Figure 8B). It also interacted, to a lesser extent, with a protein of higher molecular weight (116 kDa) in the sample of the BBS-K_v10.2 overexpressing cells. In total mouse brain protein lysate, only weak signals were obtained in the molecular weight range of 100 - 130 kDa. This rendered the protein recognized by this antibody indistinguishable of being K_v10.1 or K_v10.2. These results show that the *Santa Cruz Biotechnolog*y anti-K_v10.2 antibody is not specific for K_v10.2 detection.

The *Sigma-Aldrich* anti-K_v10.2 antibody, targeting the third extracellular loop of K_v10.2, recognized a protein compatible with BBS-K_v10.2 of approximately 116 kDa in the HEK293 BBS-K_v10.2 cell lysate only (Figure 8C). We observed in all samples a non-specific protein band that is of slightly lower molecular weight than the protein detected in HEK293 BBS-K_v10.2 cell lysate. Using mouse total brain lysate, the antibody recognized a protein with the predicted molecular weight of 112 kDa of K_v10.2. Since we observed a non-specific protein band at the same molecular weight as K_v10.2 in the HEK293 cells, the antibody seems to be not specific for detection of K_v10.2.

The *Abcam* C-terminal anti-K_v10.2 antibody recognized a protein with a molecular weight of approximately 116 kDa within all HEK293 cell samples (Figure 8D). Interaction with this non-specific protein in HEK293 Wt and HEK293 BBS-K_v10.1 cells showed that the Abcam C-terminal anti-K_v10.2 antibody is not specific to detect K_v10.2.

The *Alomone Biolabs* anti-K_v10.2 antibody recognized a protein at approximately 116 kDa in lysates of BBS-K_v10.1 and BBS-K_v10.2-overexpressing HEK293 cells (Figure 8E). This

indicates interaction of the anti-K_v10.2 antibody towards K_v10.1, pointing to a non-specific detection of K_v10.1 by this antibody. Hence, this anti-K_v10.2 antibody is also not suitable for K_v10.2 expression analysis.

In summary, Western blot analysis showed that all commercially available anti-K_v10.2 antibodies were either not sensitive to detect K_v10.2 or were cross-reactive with K_v10.1 with our protocol. Hence, these antibodies were not acceptable for our aim to unravel the K_v10.2 protein expression. We approached this issue by generating a novel polyclonal anti-K_v10.2 antibody.

4.2 Generation of a novel anti-K_v10.2 polyclonal antibody

4.2.1 Generation of a C-terminal human K_v10.2 construct

Since all tested commercially available antibodies analyzed for their ability to detect K_v10.2, showed no specificity for K_v10.2, we decided to generate a novel antibody. The aim was to generate an antibody that is not only capable of distinguishing between K_v10.1 and K_v10.2, but also recognizing both the human and murine form of K_v10.2. Therefore, we choose the human C-terminus of K_v10.2 as the antigen. This region of K_v10.2 is characterized by the least homology (44 %) towards K_v10.1 in human and human and mouse protein sequence is 94% identical (Figure 9).

The C-terminus of the human K_v10.2 ion channel cloned in the pET16b protein expression plasmid was already available in our department. The plasmid contains an IPTG inducible T7 promoter and a 10xHis-tag N-terminal of the cloned *KCNH5* sequence to allow purification of the C-terminus of K_v10.2 by Ni-affinity chromatography. Sequencing of the construct confirmed the correct *KCNH5* sequence. From here on, the expressed His-tagged C-terminus of human K_v10.2 will be referred to as His-K_v10.2-CTerm.

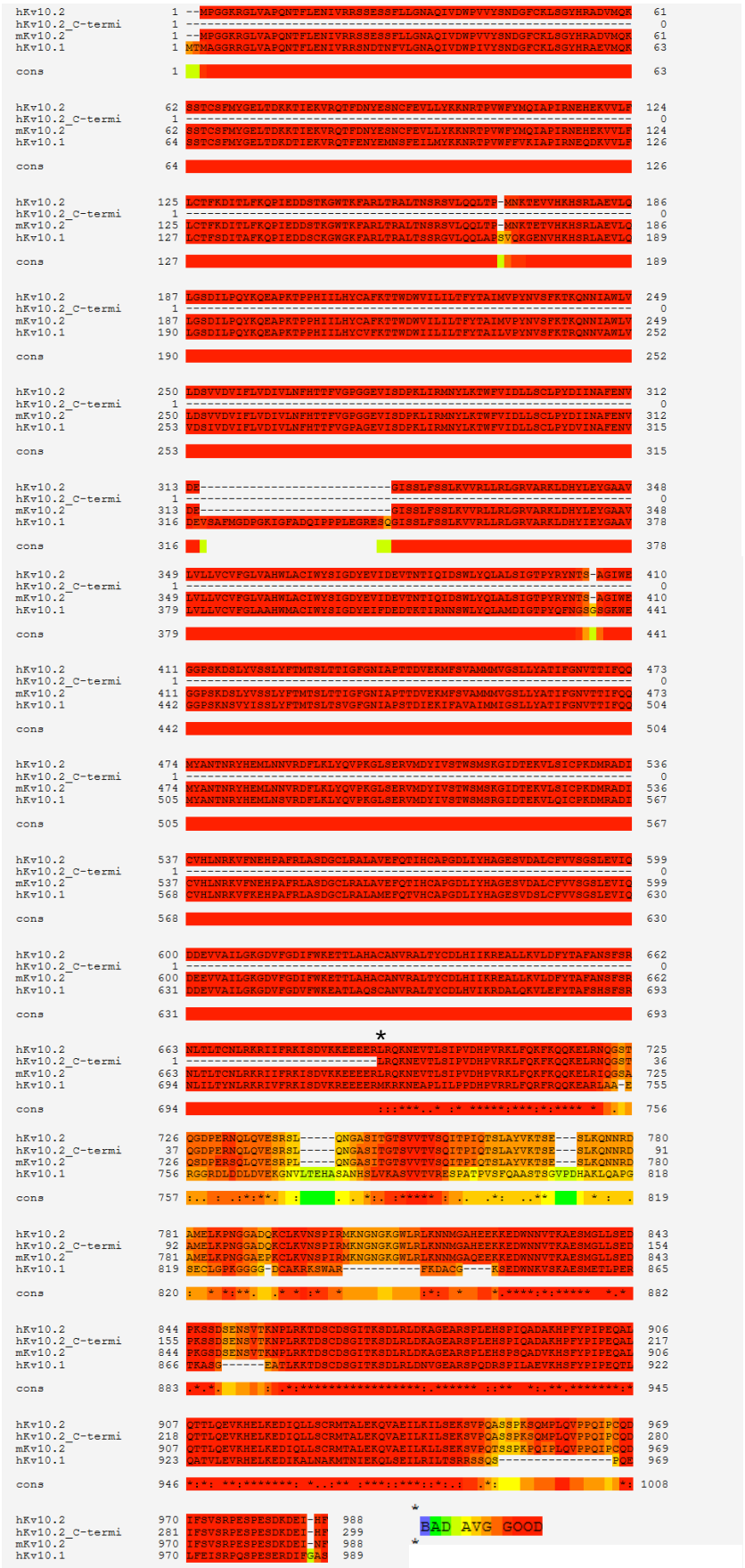

Figure 9: Protein sequence alignment of K_v10.2, K_v10.2 C-terminus K_v10.1

Protein sequence alignment of human K_v10.2 (hK_v10.2), C-terminus of human K_v10.2 (hK_v10.2-C-terminus), mouse K_v10.2 and human K_v10.1. The C-terminus of human K_v10.2 has the lowest homology

(44 %) with K_v10.1. Mouse and human full-length K_v10.2 protein sequence share a high homology (98 %), also in the C-terminus (94 %). Sequence homology is colour coded as indicated in lower right panel. Asterix indicates start C-terminus expressed for antibody generation. Sequence alignment was performed by T-Coffee (Notredame et al., 2000, Di Tommaso et al., 2011).

4.2.2 Heterologous expression of human His-K_v10.2-CTerm in *E.coli*

We transformed *E.coli* BL21 with the pET16b plasmid containing the His-K_v10.2-CTerm. These cells are a common prokaryotic expression system for protein synthesis. Samples were collected before IPTG induction and at an interval of 1 h starting 2 h after IPTG induction. Different temperatures (30°C and 37°C) as well as different concentrations of IPTG (0.3 mM, 0.7 mM and 1 mM) were used to optimize the expression conditions (data not shown). Analysis of bacterial protein expression was performed by SDS-PAGE. After Coomassie staining we found an approximately 46 kDa protein expressed in the IPTG induced samples, but not in the non-induced sample (Figure 10A).

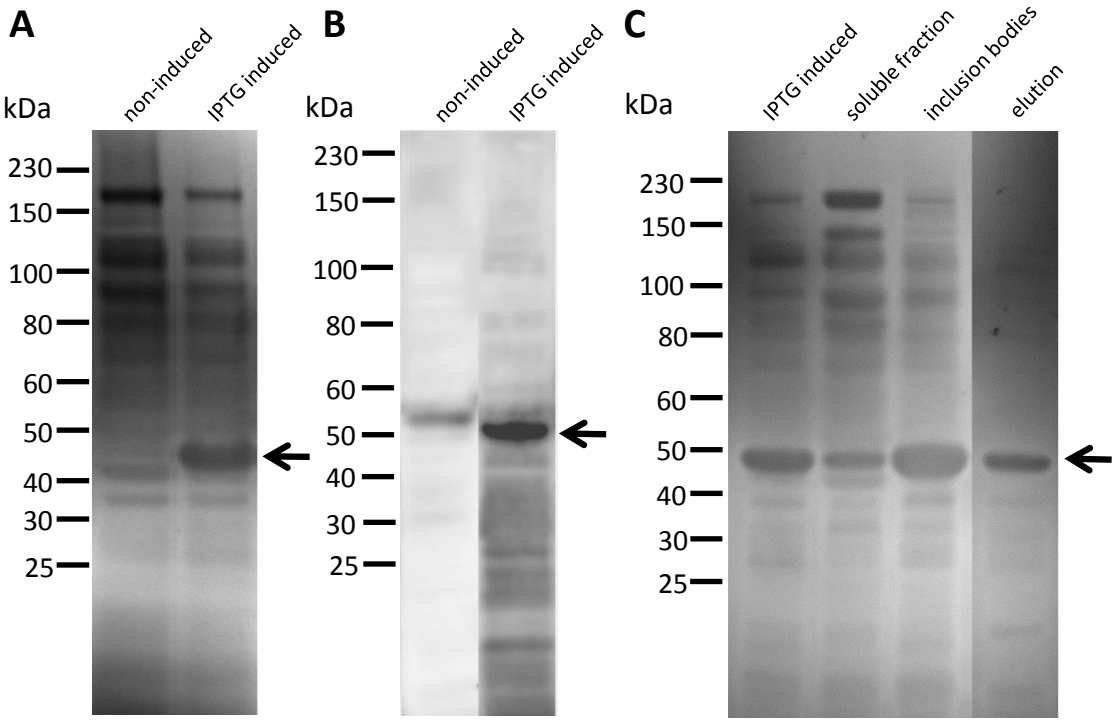

Figure 10: Prokaryotic protein expression of the C-terminus of K_v10.2 analyzed by SDS-PAGE and Coomassie staining

A: *E.Coli* BL21 cells were transfected with the His-K_v10.2-CTerm expression construct and expression was induced with IPTG. His-K_v10.2-CTerm expression was detected only in the induced sample at approximately 46 kDa (arrow), verified by SDS-PAGE and subsequent Coomassie staining. **B:** Verification of His-K_v10.2-CTerm protein expression by Western blot analysis with anti-His antibody. An approximately 50 kDa protein (arrow) was detected only in the induced cell lysate. **C:** Analysis of soluble (periplasmic space) and insoluble (inclusion bodies) fractions and elution after Ni-affinity chromatography in Coomassie stained SDS-gel revealed His-K_v10.2-CTerm protein in low amounts in the soluble fraction and highly abundant in inclusion bodies (arrow).

In order to confirm, that this protein is indeed the His-K_v10.2-CTerm, we performed Western Blot analysis of non-induced and IPTG induced cells with an anti-His antibody (Figure 10B). The result that a protein band at approximately 50 kDa was detected by the anti-His antibody only in IPTG-induced cell lysate confirmed the expression of the His-K_v10.2-CTerm protein.

Upon overexpression, proteins often form inclusion bodies. Hence, we investigated whether the His-K_v10.2-CTerm protein was expressed into the periplasmic space or formed inclusion bodies. We observed the protein at 46 kDa in the soluble fraction (periplasmic space), but also to a high amount in the insoluble fraction (inclusion bodies) indicating that the expressed His-K_v10.2-CTerm protein is packed into inclusion bodies during protein synthesis in *E.coli* (Figure 10C). Therefore, we used a denaturation procedure to solubilize the aggregated protein.

4.2.3 Purification of His-K_v10.2-CTerm protein by Ni-affinity chromatography

The solubilized protein extract containing the His-K_v10.2-CTerm protein was subjected to nickel-affinity purification, based on the His-tag. We tested urea or guanidinium hydrochloride (GuHCl) for elution and dialyzation of His-K_v10.2-CTerm. In comparison to urea, Figure 11 shows that GuHCl yielded a purer protein and a higher protein concentration. When dialyzed overnight against PBS, the protein partially precipitated. Therefore, we maintained the protein in 2 M GuHCl in PBS. The GuHCl did not allow for total protein concentration measurement by a bicinchoninic acid (BCA) protein assay. Hence, the concentration of the protein was analyzed by SDS-PAGE with an albumin as standard and subsequent Coomassie staining (Figure 11). The concentration of the protein was adjusted to 2 mg/ml and sent to Aldevron (Freiburg) for immunization of two rabbits. 57 days after immunization the animals were sacrificed. Sera of two rabbits were pooled and the antibody purified by protein A affinity chromatography. All these steps were performed by Aldevron.

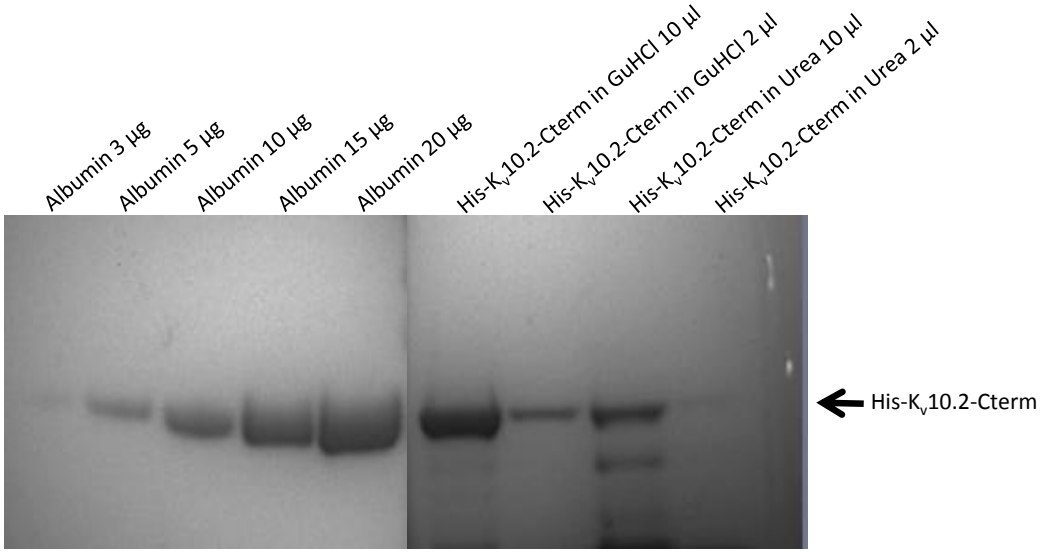

Figure 11: His-K_v10.2-CTerm protein concentration determination by SDS-PAGE
3 µg, 5 µg, 10 µg, 15 µg and 20 µg albumin were loaded on a SDS-gel to serve as concentration standard. SDS-gel is shown loaded with 10 µl purified His-K_v10.2-CTerm maintained in 2 M guanidinium hydrochloride (GuHCl) and 2 M urea together with 1:5 dilutions of each approach. Subsequent Coomassie staining revealed a higher purity and protein concentration when eluted and dialyzed with GuHCl in comparison to urea.

4.3 Determination of the specificity of the novel anti-K_v10.2 antibody

4.3.1 Anti-K_v10.2 antibody recognizes its antigen in indirect ELISA

Having generated a new antibody against K_v10.2, we first ensured that this antibody is specific for detection of its His-K_v10.2-CTerm antigen. In particular, we excluded cross-reactivity towards K_v10.1. As the antigen was a His-tagged form of the K_v10.2 C-terminus, we also ruled out reactivity towards the His-tag.

The interaction of the newly generated polyclonal IgG antibody towards its antigen was determined by indirect enzyme-linked immuno sorbent assay (ELISA) (Figure 12, black columns). To investigate cross-reactivity towards K_v10.1, we used H1X, a fusion protein of the pore and C-terminus of human K_v10.1 previously generated in our department (Hemmerlein et al., 2006). To investigate cross-reactivity of the anti-K_v10.2 antibody towards the His-tag, we used a His-tagged Ubiquitin C (UbcH5) protein as antigen. UbcH5 is a fusion protein of a member of the Ubiquitin C family with a C-terminal 6xHis-tag, which shares no homology with K_v10.2 determined by BLAST analysis (data not shown). All of the antigens were coated directly to the wells, while uncoated wells incubated with PBS served as negative controls. Further

controls included detection of the antigens with either anti-K_v10.2 antibody (Figure 12, grey columns) or secondary HRP conjugated anti-rabbit antibody alone (Figure 12, white columns).

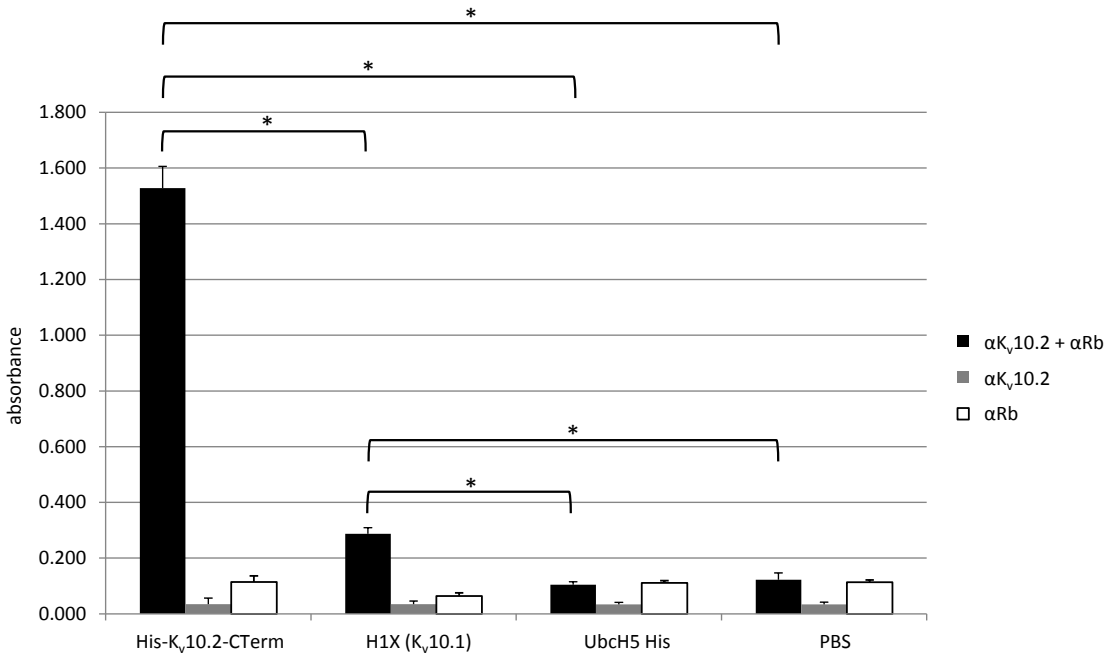

Figure 12: Analysis of binding specificity of anti-K_v10.2 antibody by ELISA
The anti-K_v10.2 antibody (black columns) recognized the His-K_v10.2-CTerm antigen that was used for antibody generation. The antibody was also probed against H1X, a human K_v10.1 fusion protein. The affinity of the antibody was approximately 5 times higher to the His-K_v10.2-CTerm antigen than to H1X (K_v10.1). UbcH5His protein served as control for investigation of His-tag detection by the anti-K_v10.2 antibody, which was not observed. Further controls included uncoated (PBS) wells or incubation of antigens with HRP labeled secondary anti-rabbit antibody only. Black columns: anti-K_v10.2 antibody and secondary HRP conjugated anti-rabbit antibody (anti-Rb). Grey columns: anti-K_v10.2 antibody, only. White columns: HRP conjugated anti-rabbit antibody only. Measurements performed in triplicates. *= P <0.01. Statistical significances were calculated with the one-way ANOVA and the Post hoc test of Tamhane.

As shown in Figure 12, the anti-K_v10.2 antibody recognized the His-K_v10.2-CTerm protein applied for antibody generation (high significance, P <0.01) and bound to the H1X antigen (high significance, P <0.01). However, the signal obtained was approximately five times weaker in the H1X coated wells in comparison to wells coated with the His-K_v10.2-CTerm antigen. The anti-K_v10.2 antibody did not bind to the UbcH5 antigen. Since the signal obtained from the combination of the anti-K_v10.2 antibody together with the secondary antibody was at the same level compared to the controls, it can be concluded that the anti-K_v10.2 antibody did not interact with the His-tag.

In summary, the K_v10.2 antibody binds to the His-K_v10.2-CTerm protein. With the indirect ELISA we could demonstrate weak cross-reactivity towards H1X, a K_v10.1 fusion protein representing the C-terminus of K_v10.1 and no interaction with the His-tag of the UbcH5 protein.

4.3.2 Anti-K_v10.2 antibody detects K_v10.2 in Western blot analysis

To evaluate the specificity of the anti-K_v10.2 antibody in Western blot, we used cell lysates from human HEK293 Wt, HEK293 BBS-K_v10.1 and HEK293 BBS-K_v10.2 cells. Furthermore, total mouse brain lysates were applied on SDS-gel to verify recognition of mouse K_v10.2 by the newly generated antibody. The lysates derived from HEK293 Wt and HEK293 BBS-K_v10.1 overexpressing cells served as controls. As shown in Figure 13, the anti-K_v10.2 antibody detected a protein at the predicted molecular weight of 116 kDa in HEK293 BBS-K_v10.2 overexpressing cells only. At this particular molecular weight, no protein was recognized in the controls (Figure 13, arrow). The anti-K_v10.2 antibody did not bind to BBS-K_v10.1. In total mouse brain lysate the antibody recognized a protein at approximately 112 kDa, the predicted molecular weight of Wt K_v10.2 (Figure 13). It is noteworthy, that the weight difference of 4 kDa between the BBS-K_v10.2 sample and the total brain lysate can be explained by the 27 amino acid (aa) sequence containing the α-bungarotoxin binding site in the BBS-K_v10.2 protein. Although partial recognition of K_v10.1 (H1X) by the anti-K_v10.2 antibody occurred in ELISA, cross-reactivity against K_v10.1 was not observed in Western blot analysis. A representative image of the whole Western blot is illustrated in the appendix section. We concluded that the anti-K_v10.2 antibody generated by us was sensitive to differentiate between K_v10.1 and K_v10.2 protein and to detect the human K_v10.2 in samples of overexpressing K_v10.2 cells as well as identify the mouse K_v10.2 in total mouse brain lysate.

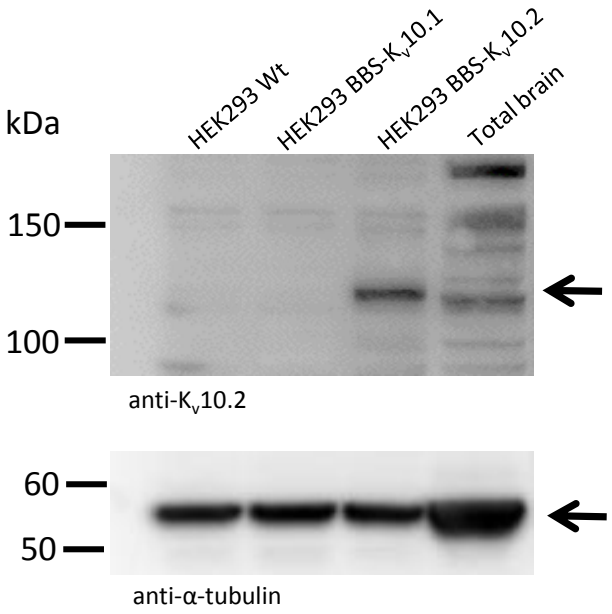

Figure 13: Validation of binding of the newly-generated anti-K_v10.2 polyclonal antibody to K_v10.2 by Western blot analysis
Western blot analysis of protein lysates from human HEK293 Wt, HEK293 BBS-K_v10.1 and HEK293 BBS-K_v10.2 cells as well as from total mouse brain were performed in combination with anti-K_v10.2 antibody. Only in HEK293 BBS-K_v10.2 cell lysate the antibody detected a protein at the predicted molecular weight of BBS-K_v10.2, being approximately 116 kDa (arrow). In total brain lysate the antibody detected a protein of lower molecular weight (approximately 112 kDa) than in the HEK293 BBS-K_v10.2 sample, due to the 27 amino acid insert containing the BBS. Equal protein loading was determined by anti-α-tubulin (arrow).

4.3.3 Anti-K_v10.2 antibody specifically detects K_v10.2 by the use of immunocytochemistry

In order to determine the specificity of the K_v10.2 antibody to recognize human K_v10.2 in immunostaining procedures, HEK293 Wt, HEK293 BBS-K_v10.1 and HEK293 BBS-K_v10.2 overexpressing cells were grown on coverslips. Cells were fixed with paraformaldehyde, followed by the chromogenic immunocytochemistry (ICC) and counterstaining with hematoxylin was performed (Figure 14). Cells used as negative controls were treated without primary anti-K_v10.2 antibody (Figure 14G-I). The anti-K_v10.2 antibody only stained HEK293 BBS-K_v10.2. As shown in Figure 14C and F an intracellular and membranal staining were observed. Not all HEK293 BBS-K_v10.2 cells were positive for K_v10.2 since the HEK293 BBS-K_v10.2 cells are not derived from a monoclonal cell line. Besides BBS-K_v10.2 overexpressing cells, none of the control cells lines were stained for K_v10.2 (Figure 14A,B,D,E).

In summary, ICC performed with the novel polyclonal anti-K_v10.2 antibody resulted in an intracellular and membrane staining of HEK293 BBS-K_v10.2 cells only. In contrast to the result of the ELISA, but consistent with our Western blot data, no cross-reactivity towards K_v10.1 was demonstrated.

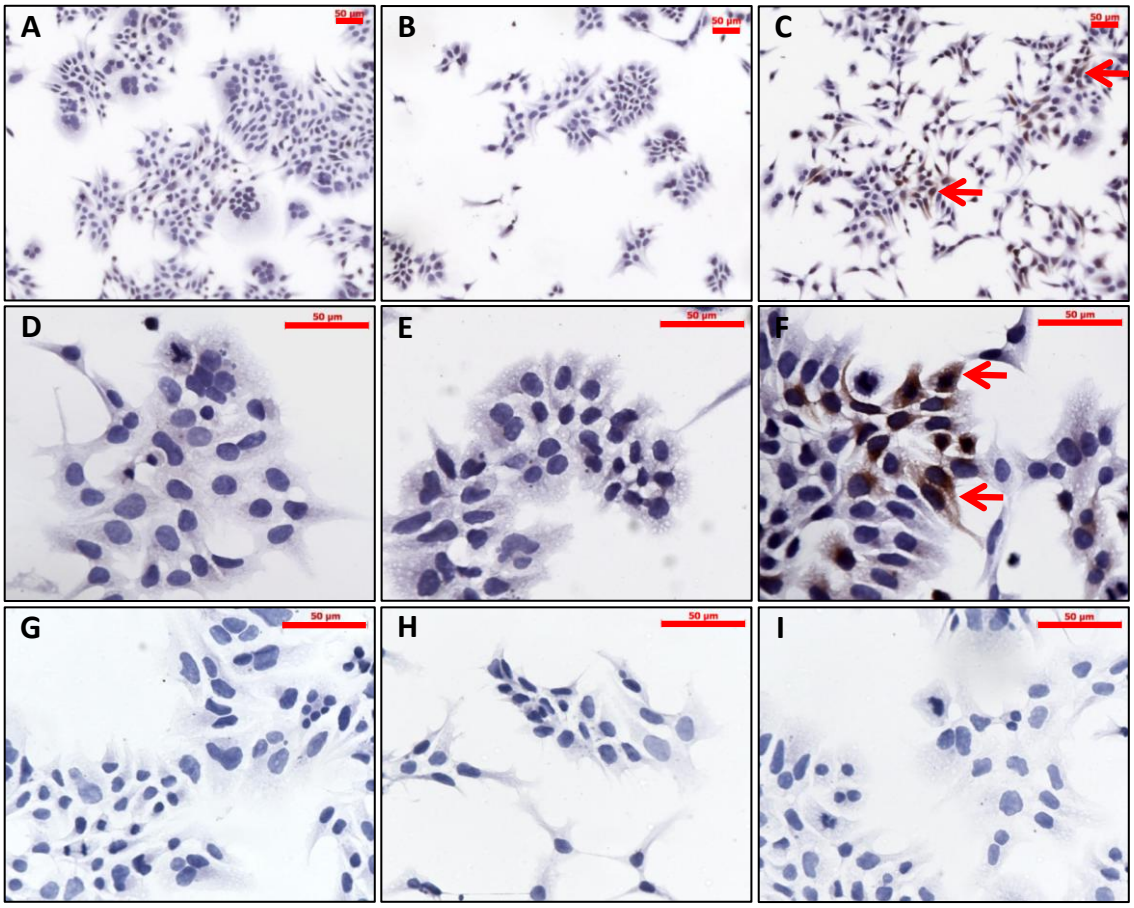

Figure 14: Immunocytochemistry with anti-K_v10.2 antibody on HEK293 Wt, HEK293 BBS-K_v10.1 and HEK293 BBS-K_v10.2 overexpressing cells
(A,D,G) HEK293 Wt, **(B,E,H)** HEK293 BBS-K_v10.1, **(C,F,I)** and HEK293 BBS-K_v10.2 cells were grown on coverslips and fixed. **(A-F)** ICC was performed on the cells by using anti-K_v10.2 antibody, secondary HRP conjugated anti-rabbit antibody and DAB substrate (brown) and counterstained with hematoxylin (blue). **(A,D)** HEK293 Wt and **(B,E)** HEK293 BBS-K_v10.1 cells were negative for K_v10.2. **(C,F)** Only HEK293 BBS-K_v10.2 overexpressing cells were positively stained with the anti-K_v10.2 antibody, where K_v10.2 was detected in the cytoplasm and in the membrane of HEK293 BBS-K_v10.2 overexpressing cells (arrows). **(G)** Negative control of HEK293 Wt cells, only secondary anti-rabbit HRP conjugated antibody and DAB substrate was used where no signal was obtained. **(H)** Negative control of HEK293 BBS-K_v10.1 cells, only secondary anti-rabbit HRP conjugated antibody and DAB substrate was used where no signal was obtained. **(I)** Negative control of HEK293 BBS-K_v10.2 cells, only secondary anti-rabbit HRP conjugated antibody and DAB substrate was used where no signal was obtained. **A-I**: Scale bar represents 50 µm.

4.4 K_v10.2 is virtually ubiquitously expressed in mouse tissues

4.4.1 K_v10.2 protein is virtually ubiquitously expressed in various mouse tissues and brain regions

Since the anti-K_v10.2 antibody specifically recognized a protein corresponding to K_v10.2 protein in Western blot analysis using the HEK293 system, we applied the antibody in Western blot to analyze the endogenous expression of K_v10.2 in protein lysates from different organs (Figure 15B-D) and brain regions (Figure 16B,C) of the adult mouse. Moreover, we analyzed lysates of various organs (Figure 15A) and brain regions (Figure 16A) for *Kcnh5* mRNA by qRT-PCR.

On every SDS-gel, we added protein lysates from the different HEK293 cells as controls as already described. Briefly, protein lysates of HEK293 Wt and HEK293 BBS-K_v10.1 served as negative controls while protein lysate of HEK293 BBS-K_v10.2 cells was used as positive control. The predicted molecular weight of K_v10.2 is 112 kDa. For internal control α-tubulin was detected with an anti-α-tubulin antibody.

Of the tissue analyzed by qRT-PCR, trachea, adrenal gland and testes showed the highest mRNA levels of *Kcnh5* (Figure 15A). Low or very low *Kcnh5* mRNA levels were found in uterus, bladder, kidney, stomach, prostate and placenta. Colon, liver, heart and lung did not contain detectable levels of *Kcnh5* transcripts.

Since the anti-K_v10.2 antibody recognized a protein corresponding to K_v10.2 protein in Western blot analysis using the HEK293 system, we used the antibody to analyze the endogenous expression of K_v10.2 protein in protein lysates from different organs (Figure 15B-D) and brain regions (Figure 16B,C) of the adult mouse in Western blot. As shown in Figure 15B, protein lysates of pancreas, spleen, liver, kidney, heart and lung from adult mice were investigated. All organs were positive; a faint band at the expected molecular weight of K_v10.2 was observed in the lung sample. Verification of equal protein loading, determined by anti-α-tubulin antibody, revealed low protein amounts in lysates of pancreas, liver and kidney. Although the loading control showed low protein amounts in lysate of kidney, a protein of the predicted molecular weight of K_v10.2 was detected in this sample with the anti-K_v10.2 antibody.

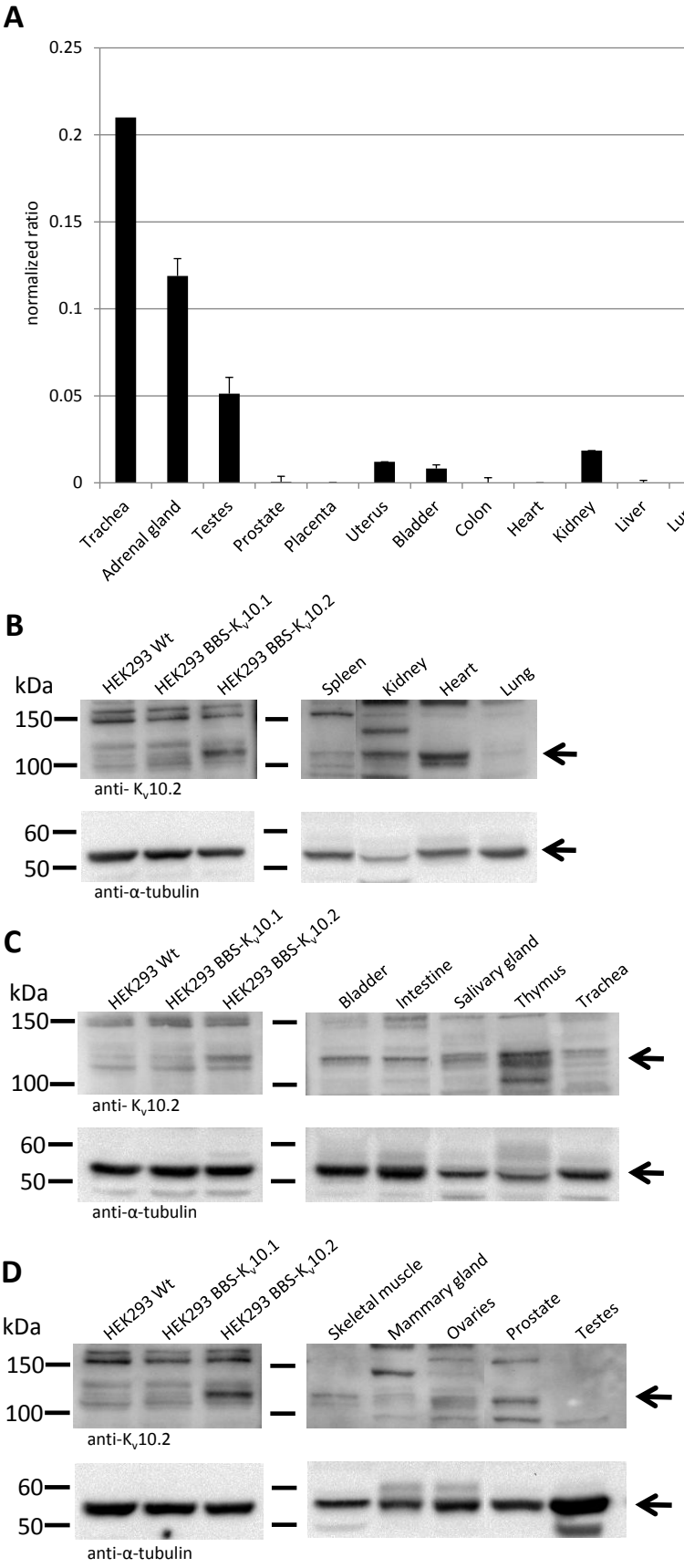

Figure 15: K_v10.2 mRNA and protein expression in organs of the adult mouse determined by qRT-PCR and Western blot analysis

A: *Kcnh5* mRNA distribution in mouse adrenal gland, testes, prostate, uterus, bladder, colon, heart, kidney, liver, lung and stomach investigated by qRT-PCR. All values were normalized to the total mouse

brain calibrator (expression =1, data not shown). Trachea, adrenal gland, testes had the highest mRNA levels of *Kcnh5* of the tissue analyzed. *Kcnh5* mRNA levels detected in uterus, prostate, placenta, bladder, stomach and kidney were low or very low, while qRT-PCR analysis of colon, liver, heart and lung and did not result in detectable transcripts of *Kcnh5*. **B:** Western blot analysis of spleen, kidney, heart and lung of adult mouse with anti-K_v10.2 antibody. Protein of the predicted molecular weight of K_v10.2 (=112 kDa) was detected in all organs. **C:** Western blot analysis of bladder, intestine, salivary gland, thymus and trachea with anti-K_v10.2 antibody. Protein of the expected molecular weight of K_v10.2 (=112 kDa) was detected in all organs. **D:** Western blot analysis of skeletal muscle, mammary gland, ovaries, prostate and testes of adult mouse with anti-K_v10.2 antibody. Protein of the predicted molecular weight of K_v10.2 (=112 kDa) was detected in all organs, except in testes. **B-D:** Equal protein loading was determined by anti-α-tubulin (arrows). HEK293 Wt and HEK293 BBS-K_v10.1 cell lysates served as negative and HEK293 BBS-K_v10.2 as positive controls. A protein of the predicted molecular weight of BBS-K_v10.2 (=116 kDa) was detected only in HEK293 BBS-K_v10.2 lysates. Arrows indicate approximate weight of BBS-K_v10.2 (=116 kDa) overexpressed in HEK293 BBS-K_v10.2 cells.

Furthermore, bladder, intestine, stomach, salivary gland, thymus and trachea were analyzed (Figure 15C). In all tissues analyzed a band of the molecular weight corresponding to K_v10.2 was detected. A strong signal at the expected molecular weight of to K_v10.2 was observed in the sample of the thymus, albeit low protein loading was observed. In addition, we demonstrated that from the analyzed tissues of skeletal muscle, mammary glands, ovaries, prostate and testes, K_v10.2 was detected in the lysates of skeletal muscle, prostate and very faintly in the mammary glands and ovaries, while no K_v10.2 was observed in the testes (Figure 15D).

Next, we assessed K_v10.2 distribution in different regions of the CNS by qRT-PCR and Western blot analysis. As shown in Figure 16, on the mRNA and protein level, we detected a ubiquitious expression of K_v10.2 throughout the samples investigated. The qRT-PCR, which was normalized against total mouse brain calibrator, was performed on cortex, cerebellum, mesencephalon, hippocampus, spinal cord, brainstem, hypothalamus and striatum. *Kcnh5* transcription was most prominent in the cortex and striatum, while the lowest expression was found in the cerebellum (Figure 16A). Western blot analysis was performed on lysates of cortex, hippocampus, hypothalamus, thalamus and brainstem (Figure 16B), as well as on lysates of olfactory bulb, striatum, tectum, pituitary gland, cerebellum and spinal cord (Figure 16C). All brain regions analyzed by Western blot were positive for K_v10.2 protein. Only in pituitary gland the protein was detected at low level, which might correlate to low protein loading in this sample determined with anti-α-tubulin antibody (Figure 16C).

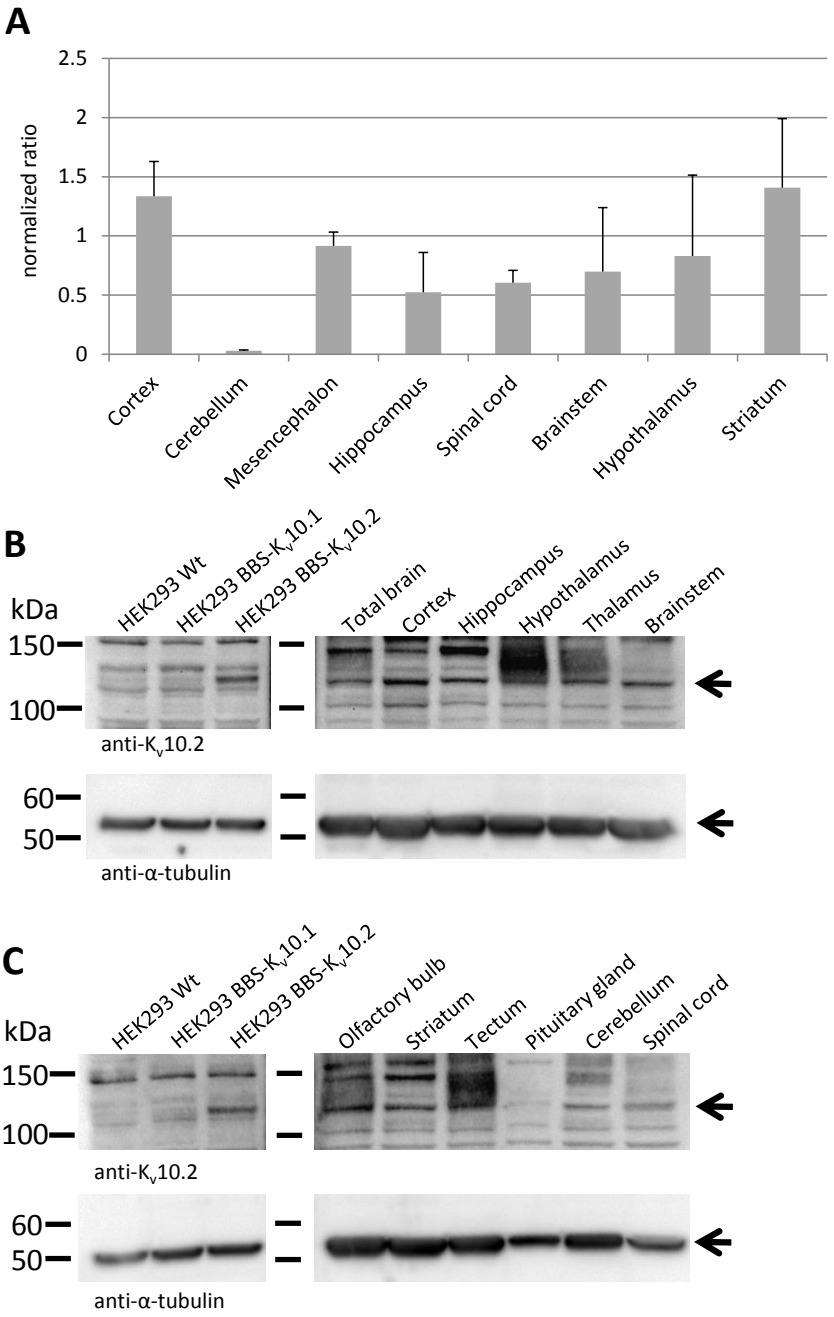

Figure 16: K_v10.2 mRNA and protein expression in brain regions of the adult mouse by qRT-PCR and Western blot analysis

A: *Kcnh5* mRNA levels were analyzed by qRT-PCR in different regions of the mouse brain. All values were normalized to the total mouse brain calibrator (expression=1, data not shown). All brain regions investigated were positive for *Kcnh5*. *Kcnh5 is* abundantly expressed in the cortex and striatum, while the cerebellum showed the lowest amount of *Kcnh5* transcripts. **B**: Western blot analysis of adult mouse total brain, cortex, hippocampus, hypothalamus, thalamus and brainstem with anti-K_v10.2 antibody. Protein corresponding to the predicted molecular weight of K_v10.2 (=112 kDa) was detected in total brain and all brain regions investigated. **C**: Western blot analysis of adult mouse olfactory bulb, striatum, tectum, pituitary gland, cerebellum and spinal cord with anti-K_v10.2 antibody. Protein of the expected molecular weight of K_v10.2 (=112 kDa) was detected in all brain regions investigated. **B,C**: Equal protein loading was determined by anti-α-tubulin (arrows). HEK293 Wt and HEK293 BBS-K_v10.1 cell lysates served as negative and HEK293 BBS-K_v10.2 as positive controls. A protein of the predicted molecular weight of BBS-K_v10.2 (=116 kDa) was detected only in HEK293 BBS-K_v10.2 lysates. Arrows indicate approximate weight of BBS-K_v10.2 (=116 kDa) overexpressed in HEK293 BBS-K_v10.2 cells.

Taken together, qRT-PCR results indicates varying *Kcnh5* transcript levels in different mouse organs, while all brain regions analyzed were *Kcnh5* mRNA positive. Western blot analysis with the anti-K_v10.2 antibody revealed a ubiquitous expression of a protein of the predicted molecular weight of K_v10.2 in regions of the CNS such as cortex, hippocampus, hypothalamus, thalamus, brainstem, olfactory bulb, striatum, tectum, pituitary gland, cerebellum and spinal cord and various organs of mouse such as spleen, kidney, heart, bladder, intestine, salivary gland, thymus, trachea, skeletal muscle, mammary gland, ovaries, lung and prostate, with the exception of testes.

4.4.2 K_v10.2 protein is localized to distinct regions in adult mouse brain

The investigation of protein expression in mouse tissues by Western blot resulted in the detection of a protein of the predicted molecular weight of K_v10.2 in virtually all samples. We further analyzed the distribution and localization of K_v10.2 with the anti-K_v10.2 antibody by the use of immunohistochemistry (IHC) on adult mouse brain sections.

As control, the tissues were incubated with secondary HRP conjugated anti-rabbit antibody and the detection system only. IHC in combination with the anti-K_v10.2 antibody resulted in a distinct staining pattern in the adult mouse brain (Figure 17A). Regions containing cells that stained positive for K_v10.2 include the mitral cell layer (Figure 18A, MCL) and the external plexiform layer of the olfactory bulb (Figure 17A, OB; Figure 18A). In the mitral cell layer the K_v10.2 staining suggests a localization of K_v10.2 to cell processes (Figure 18A, arrow) K_v10.2 protein in the cortex can be detected in the middle layers (Figure 17A, Cx; Figure 18B). Here, the results of the IHC suggested that the ion channel was localized to the membrane. Within the hippocampus the cornu ammonis area (CA) 3 and, to a lesser extend, CA2 were stained. Additionally the hilus was K_v10.2 positive (Figure 17A, Hil). Within the cerebellum, staining was observed in the Purkinje layer (Figure 18C, arrow) and the lateral cerebellar dentate nucleus (Figure 17A, Cdn) in the white matter. In the globus pallidus and thalamus, we detected K_v10.2 protein localization outside of cytoplasm of the cells (Figure 18D,E). Since the regions were intensely stained, a localization to the membrane was not possible. The intense staining was also observed in the amygdala, zona inserta, genicular nuclei and partially in the cochlear nuclei of the brainstem (Figure 18F). In contrast to the surrounding areas, the capsula interna did not show any signal. The negative control did not result in any staining (Figure 17B).

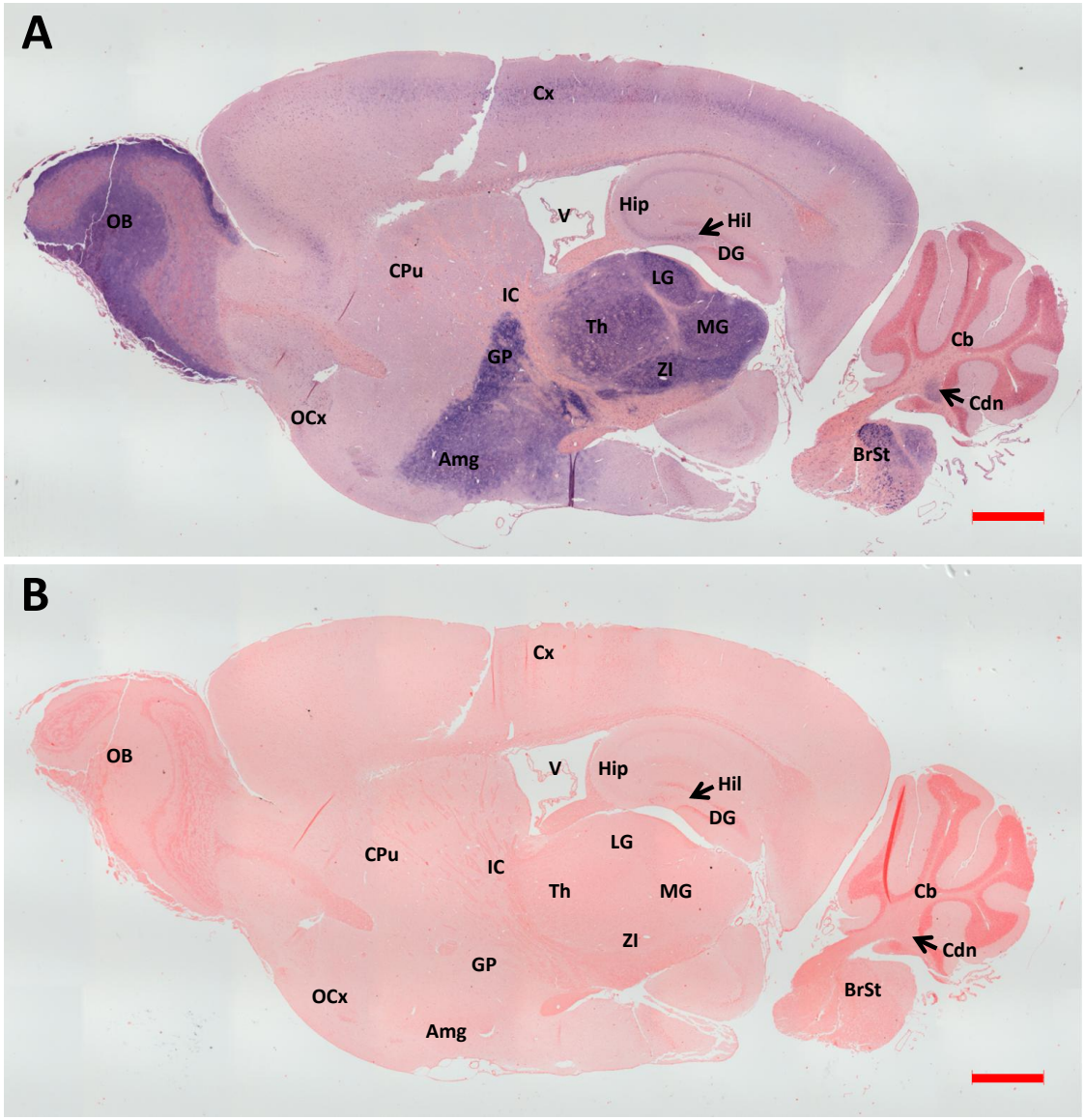

Figure 17: IHC analysis with anti-K_v10.2 antibody in adult sagittal mouse brain sections
A: K_v10.2 protein expression pattern was detected by immunohistochemistry with anti-K_v10.2 antibody (NBT/BCIP; blue) on paraffin mouse brain sections with counterstain (NFR; red). Regions stained by IHC with the anti-K_v10.2 antibody are: olfactory bulb (OB), cortex (Cx), amygdala (Amg), thalamus (Th), zona incerta (ZI), globus pallidus (GP), medial genicular nucleus (MG), lateral geniclar nucleus (LG), brainstem (BrSt). The CA3 region of the hippocampus (Hip) and the hilus (Hil) were stained. Inside of the cerebellum (Cb) the piriform layer and the lateral cerebellar dentate nucleus (Cdn) were K_v10.2 positive. No staining was observed in the caudate putamen (CPu), dentate gyrus (DG) the internal capsula (IC), lateral ventricle (LV), olfactory cortex (OCx) and hippocampus (Hpc). **B:** The negative control, consisting of the HRP conjugated secondary anti-rabbit antibody, the detection system and counterstain (NRF; red), showed no staining. **A,B:** Paraffin sections obtained at 7 µm. Scale bar represents 1000 µm.

IHC analysis of mouse brain performed with the anti-K_v10.2 antibody resulted in positive staining of the middle layers of the cortex and the cochlear nuclei of brainstem. Furthermore, the olfactory bulb, thalamus, globus pallidus, amygdala, zona inserta, genicular nuclei, middle layers of the cortex, CA3, CA2, hilus, choclear nucleus of the brainstem and lateral cerebellar dentate nucleus were positively stained.

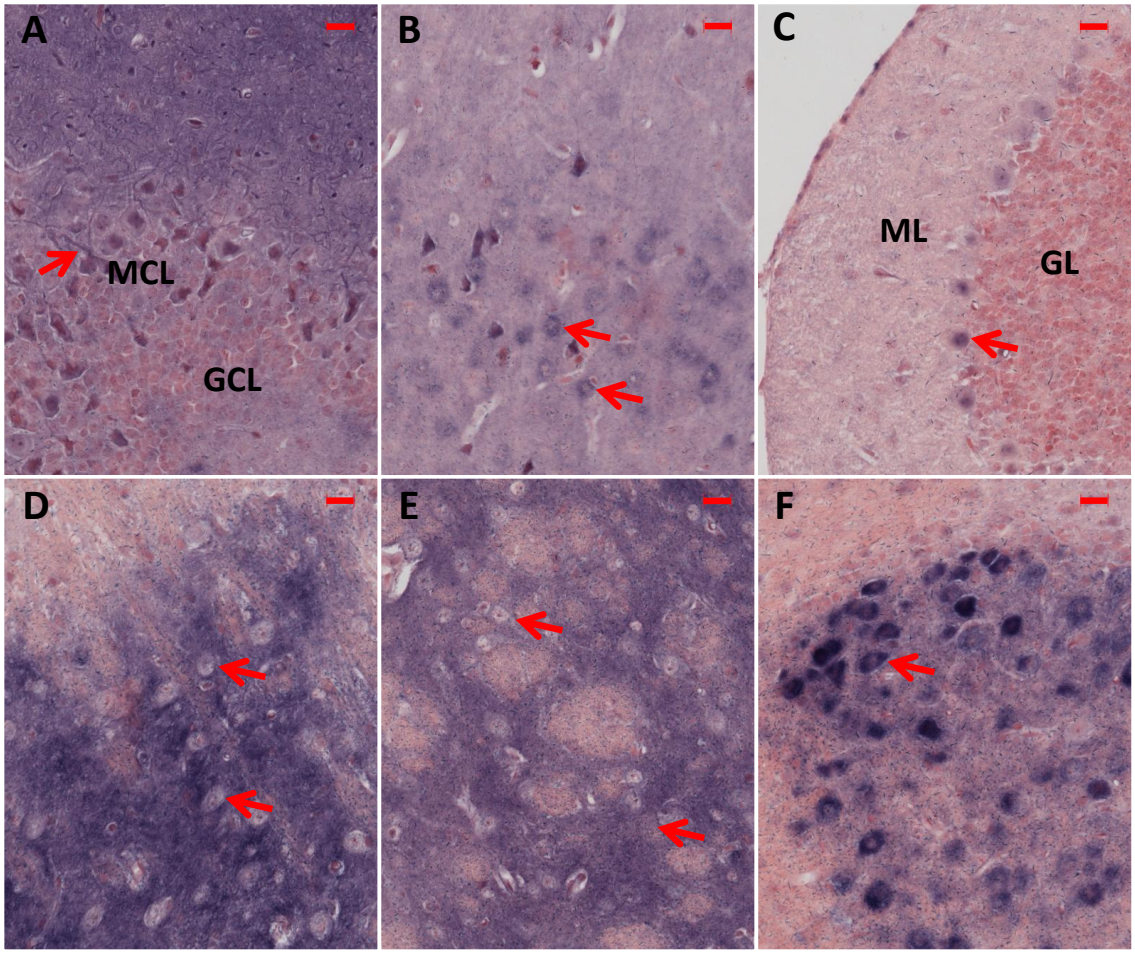

Figure 18: IHC analysis with anti-K_v10.2 antibody in selected brain regions of the adult mouse
A: Olfactory bulb: in the mitral cell layer (MCL) K_v10.2 was detected at the membrane of cells and in cellular processes (arrow). Granular cell layer (GCL) was negative for K_v10.2. **B:** Cortex: membrane staining was observed in a layer of cells that were positive for K_v10.2 (arrows). **C:** Cerebellum: Purkinje layer was K_v10.2 positive (arrow). Molecular layer (ML) and granular layer (GL) were K_v10.2 negative. **D:** Globus pallidus: IHC analysis resulted in neuropil staining, while the cell bodies (arrows) remained negative. It is indiscernible, if membranes of the cells were also stained. **E:** Thalamus: similar to the globus pallidus, IHC analysis resulted in neuropil staining, while the bodies of cells (arrows) were not stained. **F:** Brainstem: Cells of the cochlear nucleus were stained (arrow). **A-F:** IHC performed with anti-K_v10.2 antibody (NBT/BCIP; blue) in paraffin mouse brain sections with counterstain (NFR; red). Sections obtained at 7 µm. Scale bar represents 20 µm.

4.4.3 *Kcnh1* mRNA is ubiquitously expressed in the murine brain

Since favorable controls like tissue sections of K_v10.2 knockout mice were not available and blocking experiments could not be performed, cross-reactivity of the anti-K_v10.2 antibody against other proteins cannot be ruled out.

As another approach, in order to have a further proof of K_v10.2 detection by the anti-K_v10.2 antibody, we wanted to compare the expression pattern of *Kcnh5* in brain slices on mRNA and protein level using *In Situ* hybridization (ISH) and IHC, respectively. In order to

obtain a specific protocol for the *Kcnh5* probe, we first established the *Kcnh1* ISH probe. Since a *Kcnh1* total knockout mouse (Ufartes et al., 2013), was available in our department that served as negative control, the *Kcnh1* probe was used as a reference. Moreover, K_v10.1 protein distribution in rat brain is already published, allowing correlation of protein and mRNA distribution.

Kcnh5 and *Kcnh1* ISH riboprobes were designed to fulfill the following criteria: First, sequences of the probes were specific for their targets in mouse and rat, which were validated by BLAST analysis. Second, probes were designed virtually equal in size and base pair content, indicating highly similar ISH parameters required for specific annealing.

Both probes were digoxigenin labeled mRNA, which were obtained by *in vitro* transcription. The *Kcnh1* probe was 66 bases and the *Kcnh5* probe 63 bases in length. DNA templates were amplified by primers, which were directly linked to T7 promoters on the 5' end of either forward or reverse primers. Sequencing validated amplification products obtained. Following *in vitro* transcription, mRNA probes were analyzed by agarose gel electrophoreses (data not shown). To investigate the specificity and cross reactivity of the probes, a dot blot assay was performed with the antisense probes (see Appendix section), which resulted in specific probe annealing.

Strong hybridization with the *Kcnh1* antisense probe was seen in piriform cortex (Figure 19, Pfc), hippocampus (Figure 19, Hip), dentate gyrus (Figure 19, DG) and cerebellum (Figure 19A, Cb). Application of *Kcnh1* antisense and sense probe resulted in high background staining on adult Wt mouse brain sections (Figure 19A,B). The signal obtained with the sense probe partially outlined the same brain regions as detected with the antisense probe, but only slightly above the background level (Figure 19B). Both ISH probes did not hybridize to any target in the *Kcnh1* deficient mouse, demonstrating specificity of the probes (Figure 19C,D).

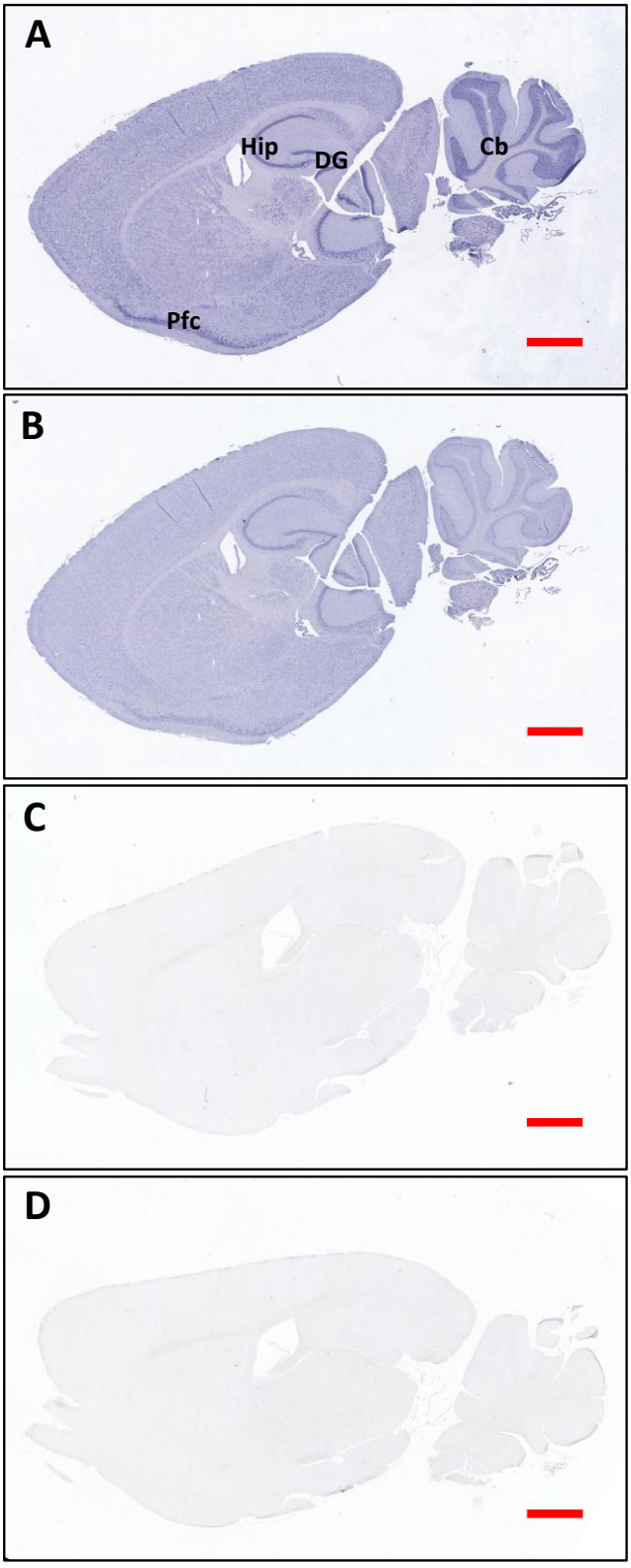

Figure 19: mRNA distribution of *Kcnh1* in adult mouse brain determined by ISH
A: In Situ hybridization with the *Kcnh1* antisense RNA probe detected *Kcnh1* transcripts ubiquitously throughout the wild type mouse brain. The strongest expression is detected in the piriform cortex (Pfc), hippocampus (Hip), dentate gyrus (DG) and cerebellum (Cb). **B:** The *Kcnh1* sense probe applied on Wild type section revealed a high background staining. **C:** Antisense *Kcnh1* RNA probe did not result in any signal obtained in the *Kcnh1* deficient mouse. **D:** Sense *Kcnh1* RNA probe did not result in any signal obtained in the *Kcnh1* deficient mouse. **A-D:** ISH performed with *Kcnh1* ISH probes (NBT/BCIP; blue) on paraffin sagittal mouse brain sections obtained at 7 µm. Scale bar represents 1000 µm.

In order to correlate the mRNA expression pattern with published protein expression pattern, we performed ISH on adult rat brain sections. Similar to our observation in the mouse brain, we detected *Kcnh1* transcripts ubiquitously in the rat brain (Figure 20A). This is in perfect accordance to published IHC results for $K_v10.1$ protein distribution (see Introduction section). The strongest expression detected was in the cortex, cerebellum, dentate gyrus, hippocampus, olfactory bulb, the olfactory cortex and brainstem. Also a strong signal was visible in the olfactory tubercle and in the Purkinje cells and granular layer of cerebellum. The ISH performed with the sense *Kcnh1* probe resulted in weak background staining (Figure 20B).

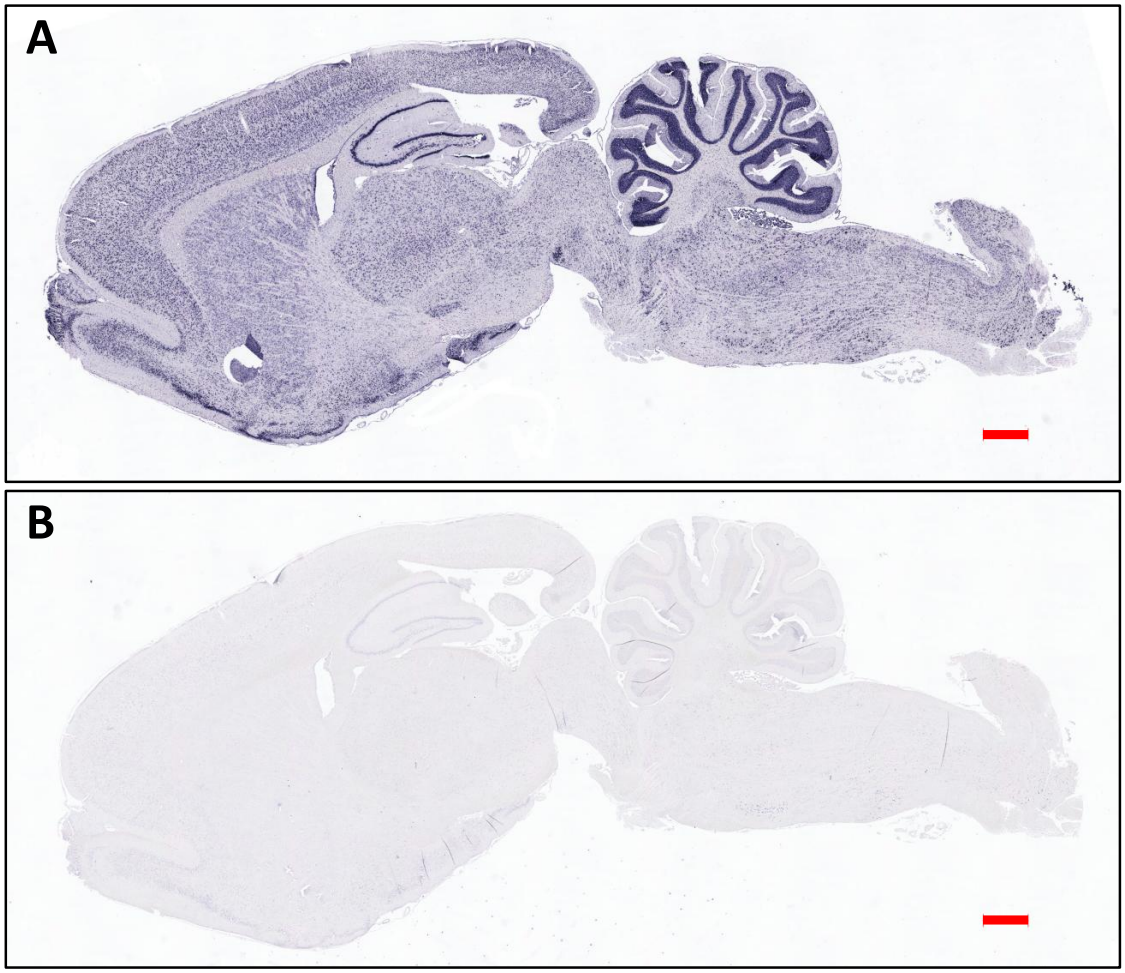

Figure 20: *Kcnh1* mRNA distribution in adult rat brain determined by ISH
A: ISH with *Kcnh1* antisense probe detected transcripts ubiquitously in the adult rat brain. The highest levels of transcripts were observed in the cortex, cerebellum, dentate gyrus, hippocampus, olfactory bulb, brainstem and the olfactory cortex. **B:** Application of the sense probe led to weak background staining all over the rat brain. **A,B:** ISH performed with *Kcnh1* ISH probes (NBT/BCIP; blue) on paraffin-acrolein sagittal rat brain sections obtained at 7 µm. Scale bar represents 1000 µm.

For *Kcnh1* we showed that the detected mRNA distribution correlates with published protein distributions in rat. The next step was to establish ISH for *Kcnh5* in order to investigate its mRNA distribution and to correlate it with its protein distribution.

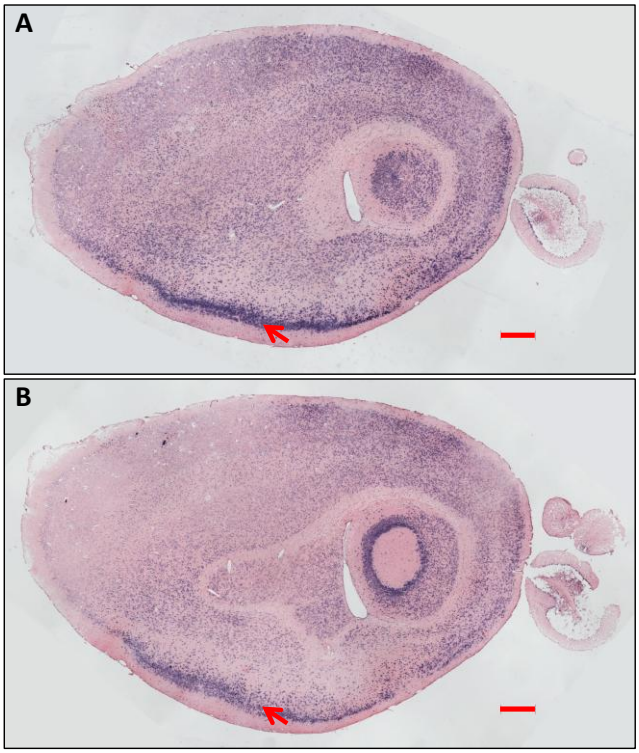

Figure 21: *Kcnh5* mRNA distribution in mouse brain determined by ISH
Application of the **(A)** *Kcnh5* antisense and **(B)** sense probe resulted in similar signals and patterns obtained by ISH. The *Kcnh5* sense probe, serving as negative control, hybridized in virtually the same pattern as the antisense probe. Especially in the piriform cortex application of the antisense and sense probes resulted in strong signals (**A,B** arrow). **A,B:** ISH performed with *Kcnh5* ISH probes (NBT/BCIP; blue) on paraffin mouse brain sections obtained at 7 µm and counterstained with NFR (red). Scale bar represents 500 µm.

ISH for *Kcnh5* on mouse brain sections was performed with the same protocol established for the *Kcnh1* probe. Since no *Kcnh5* knockout mouse was available, the negative control for *Kcnh5* antisense probe was the sense probe. The use of the *Kcnh5* antisense probe hybridized in similar pattern as obtained by to the sense probe (Figure 21A,B). In order to obtain specificity of the antisense probe, we:

1. increased hybridization temperature,
2. increased temperature of washing steps,
3. combined 1 and 2,
4. titrated the probes,
5. shortened the hybridization time.

None of these these steps were successful. Temperatures of hybridization and washing steps below 56°C resulted in hybridization of the sense probe, while temperatures above 56°C did not lead to hybridization signals obtained by the antisense probe. Therefore, determination of the *Kcnh5* mRNA expression pattern by ISH was not possible with the used protocols.

With the lack of specificity of the *Kcnh5* ISH probe, we were not able to investigate the cellular *Kcnh5* mRNA distribution to correlate it with its protein distribution.

4.4.4 K_v10.2 protein is expressed during mouse brain development

So far, we investigated the K_v10.2 protein distribution on the adult mouse by Western blot analysis and IHC. Preliminary data of our group indicate an embryonic lethality of the homozygous K_v10.2 constitutive knockout mouse (Dr. R. Ufartes, personal communication).

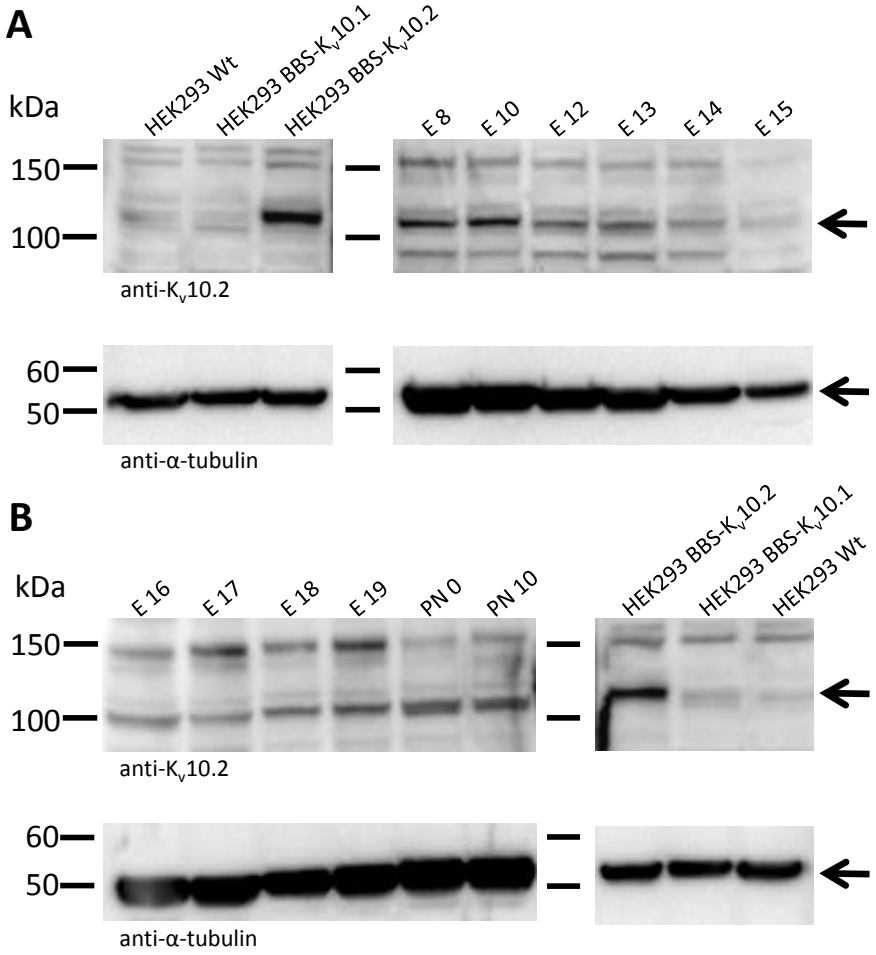

Figure 22: K_v10.2 expression in developing and postnatal mouse brain by Western blot analysis
A: Western blot analysis of protein lysates of embryonic (E) mouse stages E 8, E 10, E 12, E 13, E 14 and E 15 for K_v10.2 protein expression. Protein at the predicted molecular weight of K_v10.2 (=112 kDa) was detected in all E stages investigated. **B:** Western blot analysis of protein lysates of embryonic (E) mouse stages E 16, E 17, E 18 and E 19 and postnatal (PN) stages PN 0 and PN 10 for K_v10.2 protein expression. Protein at the predicted molecular weight of K_v10.2 (=112 kDa) was detected in all E and PN stages investigated. **A,B:** Equal protein loading was determined by anti-α-tubulin (arrows). HEK293 Wt and HEK293 BBS-K_v10.1 cell lysates served as negative and HEK293 BBS-K_v10.2 as positive controls. A protein of the expected molecular weight of K_v10.2 was detected only in HEK293 BBS-K_v10.2 lysates. Arrows indicate approximate weight of BBS-K_v10.2 (=116 kDa) overexpressed in HEK293 BBS-K_v10.2 cells.

To investigate the temporal expression of K_v10.2 during brain development, total brain lysates of embryonic (E) stages E 8, E 10, E 12 until E 19 and postnatal (PN) stages, PN 0 and PN 10, were investigated by Western blot analysis with the anti-K_v10.2 antibody. Throughout all embryonic stages tested here we could detect a protein of predicted molecular weight of K_v10.2 (= 112 kDa) in the developing mouse brain (Figure 22A,B). The same was observed in the total brain lysates of PN 0 and PN 10 (Figure 22B). Protein lysates of HEK293 Wt, HEK293 BBS-K_v10.1 and HEK293 BBS-K_v10.2 cells were used as negative and positive controls, respectively and applied on every SDS-gel.

Concluding, we demonstrated a K_v10.2 expression starting from the earliest time point of embryonic tissue investigated, E 8, until postnatal stage PN 10.

Next, we assessed the spatial distribution of K_v10.2 protein in embryonic mouse stages using IHC. According to the Western blot analysis, E 8.5 and later embryonic stages are positive for K_v10.2. To analyze not only the embryos but also the maternal supplementing tissue, the uteri of E 8.5, E 9.5 and E 11.5 pregnant mice were sectioned and stained for K_v10.2 (Figure 23A, Figure 24A, Figure 25A). At E 8.5 the primitive ectoderm of the implanted blastocyst has generated the germ layers. After the gastrulation, the organogenesis follows when tissues and organs of the embryo develop.

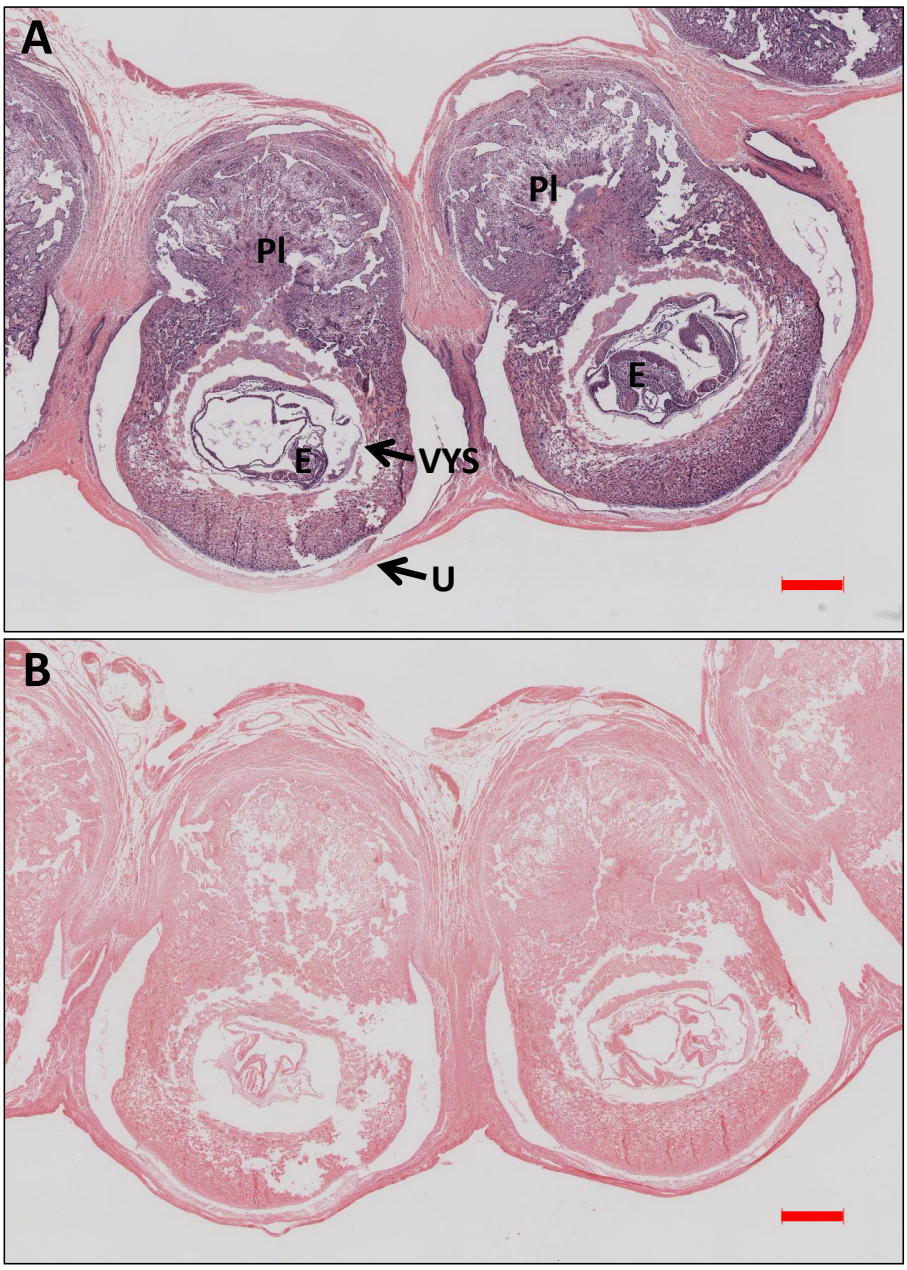

Figure 23: K_v10.2 protein distribution in the embryo and in uterine tissue of mouse embryonic stage 8.5 determined by IHC

A: Detection of K_v10.2 protein distribution in embryonic stage (E) 8.5, determined by anti-K_v10.2 antibody. The embryo (E), placenta (Pl) and visceral yolk sac (VYS) were K_v10.2 positive. The uterus (U) remained negative except for a cell layer towards the embryo. **B:** Negative control of E 8.5 embryo: Secondary HRP conjugated anti-rabbit antibody and detection system was applied; no staining was observed. **A,B:** Sections were counterstained with NFR. Paraffin sections obtained at 7 µm. Scale bar represents 500 µm.

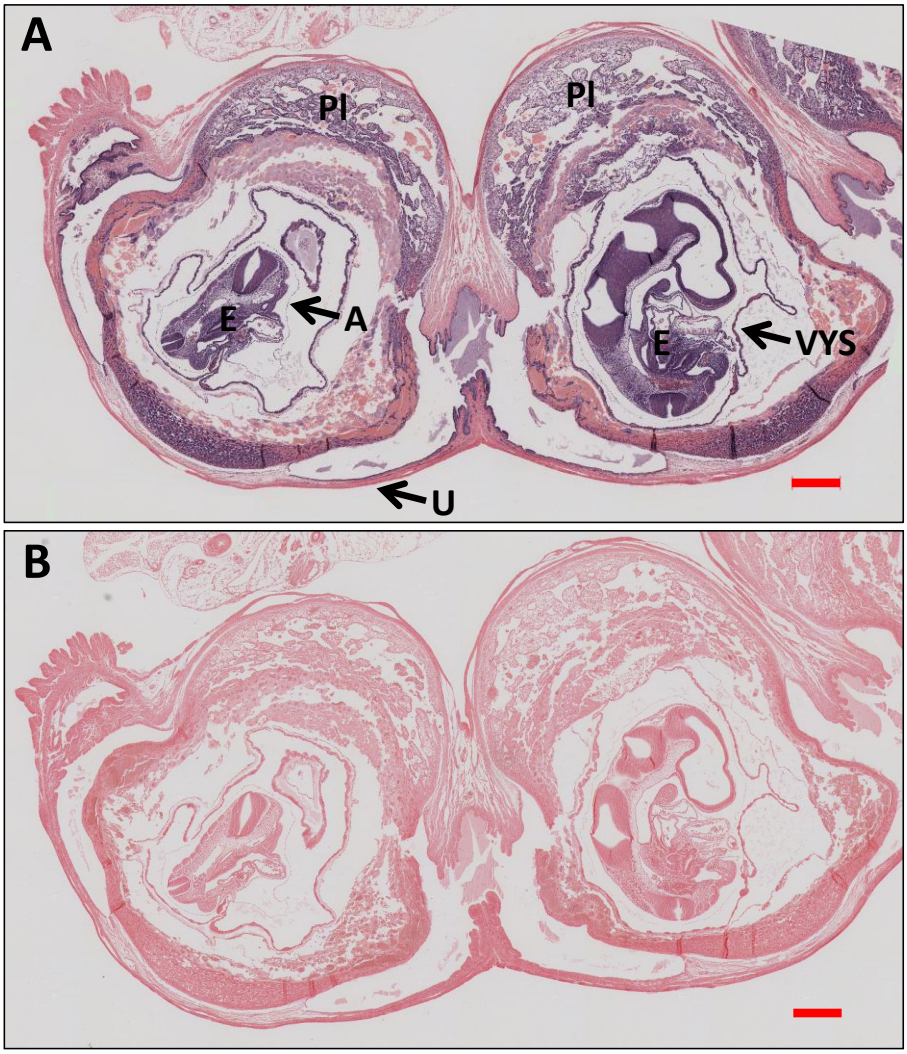

Figure 24: K_v10.2 protein distribution in the embryo and in uterine tissue of mouse embryonic stage 9.5 determined by IHC
A: Detection of K_v10.2 protein distribution in E 9.5, determined by anti-K_v10.2 antibody. The embryo (E), visceral yolk sak (VYS), amnion (A) and placenta (Pl) were positive for K_v10.2. The uterus (U) remained negative except for a cell layer towards the embryo, possibly the endometrium. **B:** Negative control of E 9.5 embryo: Secondary HRP conjugated anti-rabbit antibody and detection system was applied; no staining was observed. **A,B:** Sections were counterstained with NFR. Paraffin sections obtained at 7 µm. Scale bar represents 500 µm.

Negative controls were treated without primary anti-K_v10.2 antibody (Figure 23B, Figure 24B, Figure 25B). In all three embryonic stages, E 8.5, E 9.5 and E 11.5, the uterus (U) was mainly K_v10.2 negative except for a cell layer towards the embryo (Figure 23A, Figure 24A, Figure 25A). Furthermore, the placenta (Pl) and the visceral yolk sack (VYS) were K_v10.2 positive (Figure 23A, Figure 24A, Figure 25A). Also the embryos of all stages investigated, ubiquitously express K_v10.2, except for the E 11.5 embryo in which the developing cartilage of the spinal cord was negative (Figure 25A). At E 11.5 the parietal yolk sac (PYS) was K_v10.2 positive (Figure 25A).

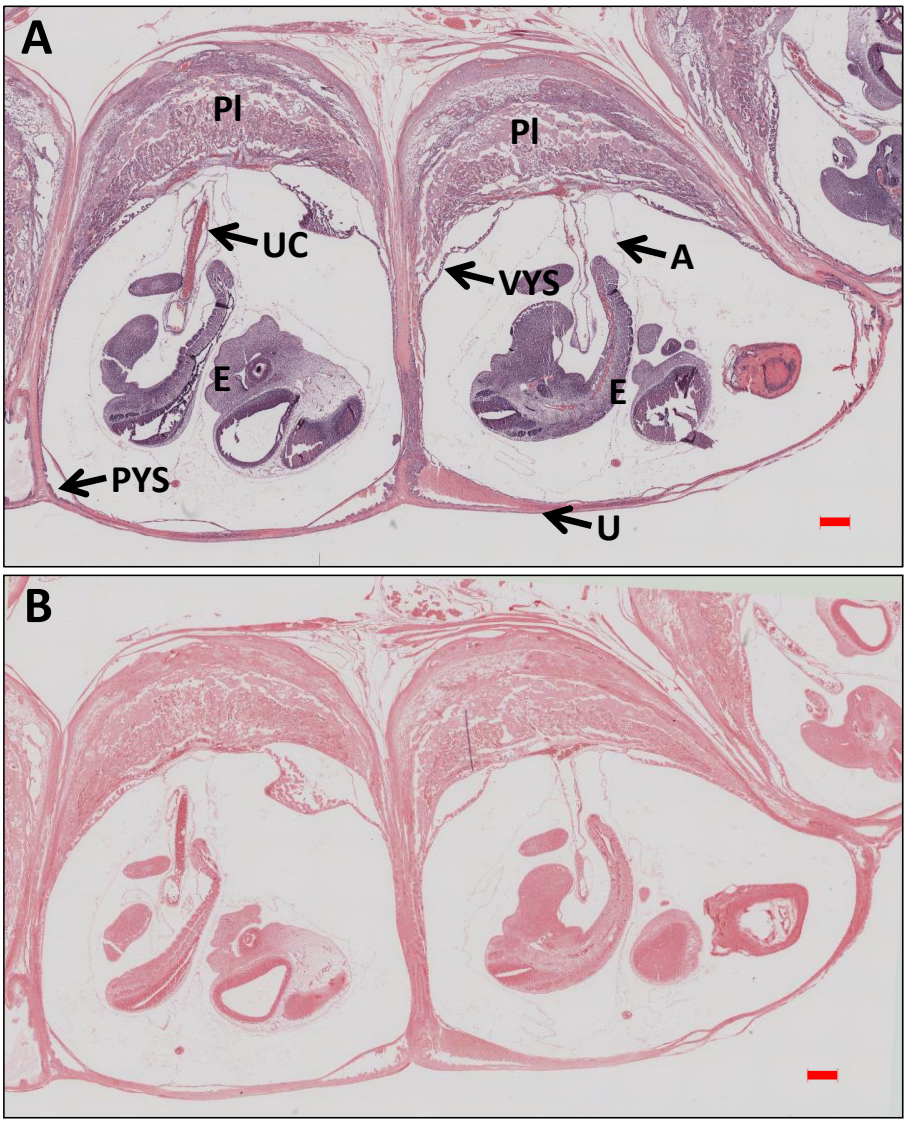

Figure 25: K_v10.2 protein distribution in the embryo and in uterine tissue of mouse embryonic stage 11.5 determined by IHC
A: Detection of K_v10.2 protein distribution in E 11.5, determined by anti-K_v10.2 antibody. The embryo (E), placenta (Pl), visceral yolk sac (VYS) and parietal yolk sac (PYS) were positive for K_v10.2. The amnion (A) and the uterus (U) remained negative except a region at the rostral side between the placentas. The umbilical cord (UC) remained negative. **B:** Negative control of E 11.5 embryo: Secondary HRP conjugated anti-rabbit antibody and detection system was applied; no staining was observed. **A,B:** Sections were counterstained with NFR. Paraffin sections obtained at 7 µm. Scale bar represents 500 µm.

In summary, K_v10.2 is virtually ubiquitously expressed in the fetal mouse as well as in the placenta and to a low extent in the uterus of the pregnant mouse.

4.4.5 K_v10.2 protein expression is not altered in brain regions of *Kcnh1* total knockout mice

The *Kcnh1* total knockout mouse was previously generated in the lab. Behavior studies of the *Kcnh1* total mouse demonstrated a mild hyperactive phenotype (Ufartes et al., 2013). We investigated if K_v10.2 expression was regionally altered in the homozygous *Kcnh1* total knockout mouse compared to Wt mouse. Therefore, we immunoblotted protein derived from different brain regions of the homozygous *Kcnh1* total knockout mouse to analyze a regional differences in K_v10.2 expression. For internal control tubulin was detected with an anti-α-tubulin antibody (Figure 26A,B). HEK293 BBS-K_v10.1 and HEK293 BBS-K_v10.2 cells served as positive and negative controls, respectively. Brain regions investigated included brain stem, thalamus, hypothalamus, hippocampus, cortex, olfactory bulb, striatum, tectum, pituitary gland, cerebellum and spinal cord (Figure 33A,B).

To investigate differential regulation of K_v10.2 protein expression in the *Kcnh1* total knockout mouse, we directly compared protein lysates of the olfactory bulb, cortex, brain stem, cerebellum, tectum, and striatum from *Kcnh1* total knockout mouse with the appropriate Wt mouse brain regions by Western blot analysis (Figure 27A,B). In all analyzed brain regions, with the exception of tectum and striatum, no obvious difference in K_v10.2 protein levels were detected. To further analyze possibly altered protein levels, we performed densitometric analysis (Figure 27C) of K_v10.2 expression normalized to detected actin. As a result, only in samples of the tectum and striatum a difference was found. In the tectum the homozygous *Kcnh1* total knockout mouse had lower levels of K_v10.2, while in the striatum it was vice versa. It is noteworthy, that the diffuse band of 120 – 150 kDa observed in the tectum could have altered the result. The results are only an indicator that no difference in protein levels of K_v10.2 in the homozygous *Kcnh1* knockout exists, since only one sample of each region was quantified (N=1).

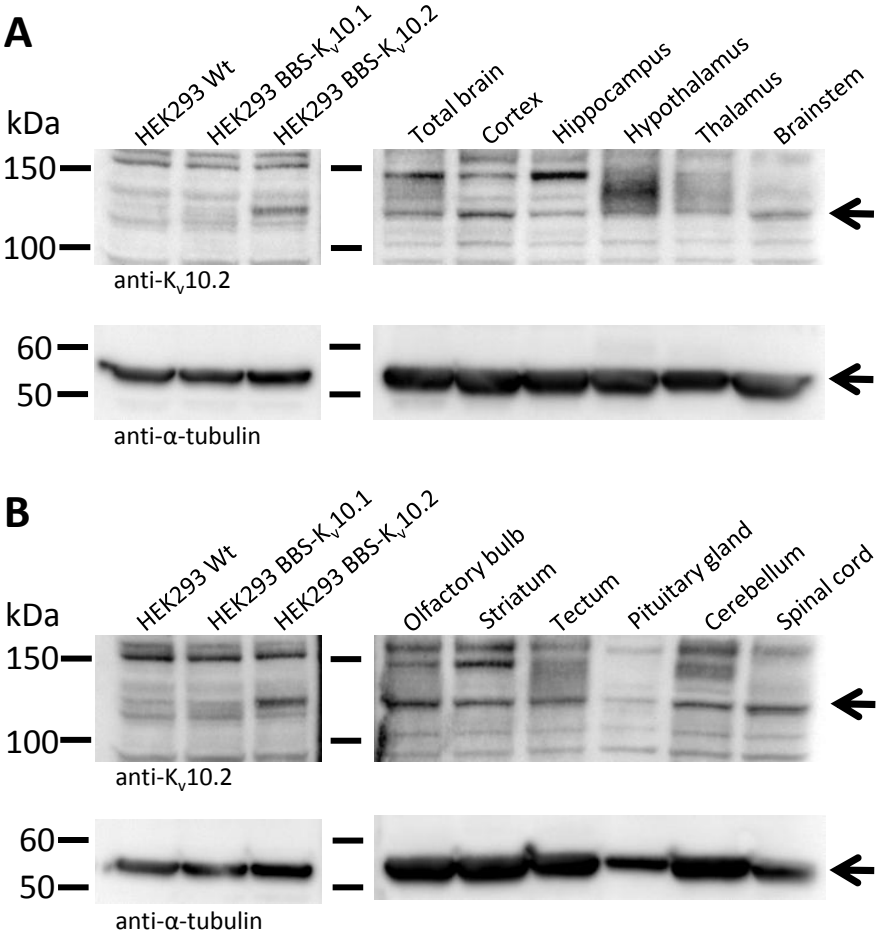

Figure 26: Western blot analysis with anti-K_v10.2 antibody of brain regions of the *Kcnh1* complete knockout mouse

A: Western blot analysis with anti-K_v10.2 antibody of adult homozygous *Kcnh1* total mouse total brain, cortex, hippocampus, hypothalamus, thalamus and brainstem. Protein of the predicted molecular weight of K_v10.2 (=112 kDa) was detected in all brain regions investigated. **B:** Western blot analysis with anti-K_v10.2 antibody of adult homozygous *Kcnh1* total knockout mouse olfactory bulb, striatum, tectum, pituitary gland, cerebellum and spinal cord with anti-K_v10.2 antibody. Protein of the predicted molecular weight of K_v10.2 (=112 kDa) was detected in all regions investigated. **A,B:** Equal protein loading was determined by anti-α-tubulin (arrows). HEK293 Wt and HEK293 BBS-K_v10.1 cell lysates served as negative and HEK293 BBS-K_v10.2 as positive controls. A protein of the predicted molecular weight of BBS-K_v10.2 (=116 kDa) was detected only in HEK293 BBS-K_v10.2 lysates. Arrows indicate approximate weight of BBS-K_v10.2 (=116 kDa) overexpressed in HEK293 BBS-K_v10.2 cells.

In summary, the investigation of the K_v10.2 expression in *Kcnh1* total knockout mouse did not show a clear upregulation of the protein detected by the anti-K_v10.2 antibody due to the loss of K_v10.1. Furthermore, detection by anti-K_v10.2 antibody did not result in a regional difference of K_v10.2 expression.

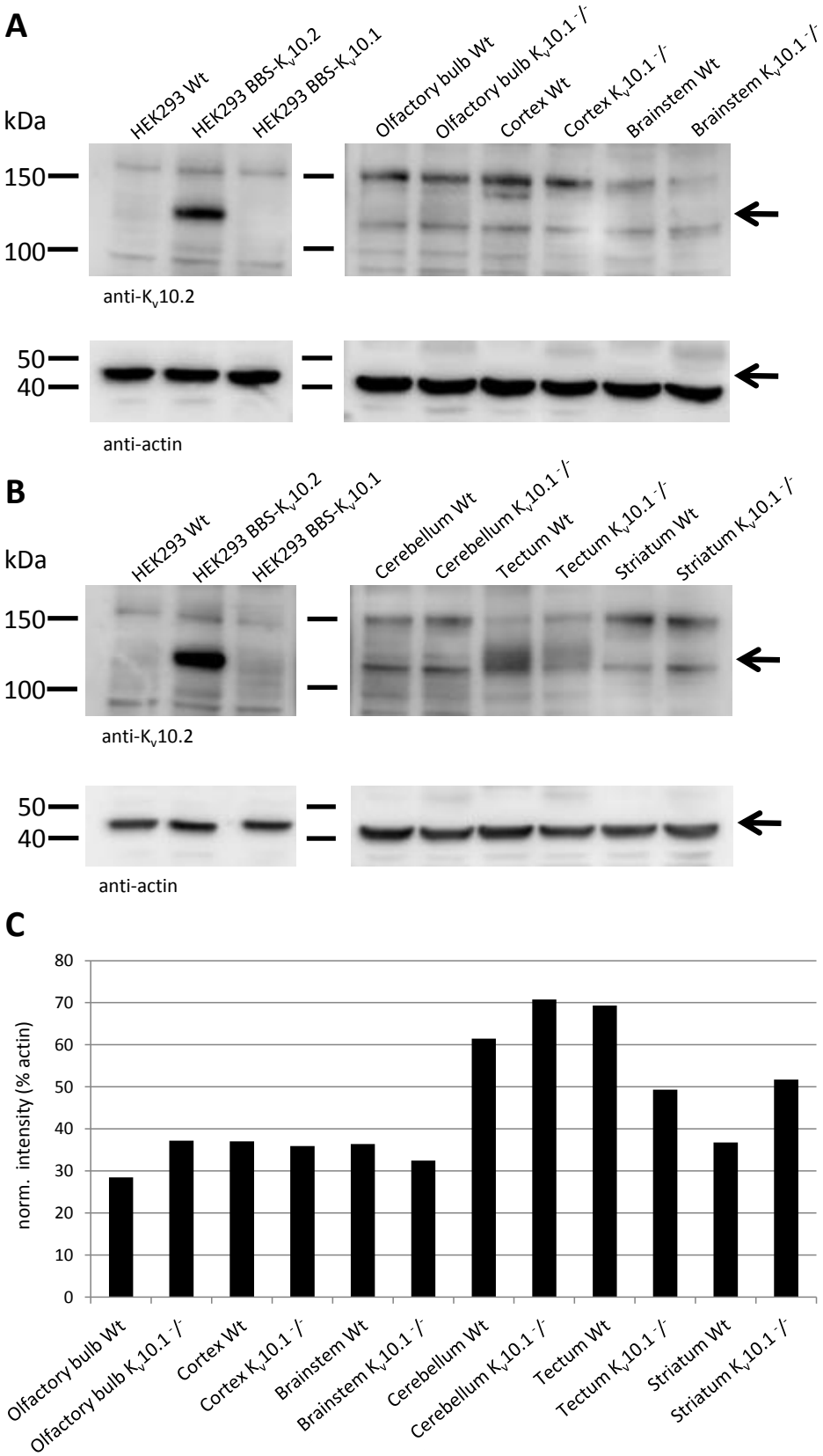

Figure 27: Western blot analysis with anti-K_v10.2 antibody of brain regions of the homozygous *Kcnh1* total knockout mouse compared to Wt mouse

A: Protein lysates of adult mouse olfactory bulb, cortex and brainstem of Wt and homozygous *Kcnh1* total knockout mouse ($K_v10^{-/-}$) were immunoblotted and analyzed for K_v10.2 expression with the anti-K_v10.2 antibody. No obvious differences of protein levels of K_v10.2 in Wt and K_v10.1 deficient mouse were ascertained. **B:** Protein lysates of adult mouse cerebellum, tectum and striatum of Wt and

homozygous *Kcnh1* deficient mouse ($K_v10.1^{-/-}$) were immunoblotted and analyzed for $K_v10.2$ expression with the anti-$K_v10.2$ antibody. No obvious differences of protein levels of $K_v10.2$ in Wt and $K_v10.1$ deficient mouse were found. **A,B:** Equal protein loading determined by anti-actin revealed no differences in protein loading (arrows). HEK293 Wt and HEK293 BBS-$K_v10.1$ cell lysates served as negative and HEK293 BBS-$K_v10.2$ as positive controls. A protein of the predicted molecular weight of BBS-$K_v10.2$ (=116 kDa) was detected only in HEK293 BBS-$K_v10.2$ lysates. Arrows indicate approximate weight of BBS-$K_v10.2$ (=116 kDa) overexpressed in HEK293 BBS-$K_v10.2$ cells. **C:** Densitometric analysis of $K_v10.2$ protein expression in different regions of adult Wt and *Kcnh1* total knockout mouse. $K_v10.2$ expression is presented as % of actin. No standard deviation was performed (N=1). Only in the tectum and striatum a difference of $K_v10.2$ protein level between Wt and *Kcnh1* total knockout mouse was observed.

4.5 Investigation of a possible physiological function of $K_v10.2$

4.5.1 LoxP construct of *Kcnh5* conditional knockout mouse was non-functional

In order to address the physiological function of *Kcnh5* and to avoid the embryonic lethality, we decided to use a conditional knockout mouse. Therefore, our lab generated a floxed *Kcnh5* mouse. This mouse possessed loxP sites flanking the exon 7 of *Kcnh5*. Cross breading of this knockout mouse strain with a Cre-recombinase expressing mouse would result in excision of exon 7 leading to a truncated protein with no channel conducting properties. A Cre-recombinase under the control of the Emx1 promoter was chosen to inactivate *Kcnh5* in the developing and mature neurons of the cortex. Surprisingly, qRT-PCR analysis of cDNA of the adult homozygous *Kcnh5* conditional knockout mouse cortex cross-bred with Emx1-Cre in comparison to Wt mouse cortex resulted in no change of *Kcnh5* expression (Figure 28A). To verify the correct loxP construct and the deletion of exon 7, a genomic DNA amplification of exon 7 with the floxed loxP sites was performed. In the Wt mouse this would result in an amplification product of approximately 950 bp, while a 450 bp amplification product was expected in the conditional knockout mouse lacking exon 7. The PCR performed resulted in amplification of a 950 bp product in the Wt mouse and the homozygous *Kcnh5* conditional knockout, indicating no functional loxP construct in the *Kcnh5* conditional knockout mouse (Figure 28B). Therefore, no conditional *Kcnh5* knockout mouse was available for further analysis or evaluation of the anti-$K_v10.2$ antibody.

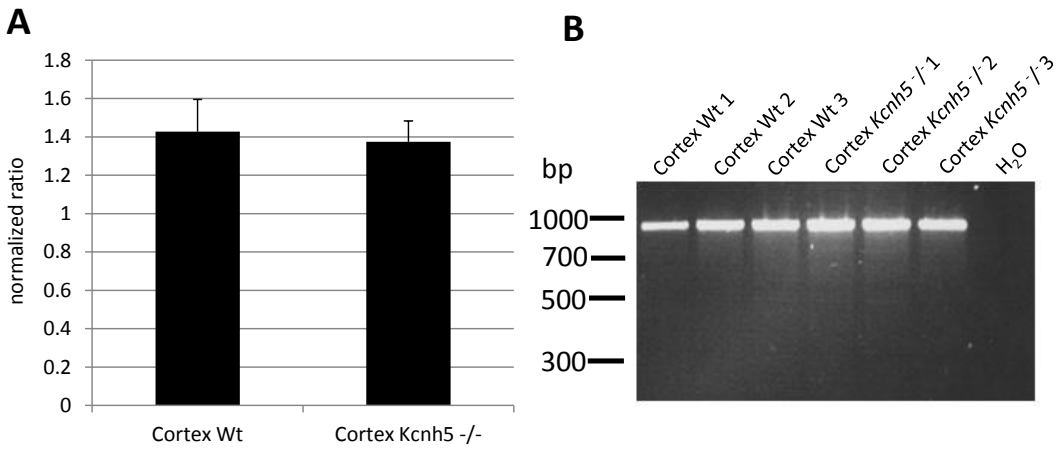

Figure 28: *Kcnh5* mRNA expression the cortex of Wt and homozygous *Kcnh5* conditional knockout mice determined by qRT-PCR and PCR amplification of the genomic loxP construct of Wt and *Kcnh5* conditional knockout mice
A: *Kcnh5* mRNA levels were analyzed by qRT-PCR in homozygous *Kcnh5* conditional knockout mice cross-bred with Emx1-Cre. No difference in *Kcnh5* expression in the homozygous conditional knockout mouse in comparison to Wt mouse was detected. All values were normalized to the total mouse brain calibrator (expression =1, data not shown). **B:** PCR analysis of cDNA of mouse Wt cortex and of homozygous *Kcnh5* conditional knockout mouse cortex cross-bred with Emx1-Cre spanning exon 6 – 8. No genomic alteration was detected after 30 cycles of amplification.

4.5.2 *Kcnh5* is expressed in primary astrocyte cultures

Since no constitutive or conditional *Kcnh5* knockout mouse was available to study the function of K_v10.2 we tried to identify cell lines expressing *Kcnh5* for functional analysis of K_v10.2 *in vitro.* Therefore, we evaluated its mRNA expression in in-house available cell lines derived from the CNS. We further assessed *Kcnh5* expression in primary astrocytic and oligodendrocytic cell cultures prepared from newborn mice.

We investigated neuronal cell lines like Neuro 2a (N2a), 108CC05 and 108CC15. The latter two are clones of a fused mouse neuroblastoma with rat glioma hybrid cell line, which mimic neurons for electrophysiological studies (Prof. Hamprecht, personal communication). In N2a cells no transcripts of *Kcnh1* and *Kcnh5* (Figure 29A) were detected. Both clones, 108CC05 and 108CC15, were also negative for *Kcnh5* and had a low expression of *Kcnh1* compared to our total mouse brain calibrator (Figure 29A). Therefore, we did not find *Kcnh5* transcripts in mouse cell lines derived from glioblastoma. To investigate if *Kcnh5* is expressed in cell lines originating from other neural cell populations, cDNA of the immortalized oligodendrocytic precursor cell line Oli-neu was analyzed by PCR for *Kcnh1* and *Kcnh5* expression. PCR analysis was performed due to the low quantity of cDNA. After 30 cycles of PCR no amplification product of *Kcnh1* or *Kcnh5* was detected (Figure 29B). As a positive control, *Kcnh1* and *Kcnh5*

were successfully amplified in total mouse brain cDNA. Amplification of hypoxanthine phosphoribosyltransferase (*HPRT*) served as an internal control and resulted in comparable levels of Oli-neu cDNA to the mouse total brain cDNA (Figure 29B).

In addition to cell lines, we further obtained two different primary astrocyte cell preparations and *in vitro* differentiated oligodendrocytes from the Cellular Neuroscience Group (Max Planck Institute of Exp. Medicine). These cells were prepared from newborn mice (PN 0) and had a purity of approximately 95% (Sebastian Schmitt, personal communication) and were analyzed by qRT-PCR (Figure 29). We detected a high expression of *Kcnh5* in primary astrocytic cell cultures (Figure 29C). In differentiated primary oligodendrocyte cell cultures, the *Kcnh5* expression was low compared to the mouse brain calibrator (Figure 29C). *Kcnh1* transcripts were also detected in both astrocytic cell cultures, but virtually absent in oligodendrocytes (Figure 29C).

In summary, no transcripts of *Kcnh5* were detected in all the cell lines investigated. Yet, *in vitro* primary astrocyte cultures express *Kcnh5* while differentiated oligodendrocytes derived from PN 0 mice express *Kcnh5* to a lesser extent as compared to total mouse brain cDNA.

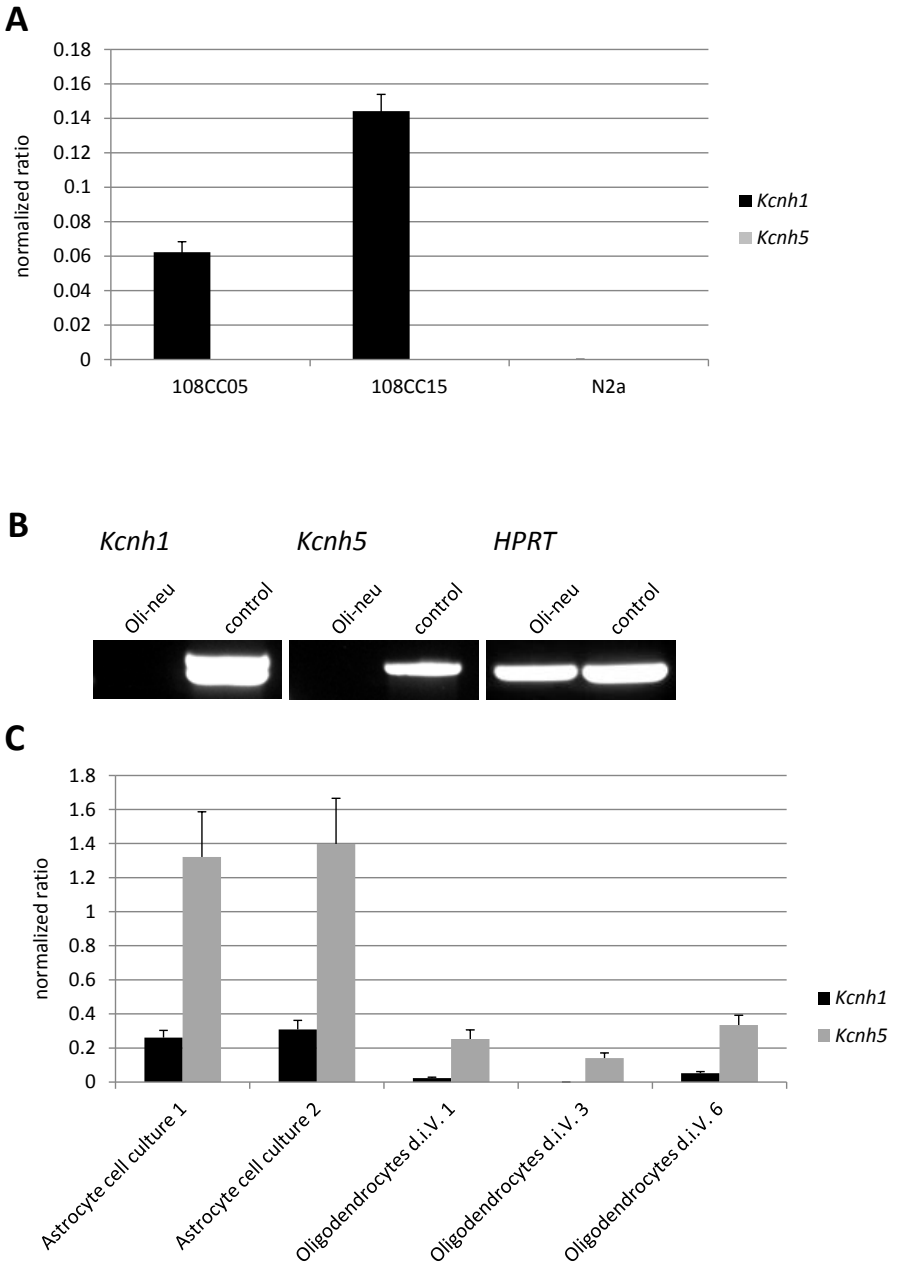

Figure 29: mRNA expression of *Kcnh5* and *Kcnh1* in neural mouse cell lines and in primary astrocytic and differentiated oligodendrocytic cell cultures

A: qRT-PCR analysis of 108CC05 and 108CC15 showed a low *Kcnh1* mRNA expression (black columns) with no detectable *Kcnh5* transcripts (grey columns). N2a cells were negative for both *Kcnh* channels. All values were normalized to the total mouse brain calibrator (expression =1, data not shown). **B:** *Kcnh1* and *Kcnh5* RT-PCR analysis on cDNA from Oli-neu cells resulted in no amplification of either channel. *HPRT* as housekeeping gene indicated equal amount of cDNA in the Oli-neu and control total mouse brain probe. *Kcnh1* and *Kcnh5* were amplified in the control reaction, with total mouse brain cDNA as template. **C:** Two separate astrocyte cell cultures (1 and 2) and differentiated oligodendrocytes were analyzed for *Kcnh1* (black columns) and *Kcnh5* (grey columns) mRNA expression. All values were normalized to the total mouse brain calibrator (expression =1, data not shown). *In vitro* astrocytes express $K_v10.2$ abundantly. Oligodendrocytes cultured are positive for $K_v10.2$ mRNA, in respect to cultured astrocytes and total brain calibrator to a low extend. *Kcnh1* expression is low in primary astrocytes and virtually absent in differentiated oligodendrocytes. d.i.V. = days *in vitro.*

4.6 K_v10.2 protein was shown to preferentially localize to neurons in the mouse brain

We demonstrated that *in vitro Kcnh5* is expressed on the mRNA level in primary cultured astrocytes. Therefore, we further wanted to unravel, if the channel is also expressed in astrocytes in the mouse brain. To do so, IHC analysis with anti-K_v10.2 antibody was performed on vibratome brain sections of transgenic heterozygous GFEA mice, which have human GFAP-driven expression of enhanced green fluorescent protein (eGFP) in astrocytes. In the cortex, no overlapping expression of K_v10.2 and eGFP positive cells was observed (Figure 30A-C). In the cerebellum, K_v10.2 did not co-localize with the majority of eGFP positive cells (Figure 30D-F, arrows F). This indicates that K_v10.2 is not expressed in astrocytes of the cortex as well as in the majority of astrocytes of the cerebellum of the adult mouse. The negative control performed with secondary Alexa-633 conjugated anti-rabbit antibody only resulted in no positive signal (Figure 30G-I).

To further investigate the localization of K_v10.2 to specific cell populations of the brain, we used the anti-K_v10.2 antibody in IHC on sagittial vibratome sections of transgenic heterozygous TYFF mice, which have thy1-driven expression of enhanced yellow fluorescent protein (eYFP) in neurons. There, the IHC showed localization of K_v10.2 to neurons of the middle layers of the mouse cortex (Figure 31A-C, arrows). Results obtained from IHC on TYFF cerebellar sections suggest a K_v10.2 localization to the soma and cell membrane of the Purkinje layer (Figure 31D-F, arrows). Within the hippocampus, results of the IHC analysis indicates that K_v10.2 localizes to the soma and to the membrane of eYFP positive neurons (Figure 31G-I, arrows). In the analyzed brain regions, especially in the cortex, only few cells were eYFP positive, suggesting not all neurons expressed eYFP. The negative control, performed with secondary Alexa-633 conjugated anti-rabbit antibody on cortical mouse brain section of eYFP positive neurons (Figure 31J-L), resulted in no signal. The negative controls of the hippocampus and the cerebellum are shown in the appendix section.

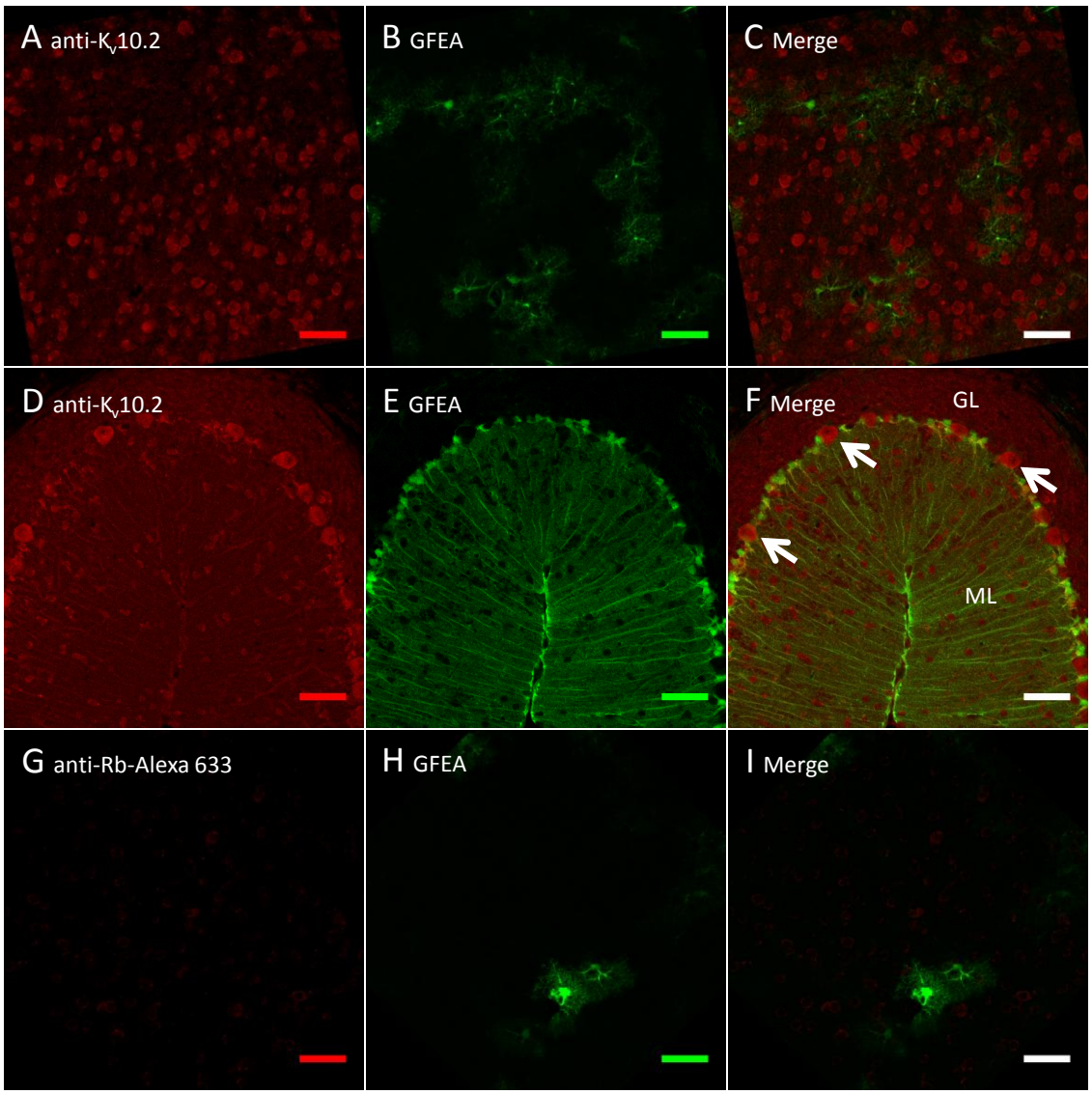

Figure 30: IHC analysis with anti-K_v10.2 antibody in cortex and cerebellum of transgenic heterozygous GFEA mouse brain

Flourescent IHC analysis of transgenic heterozygous GFEA sagittal vibratome sections of mouse cortex and cerebellum performed with anti-K_v10.2 antibody. **A-C:** Cortex: (**A**) Staining obtained by anti-K_v10.2 antibody in (**B**) cortical section with eGFP positive astrocytes. (**C**) No co-localization of eGFP positive cells and K_v10.2 was observed. **D-F:** Cerebellum: (**D**) K_v10.2 staining in (**E**) cerebellar section with eGFP positive astrocytes resulted (**F**) in a small population of K_v10.2 positive astrocytes**.** K_v10.2 positive cells were detected in the Purkinje layer (**F**, arrows) and in the granular layer (GL). (ML = molecular layer). **G-I:** Cortex: IHC performed (**G**) with Alexa-633 conjugated secondary anti-rabbit antibody only, serving as negative control, in (**H**) cortical section with eGFP positive astrocyte mouse brain sections, resulted in (**I**) no specific staining. **A-I**: Sagittal vibratome sections were obtained at 25 µm. Scale bar represents 50 µm.

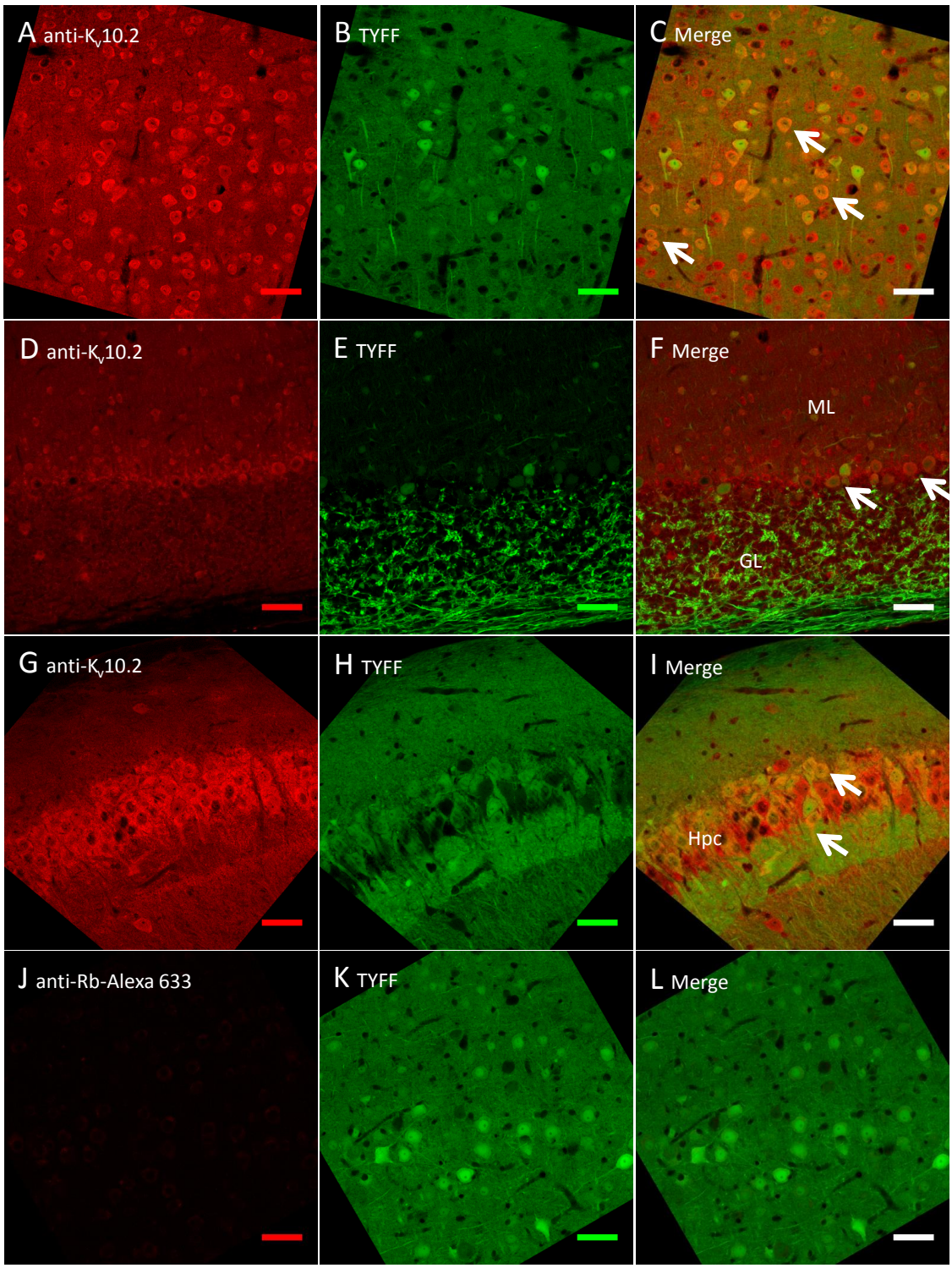

Figure 31: IHC analysis with anti-K_v10.2 in selected brain regions of transgenic heterozygous TYFF mouse

IHC analysis of heterozygous transgenic TYFF sagittal section of mouse cortex, hippocampus and cerebellum performed with anti-K_v10.2 antibody. **A-C:** Cortex: (**A**) Staining obtained by anti-K_v10.2 antibody in (**B**) section of the cortex with eYFP positive neurons (**C**, arrows) suggests a localization of K_v10.2 to the soma and the membrane of neurons. **D-F:** Cerebellum: (**D**) K_v10.2 staining of (**E**) cerebellar section with eYFP positive neurons indicating (**F**, arrows) a soma and membrane localization of K_v10.2 in the Purkinje layer. Few cells were K_v10.2 positive in the molecular layer (ML) and the granular layer (GL) (**F**). **G-I:** Hippocampus (Hpc): (**G**) K_v10.2 expressing cells and (**E**) eYFP positive neurons of the hippocampus were co-localizing (**I**). The staining suggests a localization of K_v10.2 to the soma, membrane and projections of neurons (**I**, arrows). **G-F:** Cortex: (**G**) IHC performed with Alexa-633

conjugated secondary anti-rabbit antibody only, serving as negative control, in (**H**) cortical section with eGFP positive astrocyte mouse brain sections, resulted in (**I**) no specific staining. (**L**)**. A-L:** Sagittal vibratome sections were obtained at 25 µm. Scale bar represents 50 µm.

In order to further analyze K_v10.2 expression in other cell types of the CNS, we performed IHC on transgenic heterozygous CXCR mice, which have CX3CR1-driven expression of enhanced green fluorescent protein (eGFP) in microglia. K_v10.2 did not co-localize to CX3CR1 positive microglia in the cortex (Figure 32A-C), cerebellum (Figure 32D-F) and the hippocampus (Figure 32G-I) of CXCR mice. All K_v10.2 expressing cells were morphologically different than eGFP positive microglia. The negative control, performed with secondary antibody Alexa-633 on cortical mouse brain section sections of CXCR mice (Figure 32H-J), resulted in no specific signal. For negative controls of the hippocampus and the cerebellum with secondary Alexa-633 conjugated anti-rabbit antibody only see appendix.

In summary, K_v10.2 protein was shown to localize preferentially to neurons in cortex, hippocampus and cerebellum of the adult mouse brain.

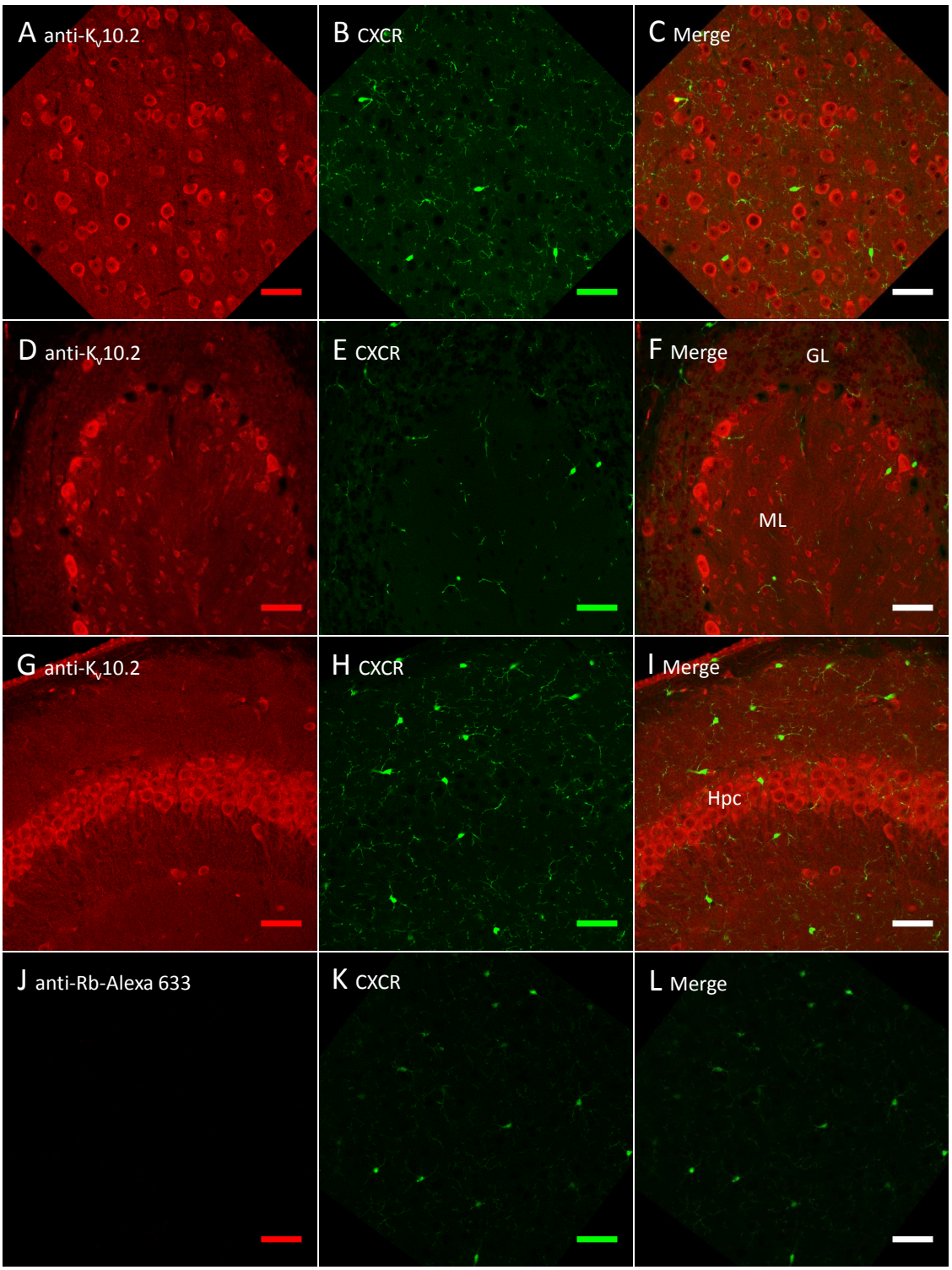

Figure 32: IHC analysis with anti-K_v10.2 antibody in selected brain regions of heterozygous transgenic CXCR mouse

IHC analysis of heterozygous transgenic CXCR sagittial mouse sections performed with anti-K_v10.2 antibody. **A-C:** Cortex: (**A**) Staining obtained by anti-K_v10.2 antibody in (**B**) cortex with eGFP positive microglia (**C**) showed no co-localization. **D-F:** Cerebellum: (**D**) K_v10.2 immunoreactive cells and (**E**) eGFP positive microglia of the cerebellum (**F**) were not co-localization. **G-I:** Hippocampus (Hpc): (**G**) K_v10.2 expressing cells and (**H**) eGFP positive microglia of the hippocampus showed (**I**) no co-localization. **J-L:** Cortex: **(J)** Negative control cortical section with secondary Alexa-633 conjugated anti-rabbit antibody only on (**K**) eGFP positive microglia resulted in no specific staining (**L**). **A-L:** Sagittal vibratome sections were obtained at 25 µm. Scale bar represents 50 µm.

4.7 The anti-K_v10.2 antibody recognized a cilia-like structure

So far, we were able to show, that the anti-K_v10.2 antibody only labeled neurons in the investigated regions of the mouse brain. To further localize the cellular localization of K_v10.2, we performed chromogenic IHC analysis of lung and liver sections of the adult mouse. As shown in Figure 33, we found only a weak staining of lung epithelial cells. Interestingly, staining of cilia-like protrusions of the cells was observed (Figure 33A, arrows). The structure recognized by the anti-K_v10.2 antibody had a high similarity with the structures detected when applying an anti-acetylated tubulin antibody in IHC (Figure 33C, arrows). The anti-acetylated tubulin is reported marker, besides others, of cilia and the primary cilium of every cell (Alieva et al., 1999).

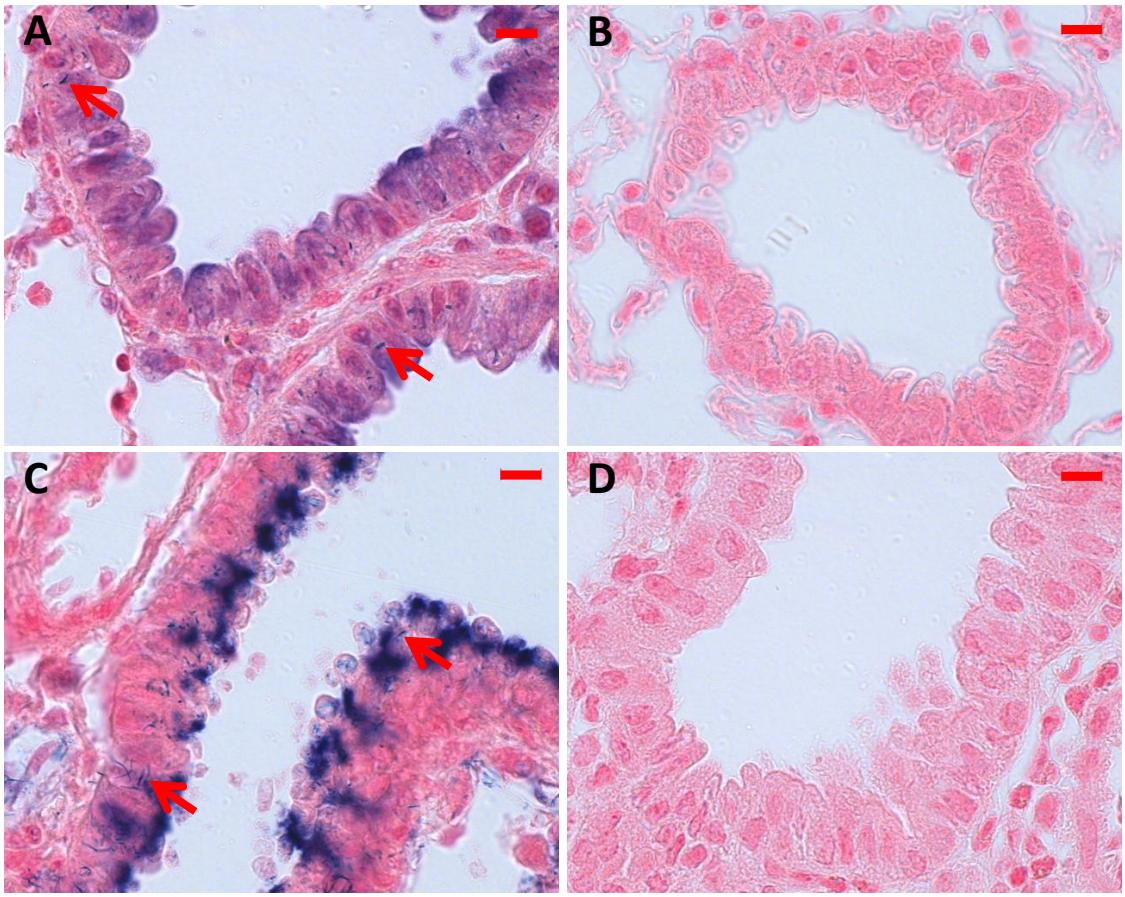

Figure 33: Anti-K_v10.2 antibody recognizes cilia-like cellular protrusion in epithelial cells of mouse lung by IHC analysis
A: Chromogenic IHC analysis of mouse lung sections performed with anti-K_v10.2 antibody (NBT/BCIP, blue) resulted in a staining of epithelial cells and of a cilia-like structure (red arrows). **B:** Negative control, consisting of the HRP conjugated secondary anti-rabbit antibody and the detection system, showed no staining. **C:** IHC analysis of mouse lung sections performed with anti-acetylated tubulin antibody (NBT/BCIP, blue) resulted in a staining of epithelial cells and a cilia-like structure similar to the structure detected by anti-K_v10.2 antibody (red arrows). **D:** Negative control, consisting of the secondary HRP conjugated anti-mouse antibody and the detection system, showed no staining. **A-D:** Sections were counterstained with NFR. Paraffin sections obtained at 7 µm. Scale bar represents 10 µm.

After detection of this cilia-like structure in lung sections with the anti-K_v10.2 antibody, we wanted to perform further IHC analysis to investigate if the anti-K_v10.2 antibody also recognizes the cilia of cells of different tissue. Hence, we analyzed liver sections by IHC. Cells of the liver only have one cilium, which is the primary cilium. Again, we observed staining of cilia-like protrusions of the cells (Figure 34A, arrows), which were similar to the staining obtained when using the anti-acetylated tubulin antibody (Figure 34C, arrows). Therefore, this finding suggests, that the anti-K_v10.2 antibody might stain in IHC analysis a structure corresponding to the primary cilium.

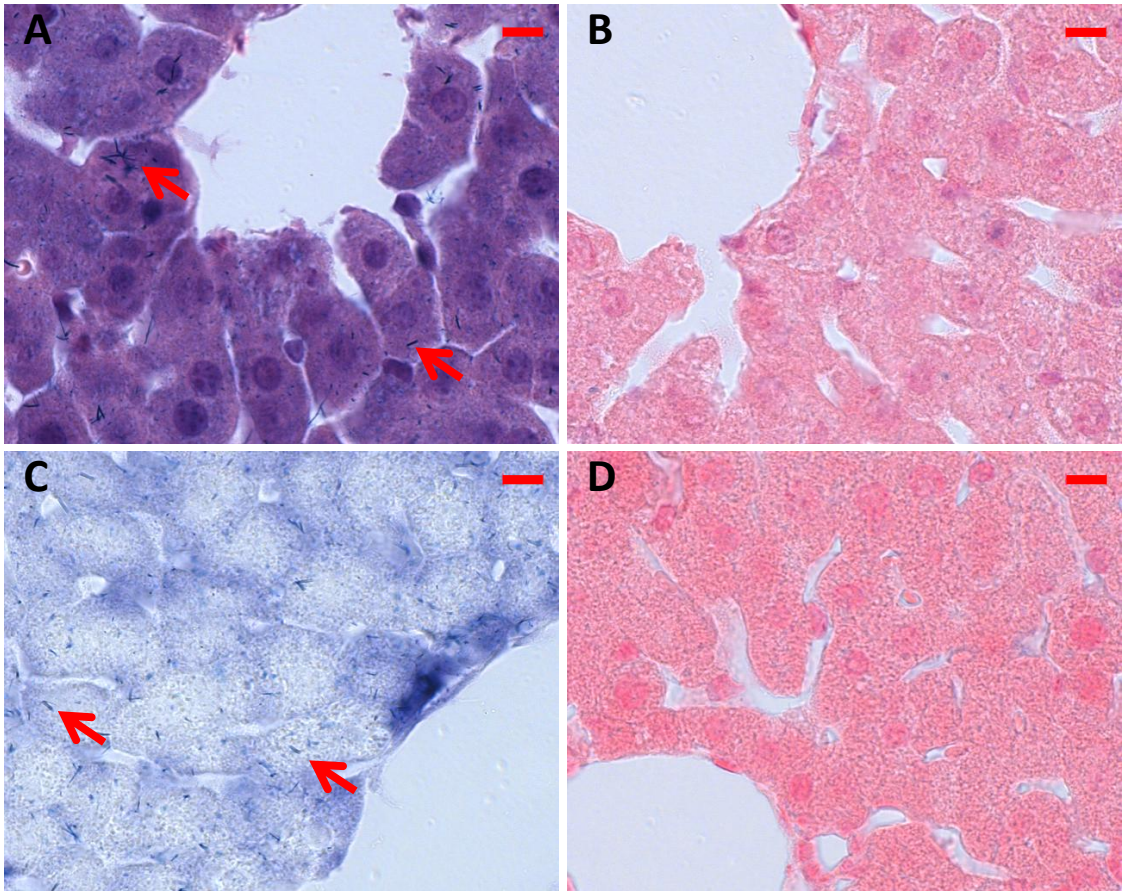

Figure 34: Anti-K_v10.2 antibody recognizes cilia-like cellular protrusion in mouse liver by IHC analysis
A: Chromogenic IHC analysis of mouse liver sections performed with anti-K_v10.2 antibody (NBT/BCIP, blue) resulted in a staining of a cilia-like structure (arrows). **B:** Negative control, consisting of the secondary HRP conjugated anti-rabbit antibody and the detection system, showed no staining. **C:** Chromogenic IHC analysis of mouse liver sections performed with anti-acetylated tubulin antibody (NBT/BCIP, blue) resulted in a staining of a cilia-like structure similar to the structure detected by anti-K_v10.2 antibody (arrows). **D:** Negative control, consisting of the secondary HRP conjugated anti-mouse antibody and the detection system, showed no staining. **A-D:** Sections were counterstained with NFR. Paraffin sections obtained at 7 µm. Scale bar represents 10 µm.

Further chromogenic IHC analysis on mouse brain sections resulted in stained cilia-like protrusions of the cells in the mouse cortex and cerebellum (Figure 35A,C, arrows). These cilia-like structures were highly similar with the structures we detected when applying the antibody

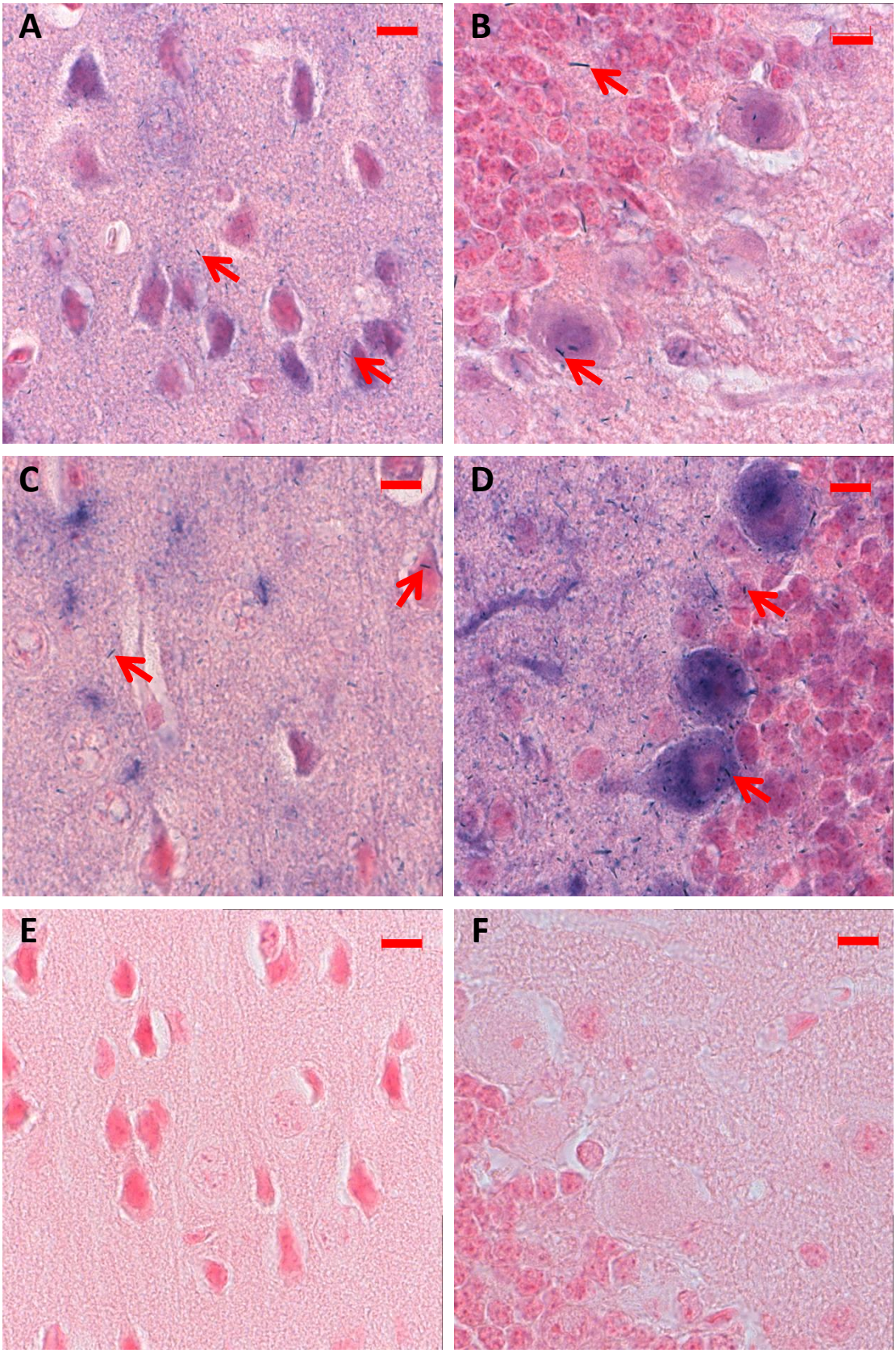

Figure 35: Anti-K_v10.2 antibody recognizes cilia-like structures in mouse cortex and cerebellum by IHC analysis

A: Chromogenic IHC analysis of mouse cortical section performed with anti-K_v10.2 antibody (NBT/BCIP, blue) resulted in a staining of a cilia-like structure (arrows). **B:** IHC analysis of the cerebellum of mouse performed with anti-K_v10.2 antibody (NBT/BCIP, blue) resulted in a staining of a cilia-like structure (red

arrows). **C:** IHC analysis of mouse cortical section performed with anti-adenylyl cyclase III (ACIII) antibody (NBT/BCIP, blue) resulted in a staining of a cilia-like structure similar to the structure detected by anti-K_v10.2 antibody (arrows). **D:** IHC analysis of mouse cortical section performed with anti-ACIII antibody (NBT/BCIP, blue) resulted in a staining of a cilia-like structure similar to the structure detected by anti-K_v10.2 antibody (arrows). **E:** Negative control of cortex section, consisting of the secondary HRP conjugated anti-rabbit antibody and the detection system, showed no staining. **F:** Negative control of the cerebellum, consisting of the secondary HRP conjugated anti-rabbit antibody and the detection system, showed no staining. **A-F:** Sections were counterstained with NFR. Paraffin sections obtained at 7 µm. Scale bar represents 10 µm.

anti-adenylyl cyclase III (ACIII) in IHC analysis of the same regions (Figure 35C,D arrows). ACIII is a known marker for primary cilia of the cells of the brain (Bishop et al., 2007). Comparing the staining pattern obtained by the antibody against acetylated tubulin and ACIII with the staining obtained by our antibody we found that the anti-K_v10.2 antibody recognizes a similar structure. This probably suggests a potential localization of K_v10.2 in cilia and to the primary cilium. However, this finding obviously needs to be analyzed in more detail in further studies.

5 Discussion

The aim of the present study was to analyze the K_v10.2 protein expression pattern in mice, to localize K_v10.2 in different cells of the CNS and to unravel K_v10.2 temporal expression during embryogenesis. Due to a lack of commercially available antibodies specific to K_v10.2, we generated and evaluated a novel polyclonal antibody directed against K_v10.2. The expression pattern of K_v10.2 in mouse tissue detected with the novel anti-K_v10.2 antibody in Western blot revealed a virtually ubiquitious K_v10.2 distribution. Studies of K_v10.2 distribution in the mouse brain with this antibody by IHC showed an expression of K_v10.2 in specific brain regions and indicated localization to neurons. Furthermore, the novel antibody anti-K_v10.2 detected a cellular structure similar to a cilium on mouse tissue such as brain, lung and liver.

5.1 Strategy to generate a novel anti-K_v10.2 antibody

We successfully generated an anti-K_v10.2 antibody that detected K_v10.2 in Western blot and ICC analysis. Since none of the commercially available antibodies were shown to be specific for K_v10.2 detection, we applied the best possible strategy to obtain an antibody that specifically recognizes K_v10.2. We chose to generate a polyclonal antibody by using a 299 amino acid (aa) long antigen, which is well in excess of the 12-20 aa needed for a peptide to function as an immunogen (Tanaka et al., 1985, Takahashi et al., 2004, Gupta et al., 2007). The 299 aa long antigen successfully exhibited immunogenicity in rabbits and contained various potential epitopes. For antigen synthesis we used prokaryotic expression in *E.coli*, which is a cost and time effective system and a widespread source of immunogens. It has been used for expression of either large fragments or full-length proteins (Wojciechowski et al., 2004, Lindskog et al., 2005, Nilsson et al., 2005). The optimization of the *E.coli* protein expression necessary to gain sufficient quantities of the antigen for vaccination led to an enrichment of the expressed protein in inclusion bodies, which has been reported for other highly expressed proteins in *E.coli* (Kane and Hartley, 1988, Fahnert et al., 2004).

Polyclonal antibodies are known to be less likely affected by conformational changes of epitopes because of the heterogeneity of polyclonal antibodies, which allows them to bind to different epitopes (Cooper and Paterson, 2001, Nakazawa et al., 2010). However, as we showed by Western blot analysis, the anti-K_v10.2 antibody detected proteins of various

molecular weights, indicating the recognition of different epitopes other than K_v10.2. The heterogeneity of the polyclonal anti-K_v10.2 antibody might have increased the sensitivity of K_v10.2 detection by recognizing different epitopes of K_v10.2.

While our strategy resulted in generation of an antibody capable of recognizing a protein of the molecular weight of K_v10.2 and of discriminating between K_v10.1 and Kv10.2, all commercially available anti-K_v10.2 antibodies that were evaluated showed no specificity for K_v10.2. They were either not sensitive enough to recognize a protein of the molecular weight of K_v10.2 or they cross reacted with another protein of the same molecular weight, possibly K_v10.1. The most plausible cause for their lack of specificity towards K_v10.2 might be the selection of the antigen sequence used for immunization, since K_v10.1 and K_v10.2 share an extensive homology throughout the entire amino acid sequence. Therefore, we selected a low or non-homologous region for the antigen used for immunization. Only two companies, Sigma-Aldrich and Alomone Labs, provide the peptide sequences that were used as antigens. BLAST analysis of these two epitopes, however, did not detect homology with K_v10.1 (data not shown). Despite the fact that the amino acid sequences of the antigen did not show homology with K_v10.1, they recognized a protein of the same molecular weight as K_v10.1 in lysates of K_v10.1 overexpressing cells, but not in the HEK293 Wt sample. Additionally, the Sigma anti-K_v10.2 antibody was considered “uncertain” by the Human Protein Atlas (Uhlen et al., 2005, Uhlen et al., 2010), when used in IHC analysis.

Therefore, published data obtained with the commercial anti-K_v10.2 antibodies should be treated with caution. Some publications exist using the Alomone Labs (Wadhwa et al., 2009) and Sigma-Aldrich (Huang et al., 2012) antibodies in IHC. Wadhwa and co-workers analyzed the K_v10.2 distribution in renal cell carcinoma by IHC, which resulted in the observation of aberrant K_v10.2 levels in cancerous tissue. In the context of diseases, Huang and colleagues indicated an upregulation of K_v10.2 expression in medullablastomas (Huang et al., 2012). Jeng and colleagues showed a localization of K_v10.2 in hippocampal neurons, which will be discussed later (Jeng et al., 2005).

5.2 Aspects of antibody evaluation

The newly generated anti-K_v10.2 antibody recognized K_v10.2 and did not cross react with K_v10.1 in Western blot analysis and ICC, which was validated by the use of HEK293 cells overexpressing human BBS-tagged K_v10.1 and K_v10.2.

The evaluation of novel antibodies on overexpressing cell lines is a reasonable approach for the investigation of the antibody binding capacity to its antigen. This system has already been applied for the evaluation of Eag1.62.mAb, an antibody targeting K_v10.1 (Hemmerlein et al., 2006). Furthermore, this system allowed us to demonstrate that the novel anti-K_v10.2 antibody discriminates between K_v10.2 and K_v10.1. This was important, since K_v10.2 and K_v10.1 share a high similarity in their entire amino acid sequence and are therefore likely to contain identical epitopes recognizable by antibodies raised against these ion channels. Our aim was to analyse K_v10.2 distibution in mouse, therefor the use of a human cell system overexpressing the human full-length proteins for antibody evaluation only indicates specificity of the antibody to mouse K_v10.2.

In order to verify the newly generated antibody the indirect ELISA system was used, which showed a strong binding to its antigen and a weak cross reactivity with H1X, a K_v10.1 fusion protein. Despite this low cross reactivity detected by ELISA we further evaluated the antibody using the HEK293 system in Western blot and ICC analysis.

It was not possible to use transgenic K_v10.2 knockout animals to investigate the antibody's specificity because K_v10.2 homozygous total knockout mice are embryonic lethal. The transgenic conditional K_v10.2 knockout mouse developed in our department could also not be applied since it did not result in genomic deletion of *Kcnh5* when crossbred with the Emx1-Cre-mouse line. By evaluation of the anti-K_v10.2 antibody in tissue samples containing the protein (Wt animal) in parallel to tissue where the K_v10.2 is deleted (transgenic knockout animal) we would be able to reach the highest certainty about the specificity of the antibody as reported for other antibodies (Pereira et al., 1996, Pradidarcheep et al., 2008).

Blocking experiments are also a useful tool to evaluate the specificity of an antibody. However, such experiments were not possible to be performed. The antigen expressed was only soluble when buffered in guanidinium hydrochloride (GuHCl), a strong denaturizing agent. Since GuHCl is known to inhibit protein activity in low concentrations (West et al., 1997, Ren et al., 2009), a preincubation of the antibody with the antigen (antibody blocking) buffered in this reagent, prior to immunoassays, would have denatured the antibody. A positive result of the blocking experiment, meaning no binding of the antibody is detectable, might be either due to a successful blocking of the antibody with its antigen or due to antibody denaturation in the presence of GuHCl in the antigen buffer. Therefore, the result would have been ambiguous.

Evaluation of the antibody specificity by Western blot analysis showed a protein band of the predicted size of K_v10.2 in lysates of the transfected HEK293 BBS-K_v10.2 cell line and

mouse brain, as well as virtually all mouse tissue investigated. Most likely, the antibody reacts with K_v10.2. However, it also recognized proteins of different molecular weight, e.g. at 90 kDa and at 150 kDa. Since no *Kcnh5* transcripts were detected in the HEK293 wt and BBS-K_v10.1 cell lines, the proteins of different molecular weight recognized by the anti-K_v10.2 antibody indicate either unspecific binding, or could represent splice forms of *Kcnh5*, which were not found by our qRT-PCR analysis. The phenomenon has also been seen for the rabbit polyclonal anti-K_v10.1 antibody 9391. K_v10.1 has at least two different splice variants that correspond to the 70 and 50 kDa band and were detected by the K_v10.1 antibody (unpublished data). Nevertheless, the anti-K_v10.2 antibody proved suitable for our aim of investigating the K_v10.2 protein distribution, since it did not recognize other proteins at the molecular weight of K_v10.2 in HEK293 cells, and therefore did not interfere with our analysis. Furthermore, in the mouse total brain sample a band at the approximate molecular weight of K_v10.2 was indeed detected, indicating its ability to recognize mouse K_v10.2.

The specificity of the anti-K_v10.2 antibody was demonstrated in ICC studies by the intracellular and membrane staining we observed in HEK293 BBS-K_v10.2 cells. This staining pattern is consistent with the ICC results of an anti-K_v10.1 antibody in HEK293 BBS-K_v10.1 cells, which also showed an intracellular and membrane staining (Kohl et al., 2011). Not all HEK293 BBS-K_v10.2 cells were K_v10.2 positive due to the properties of the polyclonal stable cell line. In contrast, native HEK293 cells and those transfected with BBS-K_v10.1 showed no immunoreactivity with the anti-K_v10.2 antibody.

The Western blot analysis detected proteins of different molecular weight while the ICC resulted in immunoreactivity in HEK293 BBS-K_v10.2 only. Therefore, the antibody may be considered more specific in ICC procedures than in Western blot analysis. A possible explanation for this discrepancy could be the difference between the techniques. Western blot analysis is performed with denatured samples, hence more epitopes become accessible to the antibody, as reported for other proteins (Garcia-Barreno et al., 2005), while conformation-dependent epitopes can disappear by denaturation (Morris, 2007). Denatured epitopes did not affect the binding of the anti-K_v10.2 antibody to K_v10.2 in Western blotting. In contrast, in ICC the proteins retain their native structure and protein complexes are maintained. Furthermore, accessibility of epitopes may not be accessible due to the fixative.

5.3 Distribution of K_v10.2 protein in mouse tissues

Since expression analysis of K_v10.2 protein has not yet been performed throughout the mouse system, this study assessed the distribution of *Kcnh5* on the mRNA and protein level in order to investigate the region-specific expression. In general, a wide K_v10.2 expression on protein level and a more restricted mRNA distribution was observed the organs investigated. Furthermore, a possible posttranslational modification was detected in certain brain regions.

The *Kcnh5* mRNA distribution pattern obtained by qRT-PCR with probes from adult mouse brain regions is in general accordance with reported data obtained by quantitative ISH on mouse brain sections reported in the Allen Brain Atlas (Lein et al., 2007) and by Northern blot analysis performed on adult rat brain tissue (Ludwig et al., 2000). The only difference occurred in the striatum, where Ludwig and co-workers did not detect transcripts of *Kcnh5* in rat (Ludwig et al., 2000). In accordance with our results, data of the Allen Brain Atlas also show a *Kcnh5* expression in the striatum of the mouse. The differences in the results might reflect variations between different mRNA detection methods, such as qRT-PCR and ISH.

It is worth noting, that with the approaches available, we show the antibody's functionality in Western blot and its specificity in ICC. As the most reliable control, i.e. K_v10.2 knockout tissue, was not available for testing, we can only have a certain degree of confidence that the antibody specifically recognizes K_v10.2. The following discussion is based on the assumption that the results obtained with the anti-K_v10.2 antibody reflect genuine K_v10.2 recognition by the anti-K_v10.2 antibody.

The data we obtained from Western blot analysis of the hypothalamus, thalamus, tectum and olfactory bulb using the anti-K_v10.2 antibody differed to the pattern we detected with other tissues. In these four samples a diffuse band in the range of 120 – 150 kDa was visible. The fact that this diffuse band is larger than the expected molecular weight excludes it as a degraded form of K_v10.2. One explanation for this could be unspecific binding of the antibody to a protein within this range in these four brain regions. Alternatively, in the case of specific binding to K_v10.2, this indicates a possible posttranslational modification of this protein in the hypothalamus, thalamus, tectum and olfactory bulb *in vivo*. *In vitro*, the human K_v10.2 is reported not to be glycosylated (Ju and Wray, 2002). For the homologous K_v10.1 it has been shown *in vivo* that posttranslational modification occurs (Napp et al., 2005). Considering the high sequence homology of K_v10.1 and K_v10.2, the latter might also be

glycosylated *in vivo*. Wether or not K_v10.2 is posttranslationally modified needs to be clarified by future experiments.

While the regional K_v10.2 protein distribution, especially in mouse brain, is in general accordance with the *Kcnh5* mRNA distribution demonstrated here, inconsistencies were observed in some tissues. Examples are the prostate, heart and intestine, where Western blot analysis from adult mouse tissues revealed the presence of K_v10.2, whereas only very low or no mRNA was detected. The reasons for this divergence are not clear, but such a difference of protein and mRNA level has already been shown for K_v10.1. Martin and co-workers investigated the protein distribution in rat brain sections (Martin et al., 2008) which did not match the patterns obtained by ISH in former publications (Ludwig et al., 2000, Saganich et al., 2001). One possibility is that the K_v10.1 protein "*in vivo* half-lives [may be altered] as the result of varied protein synthesis and degradation" (Martin et al., 2008), which may apply for K_v10.2. The synthesis and degradation of a specific protein might be tissue dependent. Additionally, the mRNA *in vivo* half-life might be differentially regulated within different tissues. A low copy, non-degraded mRNA may still lead to protein translation detectable by Western blot analysis. Another explanation for the discrepancy of protein and mRNA level might be due to the K_v10.2 detection methods applied. For our qRT-PCR we applied primers in exon 8 and 9, while our anti-K_v10.2 antibody targets the C-terminus, which is encoded by exon 11 in mouse. Although the reported alternatively spliced versions of K_v10.2 have a truncated C-terminus (Saganich et al., 1999, Ju and Wray, 2002), further isoforms or tissue specific isoforms might exist. For K_v10.1, alternatively spliced variants were detected that contain the C-terminus but not the pore domain (unpublished data). To resolve the discrepancy of the observed *Kcnh5* mRNA and protein levels, a future experiment might be to design qRT-PCR primers for the exon 11 of mouse, thereby detecting the same exon which encodes the antibody's epitope.

The K_v10.2 ubiquitious protein expression in all analyzed tissues of the adult mouse does not allow an interpretation of a possible specific physiological function. Since the channel is ubiquitously expressed throughout the CNS, it could play a role in many putative processes, such as processing of olfaction information (olfactory bulb), emotional information (limbic structures), and many functions related to other CNS structures. Furthermore, K_v10.2 protein is widely expressed throughout adult mouse tissues, further impeding assignment of a physiological function.

5.4 Clarifying the regional K_v10.2 expression

We localized the protein in different nuclei of the brain by IHC, which in general is in accordance with known mRNA expression patterns (Ludwig et al., 2000, Saganich et al., 2001). Specific immunohistochemical staining was obtained in the olfactory bulb, cortex, amygdala, thalamus, zona incerta, globus pallidus, medial genicular nucleus, lateral genicular nucleus, cochlear nucleus of the brainstem, within the hippocampus CA3 and CA2 field and the hilus. Furthermore, the Purkinje layer and the lateral cerebellar dentate nucleus were stained. ISH analysis for *Kcnh1* mRNA distribution overlapps with the protein distribution, while a cellular detection of *Kcnh5* mRNA using ISH failed.

In the regions analyzed by IHC, different patterns of immunostaining were observed. In the cortex, Purkinje layer of the cerebellum, cochlear nucleus of the brainstem, hippocampus and the lateral cerebellar dentate nucleus, the staining indicates a localization of K_v10.2 to the cell soma. In the mitral cell layer of the olfactory bulb and the hippocampus, the soma of the cells, as well as their processes were stained. A neuropil staining was observed in the regions of the olfactory bulb, thalamus, globus pallidus and the amygdala. For the olfactory bulb (Pinching and Powell, 1971), the globus pallidus (Coulter, 1988) and the thalamus (Peden et al., 2008) such a neuropil staining has been already reported, while for other regions it has been speculated that they contain neuropil elements (Chklovskii et al., 2002).

Our results of the IHC for K_v10.2 distribution are in general accordance with the different ISH performed to date (Ludwig et al., 2000, Saganich et al., 2001). Although the data obtained show some incongruences to the two ISH reports, the overlapping results are consistent with our results. Differences were found in the cerebellum in the Purkinje layer, where we detected a weak staining, while no *Kcnh5* mRNA was found by ISH (Ludwig et al., 2000, Saganich et al., 2001). In the cortical layers, the protein distribution seems to be more restricted to the middle layers, which is in accordance with the ISH results by Saganich (Saganich et al., 2001). Both ISH approaches (Ludwig et al., 2000, Saganich et al., 2001), did not detect protein in the globus pallidus, while we observed an intense staining by IHC. This also applies to the Purkinje layer, where we detected a weak K_v10.2 protein expression. In contrast to Ludwig and co-workers' finding, no protein was detected in the dentate gyrus (Ludwig et al., 2000).

Possible reasons for the discrepancy in mRNA and protein detection have already been discussed. Additionally, mRNA positive regions were not stained for K_v10.2 protein in our IHC.

While the underlying cause has not been confirmed yet, this might reflect posttranslational or –transcriptional mechanisms involved in K_v10.2 regulation.

To correlate on a cellular level the *Kcnh5* mRNA expression with protein distribution obtained with our anti-K_v10.2 antibody, we tried to establish ISH for *Kcnh5* and *Kcnh1* mRNA. The ISH probe for *Kcnh1,* which we successfully established, resulted in a specific staining in accordance with the known expression pattern for *Kcnh1* in rat on the mRNA (Dr. S. Martin, personal communication) and protein level (Martin et al., 2008). However, the application of our established protocol for *Kcnh1* was not successful for the *Kcnh5* probe.

To deduce a physiological function from the IHC is also not possible. The regions detected as K_v10.2 positive are involved in various physiological functions, for example processing of emotional information (limbic system), motor behavior (thalamus, globus pallidus), cognition (cortex, hippocampus, globus pallidus) and the diverse functions of the other regions.

It is noteworthy that the IHC staining obtained with our anti-K_v10.2 antibody is clearly distinguishable from the expression pattern of the K_v10.1 protein, which shows an ubiquitious expression in adult rat brain (Martin et al., 2008). This further underlines that our antibody does not recognize K_v10.1 in IHC studies.

One other explanation for the different results we obtained with Western blot analysis and the IHC might be that the sample preparation for tissue lysates of the brain regions involves a surgical sectioning. Thereby, errors may occur in the sampling of the tissue, especially in small brain regions, leading to K_v10.2 positive cells in K_v10.2 negative tissue. Furthermore, the IHC only displays a small area of the whole mouse brain, possibly missing K_v10.2 positive cells within brain regions. In order to resolve the difference, a future experiment may be to perform a serial sectioning of the whole brain with subsequent IHC analysis.

5.5 Neuronal localization of K_v10.2

K_v10.2 protein preferentially localizes to neurons in the cortex, hippocampus and cerebellum of mouse, while a small population of astrocytes in the cerebellum was also positive. *Kcnh5* mRNA localization to neurons has been previously reported in the mouse (Saganich et al., 1999, Ludwig et al., 2000, Saganich et al., 2001, Huang et al., 2012). For

localization of K_v10.2 in neurons of the adult mouse brain, we used heterozygous TYFF (neuron), CXCR (microglia) and GFEA (astrocyte) transgenic mice. These systems do not require a double staining of K_v10.2 with specific markers, like GFAP for astrocytes (Sofroniew and Vinters, 2010), ßIII-tubulin for neurons (Katsetos et al., 2002) or IbaI for microglias (Ito et al., 2001). For the cortex, Purkinje layer of the cerebellum and the hippocampus we showed the preferenatial localization of K_v10.2 to neurons. In the CA3 region of the hippocampus, Jeng and co-workers showed a K_v10.2 localization to neurons as well (Jeng et al., 2005). However, by using the Alomone Lab anti-K_v10.2 antibody we did not detect any specificity to K_v10.2 in Western blot analysis, which was discussed earlier. In virtually all cells investigated, the results obtained suggest a localization of K_v10.2 to the soma of neurons and most likely to the membrane of the soma, while stained neural processes were almost invisible. This is in accordance with our fluorescence IHC analysis, where K_v10.2 was detected to localize mainly to neurons in the Purkinje layer of the cerebellum, hippocampus and cortex. The possible membrane localization of K_v10.2 indicates that it may play a role in action potential repolarization of the soma. However, future experiments, such as ICC on cultured neurons, are necessary to further investigate its subcellular localization in neurons.

A co-localization of K_v10.2 with endogenously labeled neurons was not evident in all cells. The use of transgenic TYFF and GFEA mice has some limitations due to the integration site of the construct of the transgenic mice. Hirrlinger and co-workers reported that the "transgenes showed a variable percentage of labeled cells not only in different brain regions but also among different mouse lines" (Hirrlinger et al., 2005). In our analysis, we did not investigate a possible localization to oligodendrocytes, which are important glia cells of the CNS. A double staining with an oligodendrocytic marker, such as Olig2 (Yokoo et al., 2004) may further support our finding that K_v10.2 is preferentially localized to neurons in the cortex, cerebellum ant hippocampus.

5.6 Loss of function of the K_v10.2 conditional knockout mouse

In order to address the physiological role of K_v10.2, a conditional *Kcnh5* knockout mouse was previously generated in our department. The Cre-loxP system, which was applied, is a molecular tool for genome modulation by homologous recombination (Nagy, 2000). The analysis of the homozygous *Kcnh5* conditional knockout mouse cross-bred with homozygous Emx1-Cre mouse (Guo et al., 2000) did not result in Cre-mediated genomic alteration of *Kcnh5*

or knockdown of *Kcnh5* expression in the cortex. Furthermore, no alteration in the genome was observed by PCR using primers spanning exon 6 - 8 and the loxP sites. Genotyping of the 5' loxP site was successful (data not shown), indicating that the 3' loxP site is missing. This speculation is according with observations of the International Knockout Mouse Consortium, that "the 3' loxP site is often lost due to recombination events in the homology region between the targeting cassette and 3' loxP site" (http://www.knockoutmouse.org/about/targeting-strategies accessed 28.Jan.12 (2007, Skarnes et al., 2011)). Therefore, no *Kcnh5* conditional knockout was available for further analysis of the physiological function of K_v10.2. Moreover, with the *Kcnh5* conditional knockout mouse (depleted of the K_v10.2 protein) unavailable, the most effective control for our novel antibody was missing for Western blot or IHC analysis.

5.7 Subcellular localization of K_v10.2

In our chromogenic IHC analysis utilizing the anti-K_v10.2 antibody on brain sections, we detected immunoreactivity of a cilia-like structure akin to a cell protrusion detected by type III adenylyl cyclase (ACIII) staining on mouse brain sections. Since ACIII is reported to localize to the primary cilium in the brain (Bishop et al., 2007), the similarities between the stainings may indicate that the anti-K_v10.2 antibody recognizes a structure highly similar to the cilium of cells. Furthermore, anti-K_v10.2 antibody detected similar structures on cells in liver and lung sections. The structure detected also resembled a staining pattern which we obtained with acetylated tubulin-positive cilia staining in the same organs. Acetylated tubulin is widely used as a marker for the primary cilium and cilia in general for non-CNS derived tissue (Alieva et al., 1999).

Because our antibody seems to recognize a cilia-like structure, it may be possible that K_v10.2 is localized in cilia. In this context, K_v10.2 might regulate potassium efflux after Ca^{2+} influx. However, to really show this localization, it would be necessary to perform a double staining with K_v10.2 and a cilia marker such as acetylated tubulin or ACIII.

5.8 Possible physiological functions of K_v10.2

Given that no K_v10.2 localization to cortical astrocytes has been found in IHC analysis, it is interesting that *in vitro* we measured a high mRNA expression in primary astrocyte

cultures derived from prefrontal cortex and midbrain, and not in the neuronal cell lines such as N2a or Oli neu. The astrocyte cultures derive from PN 0 mice, while we performed K_v10.2 localization in tissue in adult mouse brain sections. This finding may indicate a certain maturation dependent regulation of K_v10.2 expression in astrocytes. A future experiment would be to perform laser capture microdissection on PN 0 mouse brain sections and analyze the astrocytes for K_v10.2 expression in order to unravel a possible regulation of K_v10.2 during maturation.

None of the other cell lines, 108CC05, 108CC15, Olig2 or N2a, we investigated express *Kcnh5*. While this finding is inconsistent with our IHC observations, where K_v10.2 was preferentially localized in neurons, it is possible, that the neuronal cell lines do not mimic neurons *in vivo* since they are either derived from neuroblastoma cells (108CC05, 108CC15 and N2a) or need further differentiation (Olig2 and N2a).

K_v10.2 protein expression is not altered in K_v10.1 deficient mice. The homozygous *Kcnh1* total knockout mouse displays only a slight hyperactive phenotype and no *Kcnh5* mRNA upregulation (Ufartes et al., 2013). An increased K_v10.2 protein expression has also not been detected. Hence, in the case that K_v10.2 at least partially mimics the physiological function of K_v10.1, the endogenous levels of K_v10.2 are enough to compensate for the loss of K_v10.1. Another possibility is that K_v10.2 is not involved in rescuing the phenotype of K_v10.1. A knockout mouse resulting in no alteration of phenotype has been reported for other ion channels (Guo et al., 2005, Nerbonne et al., 2008) and this is possible also for the homozygous K_v10.1 total knockout.

K_v10.2 is expressed during embryogenesis in mice. Besides the *Kcnh5* conditional knockout, a *Kcnh5* total knockout mouse was generated in our department. Data indicate that the homozygous *Kcnh5* total knockout mouse is embryonically lethal. Interestingly, the heterozygous *Kcnh5* total knockout does not display an obvious phenotype (data not shown). This indicates that expression of *Kcnh5* from one Wt allele is enough to rescue the embryonic lethality. We demonstrated the continuous expression of K_v10.2 in neuronal development of mice during all stages investigated. Furthermore, by IHC analysis, K_v10.2 was detected throughout the embryo, partially in the maternal tissue. In the context of the embryonic lethality of the homozygous *Kcnh5* total knockout, the lack of *Kcnh5* expression in maternal tissue cannot be the origin of this phenotype, since all embryos, the homozygous *Kcnh5* knockout mice as well as the heterozygous and wt mice would then be affected, which was not the case. Therefore, the embryonic lethality has to arise from the lack of K_v10.2 in the embryo

itself. Further analysis of the temporal and spatial distribution in mouse embryos of earlier stages than E 8.5 should be conducted to investigate the stage of embryonic lethality. However, the homozygous *Kcnh1* total knockout mouse displays only a mild phenotype, while the homozygous *Kcnh5* knockout causes a severe defect in embryogenesis. It is obvious that a lack of K_v10.2 at early embryonic stages is incompatible with life.

6 Summary and Conclusions

Potassium channels are one of the most heterogeneous groups of ion channels that are essential for cellular physiology. An alteration of the physiological properties of these channels as a cause of genetic mutations or aberrant expression often results in channelopathies such as long QT syndrome, congenital hyperinsulinism and seizures. In this context, K_v10.1, the first described member of the K_v10 family, has been implicated in cell cycle progression and cancer. While K_v10.1 has been extensively studied, the function and localization of K_v10.2, a second member of the K_v10 family, has not been well described especially due to non-availability of specific tools. One aspect is the lack of specific antibody, which is able to discriminate K_v10.2 from K_v10.1 as both proteins share a high amino acid homology. In my thesis, we have studied the distribution of K_v10.2 in the mouse tissues and we provide the first analyses exploring a possible physiological function of K_v10.2.

Five commercially available anti-K_v10.2 antibodies tested did not show specificity or sensitivity for K_v10.2 in Western blot analysis. Therefore, a novel polyclonal IgG antibody directed against the C-terminus of human K_v10.2 was generated. The C-terminus of human K_v10.2 shares least homology towards K_v10.1 and this region has a high homology to the mouse K_v10.2 protein. By the use of K_v10.2 and K_v10.1 overexpressing HEK293 cells, we demonstrated recognition of K_v10.2 in Western blot analysis and immunological staining procedures. The generated polyclonal anti-K_v10.2 antibody discriminated K_v10.2 against K_v10.1.

K_v10.2 protein was found to have a widespread expression pattern in various mouse tissues and brain regions using the newly generate antibody in Western blot analysis. This finding was supported by overlapping *Kcnh5* mRNA distribution in mouse brain regions, while tissues were only partially congruous. The analyzed K_v10.2 distribution was clearly distinct from reported ubiquitious K_v10.1 protein distribution in the rat brain (Martin et al., 2008), further indicating no recognition of K_v10.1 by the anti-K_v10.2 antibody. A preferentially neural localization of K_v10.2 in cortex, hippocampus and cerebellum was assessed by IHC performed on mouse brain sections of transgenic mice that express yellow fluorescent protein (YFP) under the control of neuron-specific Thy1 promoter. No co-localization by IHC was detected in mice expressing eGFP under the CX3CR1 promoter (microglia). Furthermore, only a small population of cells of the cerebellum was K_v10.2 positive in mice expressing eGFP under the control of the GFAP promoter (astrocytes). Moreover, K_v10.2 was detected in the soma of neurons in the hippocampus, cortex and cerebellum, while cell processes of the hippocampus

and mitral cell layer were also K_v10.2 positive. This indicates an altered subcellular localization of K_v10.2 in neurons of different regions of the mouse brain. Additionally, the antibody recognized a cilia-like structure on cells of mouse brain, lung and liver tissue in IHC analysis. The detected structures were highly similar to cilia that are stained by the established cilia markers, adenylyl cyclase III and acetylated tubulin.

Western blot analysis of K_v10.2 protein levels in the K_v10.1 deficient mice, which shows a slightly hyperactive phenotype, suggests no altered K_v10.2 protein levels, which is in line with reported mRNA findings.

An approach to investigate the physiological function of K_v10.2 by a Cre-recombinase mediated deletion of K_v10.2 in the homozygous *Kcnh5* conditional knockout mouse did not result in decreased levels of *Kcnh5* mRNA. No genomic alteration of the *Kcnh5* gene locus was observed, indicating a lack of the required LoxP sites for gene recombination. Therefore, the *Kcnh5* conditional knockout mouse was not available for further studies or antibody evaluation. In contrast to the homozygous *Kcnh1* conventional knockout mouse, preliminary data of the homozygous *Kcnh5* total knockout indicates embryonic lethality, while the heterozygous *Kcnh5* total knockout mouse did not show any obvious phenotype. The temporal expression of K_v10.2 protein in the developing mouse head was detected from embryonic day 8, the earliest investigated developmental stage, until postnatal stages and in the adult mouse. The spatial distribution of K_v10.2 protein showed ubiquitous expression throughout the mouse embryo and the placenta.

In conclusion, we generated a sensitive polyclonal anti-K_v10.2 antibody, which discriminates K_v10.2 towards K_v10.1. In future, our generated anti-K_v10.2 antibody might be used for investigation of an involvement of K_v10.2 in human diseases. While the K_v10.2 protein is widely expressed throughout the adult mouse, further investigation about the onset of the expression of this ion channel during embryogenesis has to be conducted. Moreover, the possible involvement of K_v10.2 in ciliary function needs to be assessed.

7 Appendixes

7.1 Nomenclature of the members of the Eag family

Table 1: Overview of the current and previous nomenclature of the Eag family after IUPHAR (Gutman et al., 2005)

Potassium channel name	Gene Name	Previous Names
K_v10.1	potassium voltage-gated channel, subfamily H (eag-related), member 1	Kv10.1a; Kv10.1b; KCNH1a; ether-a-go-go; Kv10.1; eag; h-eag; Kv10.1; r-eag; EAG channel 1; ether-a-go-go potassium channel 1; potassium voltage-gated channel subfamily H member 1; voltage-gated potassium channel subunit Kv10.1; M-eag; ether a go-go
K_v10.2	potassium voltage-gated channel, subfamily H (eag-related), member 5	Kv10.2; KCNH5; ether-a-go-go potassium channel 2; potassium voltage-gated channel subfamily H member 5; rKV10.2; voltage-gated potassium channel subunit Kv10.2
K_v11.1	potassium voltage-gated channel, subfamily H (eag-related), member 2	*ether-à-go-go*-related gene; HERG; erg1; hergb; LQT2; Kv11.1; ERG-1; RERG; eag-related protein 1; ether-a-go-go-related gene potassium channel 1; ether-a-go-go-related protein 1; potassium voltage-gated channel subfamily H member 2; r-ERG; voltage-gated potassium channel subunit Kv11.1; merg1a; M-erg; ether a go-go related; LQT; merg1b; AI326795
K_v11.2	potassium voltage-gated channel, subfamily H (eag-related), member 6	erg2; KCNH6; Kv11.2; HERG2; ERG-2; Eag-related gene member 2; eag-related protein 2; ether-a-go-go-related gene potassium channel 2; ether-a-go-go-related protein 2; potassium voltage-gated channel subfamily H member 6; voltage-gated potassium

		channel subunit Kv11.2; m-erg2
K_v11.3	potassium voltage-gated channel, subfamily H (eag-related), member 7	erg3; KCNH7; Kv11.3; HERG3; ERG-3; eag-related protein 3; ether-a-go-go-related gene potassium channel 3; ether-a-go-go-related protein 3; potassium voltage-gated channel subfamily H member 7; voltage-gated potassium channel subunit Kv11.3; 9330137I11Rik
K_v12.1	potassium voltage-gated channel, subfamily H (eag-related), member 8	elk1; elk3; Kv12.1; Ets-1; ELK channel 3; ELK1, member of ETS oncogene family; ether-a-go-go-like potassium channel 1; ether-a-go-go-like potassium channel 3; potassium voltage-gated channel subfamily H member 8; potassium voltage-gated channel, subfamily H, member 8; potassium voltage-gated channel, subfamily H, member 8; C130090D05Rik
K_v12.2	potassium voltage-gated channel, subfamily H (eag-related), member 3	BEC1; Elk2; Kv12.2; BEC1 protein; ELK channel 2; brain-specific eag-like channel 1; ether-a-go-go-like potassium channel 2; potassium voltage-gated channel subfamily H member 3; rElk2; voltage-gated potassium channel subunit Kv12.2; Melk2; ether a go-go like; AU019351; C030044P22Rik
K_v12.3	potassium voltage-gated channel, subfamily H (eag-related), member 4	BEC2; Elk1; Kv12.3; ELK channel 1; brain-specific eag-like channel 2; ether-a-go-go-like potassium channel 1; potassium voltage-gated channel subfamily H member 4; rElk1; voltage-gated potassium channel subunit Kv12.3

7.2 Anti-K_v10.2 antibody detects K_v10.2 in Western blot analysis

Figure 36 illustrates Western blot image processing based on Figure 13. Images of Western blots were obtained in the Chemi-Doc luminescence detection system with no illumination for acquisition of Western blot (Figure36, chemiluminescent acquisition) and epi-white illumination for acquisition of the protein standard (Figure36, epi-white acquisition). For better illustration, protein standard was removed from chemiluminescent images and replaced

with drawn bars to indicate the migration distance of the molecular weight standard in all Western blots presented in the results section.

As already discussed, the anti-K_v10.2 antibody detects a protein of predicted molecular weight of BBS-K_v10.2 (=116 kDa) only in the HEK293 BBS-K_v10.2 cell lysate. At this particular molecular weight, no signal was obtained in lysates of HEK293 Wt and HEK293 BBS-K_v10.1 cells. In the total mouse brain sample, a band at the predicted weight of K_v10.2 (=112 kDa) was observed. Further proteins at different molecular weight, i.e. at approximately 50 and 70 kDa were recognized.

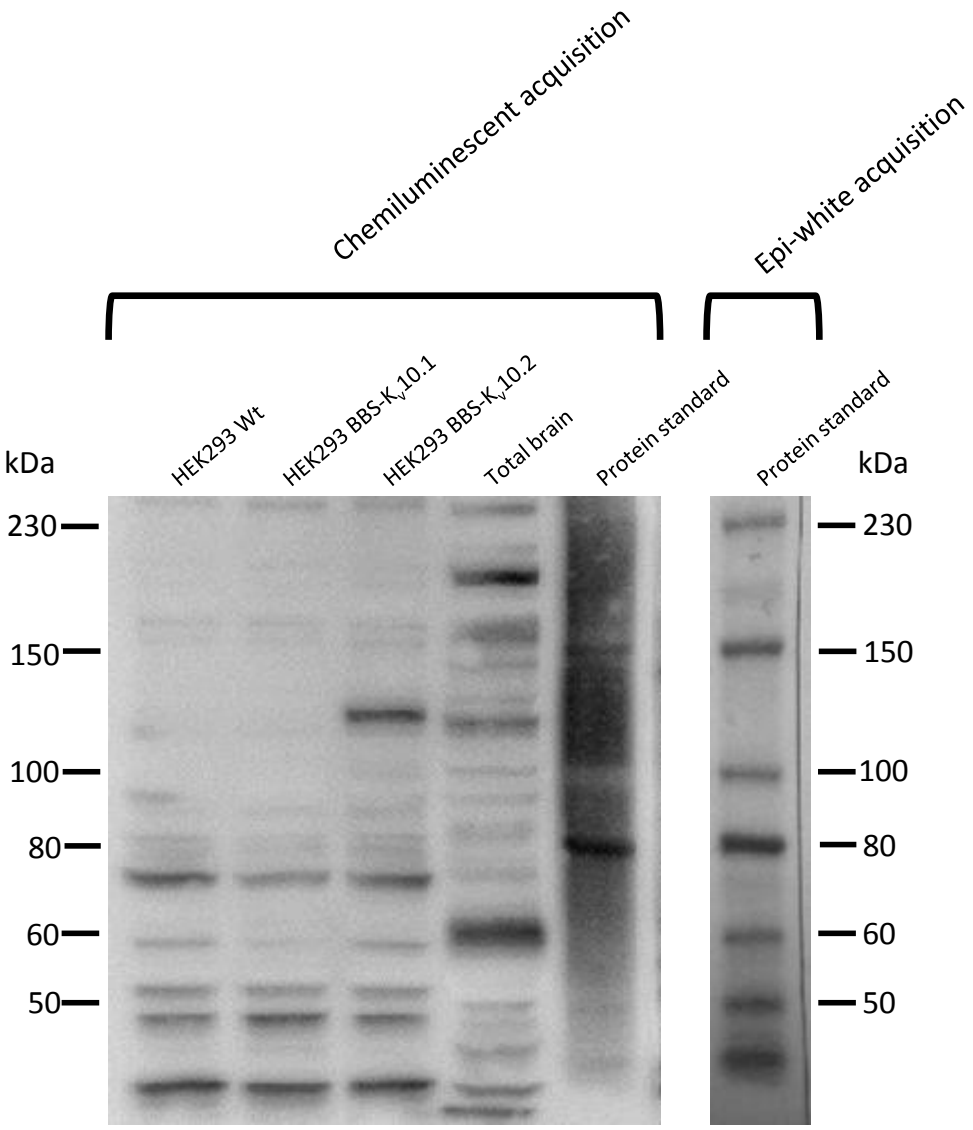

Figure 36: Representation of Western blot image processing based on Figure 13
Western blot analyses performed with anti-K_v10.2 antibody were acquired in the Chemi-Doc luminescence detection system with no illumination for acquisition of Western blot and epi-white illumination for acquisition of the protein standard. For better illustration, protein standard was removed from the images obtained and replaced with drawn bars to indicate the migration distance of the molecular weight standard. Anti-K_v10.2 antibody detected a protein of the predicted molecular weight of BBS-K_v10.2 (=116 kDa) in the lysate of HEK293 BBS-K_v10.2 cells. In total mouse brain lysate, a protein of the predicted molecular weight of K_v10.2 (=112 kDa) was recognized. At this molecular weight, no protein was detected in lysates of HEK293 Wt and HEK293 BBS-K_v10.1 cells. In all samples, bands of proteins of different molecular weight were observed, i.e. approximately at 50 kDa and 70 kDa.

7.3 *In Situ* hybridization probes are specific in dot blot assay

To examine the specificity of the *in vitro* synthesized digoxigenin labeled ribonucleic ISH probes, we performed a dot blot assay. For this we amplified the target sequences of both antisense probes as well as the whole exon 7 of both genes. Together with a negative control,

a calbindin amplification product that did not have any homology towards either *Kcnh1* or *Kcnh5*, these amplification products were blotted on a membrane and incubated with our ISH probes. We observed a strong signal at 51°C of the *Kcnh1* probe on both *Kcnh1* target sequences with decreasing signal intensity in lower target concentrations (Figure 37A). Although the probe also recognized the highest three *Kcnh5* dilutions in this dot blot assay we concluded that this was depending on the annealing temperature of the probe. The *Kcnh5* probe specifically bound to the *Kcnh5* target sequences at 55°C, while a very weak signal on the *Kcnh1* target sequence was observed (Figure 37B). The calbindin sequence was not recognized by either probe.

We concluded that our *Kcnh1* and *Kcnh5* antisense probes specifically bind to their target sequences with the appropriate temperature settings.

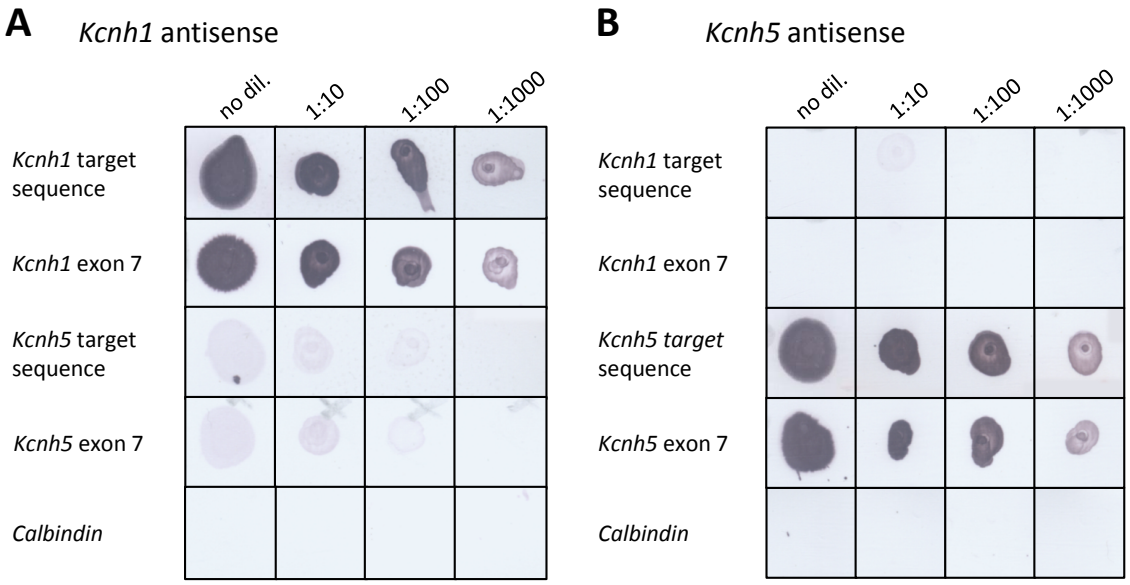

Figure 37: Specificity of *Kcnh1* and *Kcnh5* ISH RNA riboprobes determined by dot blot assay
A: Dot blot assay with *Kcnh1* antisense RNA probe performed at 51°C. The probe hybridized to *Kcnh1* target sequences with decreasing signal intensity in higher dilutions (dil). Analogous *Kcnh5* sequences, to verify cross reactivity, were weakly detected. *Calbindin* sequence serving as a negative control was not recognized by the *Kcnh1* probe. **B:** Dot blot assay with *Kcnh5* antisense RNA probe performed at 55°C. The probe detected only *Kcnh5* target sequences with decreasing signal intensity at higher dilutions (dil). *Calbindin* sequence serving as a negative control was not recognized by the *Kcnh1* probe.

7.4 Hippocampus and cerebellum negative controls of IHC on TYFF and CXCR mouse brain sections

As shown in Figure 38:, controls performed without primary anti-K_v10.2 antibody resulted in no specific staining observed in the hippocampus (Figure 38A-C) and cerebellum (Figure 38D-F) of heterozygous transgenic TYFF mice. Negative controls were performed with

Alexa-633 conjugated secondary anti-rabbit antibody. The same control was performed on sections of the hippocampus (Figure 39A-C) and cerebellum (Figure 38D-F) of CXCR animals which contain endougenous eGFP labeled microglia. In both controls no staining with secondary anti-rabbit Alexa-633 antibody was observed (Figure 39A,C,D,F).

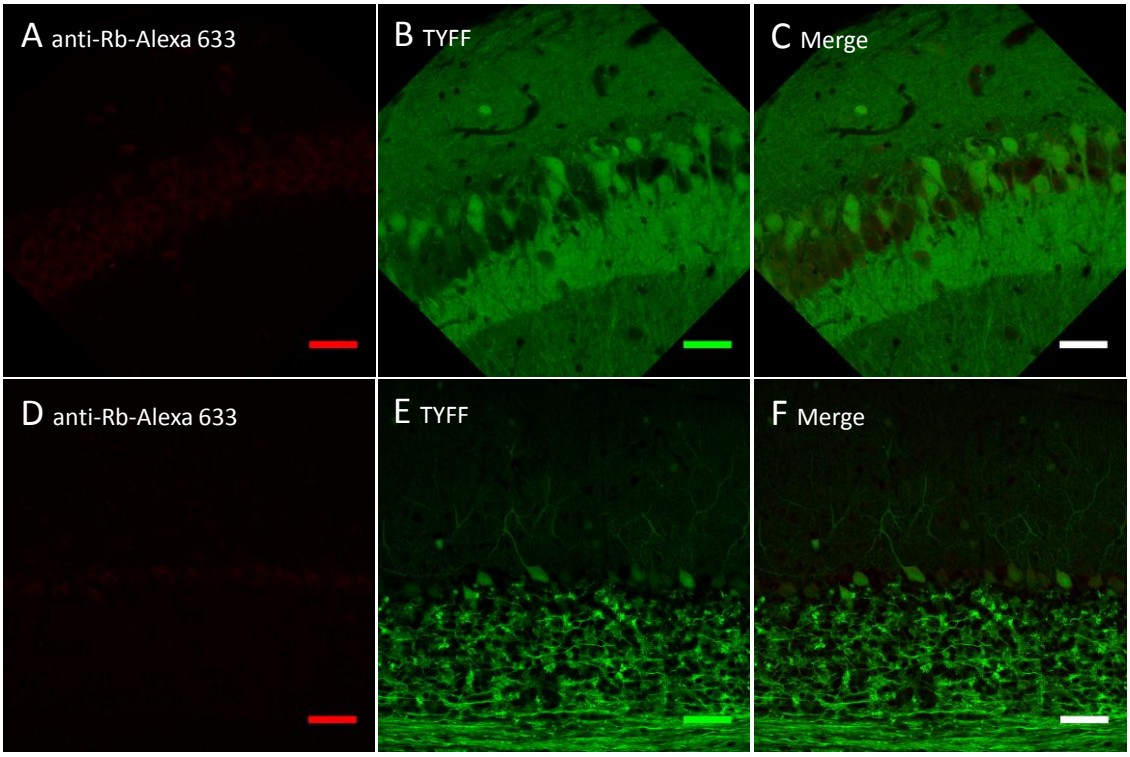

Figure 38: IHC negative controls of heterozygous transgenic TYFF mouse hippocampus and cerebellum
A-C: Hippocampus: (**A**) Negative control with Alexa-633 conjugated secondary anti-rabbit antibody on (**B**) eYFP expressing neurons resulted in (**C**) no specific staining. **D-F**: Cerebellum: (**D**) Negative control with Alexa-633 conjugated secondary anti-rabbit antibody on (**E**) eYFP expressing neurons resulted in (**F**) no specific staining. Sagittal vibratom sections obtained at 25 µm. Scale bar represents 50 µm.

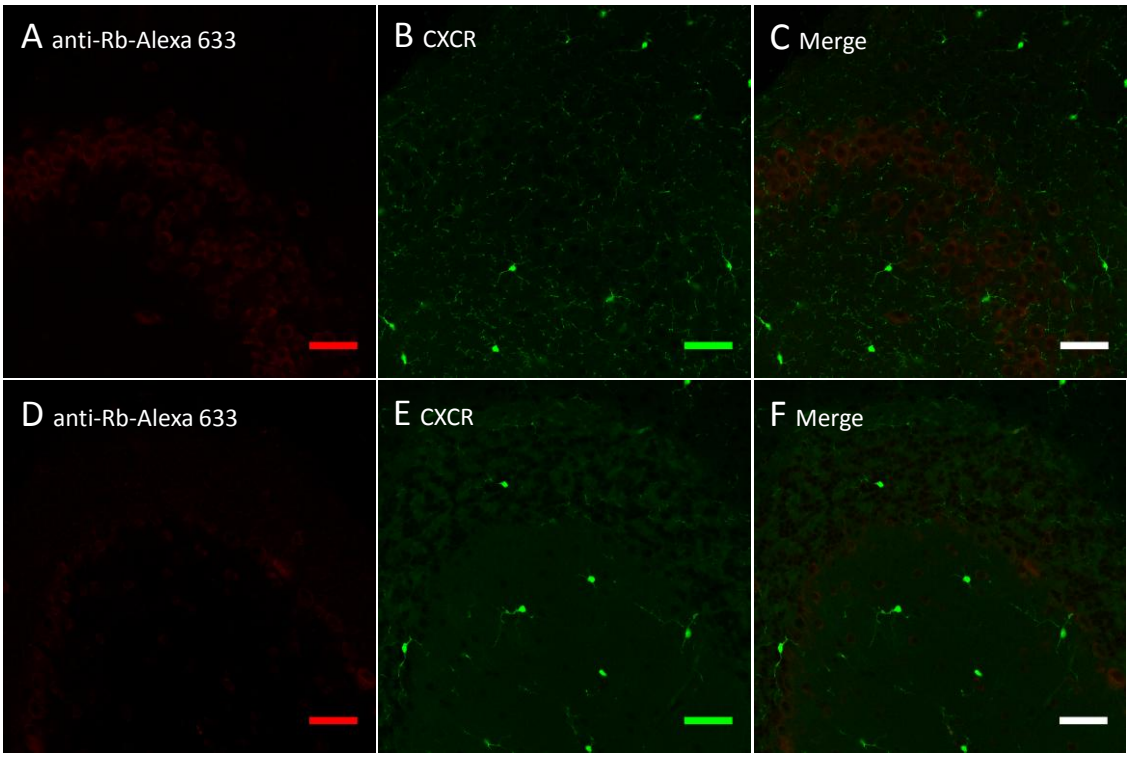

Figure 39: IHC negative control of heterozygous transgenic CXCR mouse hippocampus and cerebellum
A-C: Hippocampus: (**A**) Negative control with secondary Alexa-633 conjugated anti-rabbit antibody on (**B**) eGFP expressing microglia resulted in no specific staining (**C**). **D-F**: Cerebellum: (**D**) Negative control with secondary Alexa-633 conjugated anti-rabbit antibody on (**E**) eGFP expressing microglia resulted in (**F**) no specific staining. Sagittal vibratom sections obtained at 25 µm. Scale bar represents 50 µm.

8 Curriculum Vitae

Gerd-Marten Kuscher

Birthday: 12.07.1981

Born in: Neuruppin, Brandenburg, Germany

Unmarried

Adress:

Department of Molecular Biology of Neuronal Signals

Hermann-Rein-Str. 3

37075 Göttingen

Contact:

Office: +49 551 3899 272

E-Mail: Kuscher@em.mpg.de

Education/ Working experience

03/2009 – present	Ph.D. thesis at the Max Planck Insitute of Experimental Medicine, at the Department of Molecular Biology of Neuronal Signals. Topic: *Localization of the voltage gated K_v10.2 potassium channel in the mouse organism*
10/2002 – 03/2009	Diploma in biology at the Georg-August-University Göttingen. Diploma thesis prepared at Max Planck Institute of Experimental Medicine in the research group of Prof. Victor Tarabykin. Topic: *Identification and characterization of downstream target genes of the transcription factor SIP1 in neocortical development*
11/2001 – 07/2002	General conscription at the 2. Führungsunterstützungsregiment 20 in Hannover, Germany
07/2001	Abitur degree (general qualification for university entrance) at the Gymnasium St. Ursula-Schule, Hannover, Germany

Publications

Sausbier U, Dullin C, Missbach-Guentner J, Kabagema C, Flockerzie K, Kuscher GM, Stuehmer W, Neuhuber W, Ruth P, Alves F, Sausbier M (2011) Osteopenia due to enhanced cathepsin K release by BK channel ablation in osteoclasts. PLoS One 6(6):e21168.

9 Acknowledgements

Ich möchte mich herzlich bei Herrn Prof. Dr. Walter Stühmer bedanken, der mir die Möglichkeit gab in der Abteilung Molekulare Biologie Neuronaler Signale meine Doktorarbeit anzufertigen. Weiterhin bedanke ich mich sehr, dass er mit mir die wissenschaftlichen und nicht wissenschaftlichen Probleme und Fragen erörterte und Teil meines *Thesis Committe* war.

Mein größter Dank gilt Frau Prof. Frauke Alves und Dr. Roser Ufartes, die mir Hilfestellungen gaben, wo es nur möglich war. Des Weiteren waren sie jederzeit für Diskussion offen und waren immer da, wenn es Probleme zu lösen galt, dafür vielen Dank!

Ich möchte mich auch bei den Mitgliedern meines *Thesis Committees*, Herrn Prof. Dr. Thomas A. Bayer und Herrn Prof. Dr. Hubertus Jarry, für ihre Unterstützung und die rege Teilnahme an meinen *Thesis Committee Meetings*, die vielen konstruktiven Kritiken und Diskussionen bedanken.

Mein herzlichster Dank geht an alle Kollegen und Mitarbeiter von der Abteilung MBNS und Prof. Alves Arbeitsgruppe, insbesondere Bärbel, Hanna, Mercedes und Rosi.

Vor allem möchte ich mich bei Prof. Dr. Luis A. Pardo, Dr. Sabine Martin und Dr. Marcio Lazzarini bedanken. Ohne ihre Hilfe, Aufmunterung und Ratschläge wäre meine Arbeit nicht zu dem geworden, was sie ist. Vielen Dank!

Ganz herzlich möchte ich mich bei Dr. Miso Mitkovski bedanken, der mich nicht in der Kunst der Mikroskopie schulte, sondern vielmehr immer ein Freund war. Das Letztere gilt auch für Sebastian Schmitt, der immer da war, wenn die wissenschaftliche Not am größten war und mir die Möglichkeit gab, die Primärzellkultur zu erlernen. Mein Dank geht auch an Manuela Schwark, war nicht nur eine wichtige Freundin, sondern auch eine Hilfe bei kleinen und großen Problemen.

Ich möchte mich auch bei Prof. Dr. Victor Tarabykin und Dr. Anjana Nityanandam bedanken, die auch nach meiner Diplomarbeit immer für eine rege Diskussion offen waren.

Meinen Eltern, Helga und Gerd Kuscher, und meiner Schwester Isabelle Kuscher gilt mein besonderer Dank. Ihr habt immer an mich geglaubt.

Meiner Freundin Kristin danke ich für so viel, dass es hier nicht genügend Platz gibt es aufzuzählen. Danke für die all die Kraft, aufmunternden Worte und Lichtblicke! Du warst all die Zeit bei mir!

10 Bibliographies

Alieva IB, Gorgidze LA, Komarova YA, Chernobelskaya OA, Vorobjev IA (1999) Experimental model for studying the primary cilia in tissue culture cells. Membr Cell Biol 12:895-905.

Allen-Brain-Atlas-Consortium (2007) A Mouse for All Reasons. Cell 128:9-13.

Arcangeli A, Rosati B, Crociani O, Cherubini A, Fontana L, Passani B, Wanke E, Olivotto M (1999) Modulation of HERG current and herg gene expression during retinoic acid treatment of human neuroblastoma cells: potentiating effects of BDNF. J Neurobiol 40:214-225.

Asher V, Sowter H, Shaw R, Bali A, Khan R (2010) Eag and HERG potassium channels as novel therapeutic targets in cancer. World J Surg Oncol 8:113.

Bauer CK, Schwarz JR (2001) Physiology of EAG K+ channels. J Membr Biol 182:1-15.

Bianchi L, Wible B, Arcangeli A, Taglialatela M, Morra F, Castaldo P, Crociani O, Rosati B, Faravelli L, Olivotto M, Wanke E (1998) herg encodes a K+ current highly conserved in tumors of different histogenesis: a selective advantage for cancer cells? Cancer Res 58:815-822.

Bishop GA, Berbari NF, Lewis J, Mykytyn K (2007) Type III adenylyl cyclase localizes to primary cilia throughout the adult mouse brain. J Comp Neurol 505:562-571.

Blackiston DJ, McLaughlin KA, Levin M (2009) Bioelectric controls of cell proliferation: ion channels, membrane voltage and the cell cycle. Cell Cycle 8:3519-3528.

Bruggemann A, Stuhmer W, Pardo LA (1997) Mitosis-promoting factor-mediated suppression of a cloned delayed rectifier potassium channel expressed in Xenopus oocytes. Proc Natl Acad Sci U S A 94:537-542.

Butler A, Wei A, Salkoff L (1990) Shal, Shab, and Shaw: three genes encoding potassium channels in Drosophila. Nucleic Acids Res 18:2173-2174.

Butler A, Wei AG, Baker K, Salkoff L (1989) A family of putative potassium channel genes in Drosophila. Science 243:943-947.

Capel PJ (1974) A quantitative immunofluorescence method based on the covalent coupling of protein to sepharose beads. J Immunol Methods 5:165-178.

Chen Y, Sanchez A, Rubio ME, Kohl T, Pardo LA, Stuhmer W (2011) Functional K(v)10.1 channels localize to the inner nuclear membrane. PLoS One 6:e19257.

Cherubini A, Taddei GL, Crociani O, Paglierani M, Buccoliero AM, Fontana L, Noci I, Borri P, Borrani E, Giachi M, Becchetti A, Rosati B, Wanke E, Olivotto M, Arcangeli A (2000) HERG potassium channels are more frequently expressed in human endometrial cancer as compared to non-cancerous endometrium. Br J Cancer 83:1722-1729.

Chklovskii DB, Schikorski T, Stevens CF (2002) Wiring optimization in cortical circuits. Neuron 34:341-347.

Christensen ST, Pedersen SF, Satir P, Veland IR, Schneider L (2008) The primary cilium coordinates signaling pathways in cell cycle control and migration during development and tissue repair. Curr Top Dev Biol 85:261-301.

Coetzee WA, Rudy B (eds.) (2006) Potassium Channels: John Wiley & Sons, Ltd. www.els.net.

Cooper HM, Paterson Y (2001) Production of polyclonal antisera. Curr Protoc Immunol Chapter 2:Unit 2 4.

Corbit KC, Shyer AE, Dowdle WE, Gaulden J, Singla V, Chen MH, Chuang PT, Reiter JF (2008) Kif3a constrains beta-catenin-dependent Wnt signalling through dual ciliary and non-ciliary mechanisms. Nat Cell Biol 10:70-76.

Coulter HD (1988) Vesicular localization of immunoreactive [Met5]enkephalin in the globus pallidus. Proc Natl Acad Sci U S A 85:7028-7032.

Covarrubias M, Wei A, Salkoff L, Vyas TB (1994) Elimination of rapid potassium channel inactivation by phosphorylation of the inactivation gate. Neuron 13:1403-1412.

Cui J, Kagan A, Qin D, Mathew J, Melman YF, McDonald TV (2001) Analysis of the cyclic nucleotide binding domain of the HERG potassium channel and interactions with KCNE2. J Biol Chem 276:17244-17251.

de Oliveira RM, Martin S, de Oliveira CL, Milani H, Schiavon AP, Joca S, Pardo LA, Stuhmer W, Del Bel EA (2012) Eag1, Eag2, and SK3 potassium channel expression in the rat hippocampus after global transient brain ischemia. J Neurosci Res 90:632-640.

DeCoursey TE, Chandy KG, Gupta S, Cahalan MD (1984) Voltage-gated K+ channels in human T lymphocytes: a role in mitogenesis? Nature 307:465-468.

Di Tommaso P, Moretti S, Xenarios I, Orobitg M, Montanyola A, Chang JM, Taly JF, Notredame C (2011) T-Coffee: a web server for the multiple sequence alignment of protein and RNA sequences using structural information and homology extension. Nucleic Acids Res 39:W13-17.

Dolmetsch RE, Pajvani U, Fife K, Spotts JM, Greenberg ME (2001) Signaling to the nucleus by an L-type calcium channel-calmodulin complex through the MAP kinase pathway. Science 294:333-339.

Doxsey S, McCollum D, Theurkauf W (2005) Centrosomes in cellular regulation. Annu Rev Cell Dev Biol 21:411-434.

Drain P, Dubin AE, Aldrich RW (1994) Regulation of Shaker K+ channel inactivation gating by the cAMP-dependent protein kinase. Neuron 12:1097-1109.

Egri C, Ruben PC (2012) Action Potentials: Generation and Propagation. eLS John Wiley & Sons, Ltd: Chichester.

Fahnert B, Lilie H, Neubauer P (2004) Inclusion bodies: formation and utilisation. Adv Biochem Eng Biotechnol 89:93-142.

Feng Q, Hawes SE, Stern JE, Wiens L, Lu H, Dong ZM, Jordan CD, Kiviat NB, Vesselle H (2008) DNA methylation in tumor and matched normal tissues from non-small cell lung cancer patients. Cancer Epidemiol Biomarkers Prev 17:645-654.

Garcia-Barreno B, Steel J, Paya M, Martinez-Sobrido L, Delgado T, Yeo RP, Melero JA (2005) Epitope mapping of human respiratory syncytial virus 22K transcription antitermination factor: role of N-terminal sequences in protein folding. J Gen Virol 86:1103-1107.

Gorski JA, Talley T, Qiu M, Puelles L, Rubenstein JL, Jones KR (2002) Cortical excitatory neurons and glia, but not GABAergic neurons, are produced in the Emx1-expressing lineage. J Neurosci 22:6309-6314.

Green MR, Sambrook J (2012) Molecular Cloning : A Laboratory Manual Cold Spring Harbor, NY: Cold Spring Harbor Laboratory Press.

Griggs RC, Nutt JG (1995) Episodic ataxias as channelopathies. Ann Neurol 37:285-287.

Guirao B, Joanny JF (2007) Spontaneous creation of macroscopic flow and metachronal waves in an array of cilia. Biophys J 92:1900-1917.

Guo H, Hong S, Jin XL, Chen RS, Avasthi PP, Tu YT, Ivanco TL, Li Y (2000) Specificity and efficiency of Cre-mediated recombination in Emx1-Cre knock-in mice. Biochem Biophys Res Commun 273:661-665.

Guo W, Jung WE, Marionneau C, Aimond F, Xu H, Yamada KA, Schwarz TL, Demolombe S, Nerbonne JM (2005) Targeted deletion of Kv4.2 eliminates I(to,f) and results in electrical and molecular remodeling, with no evidence of ventricular hypertrophy or myocardial dysfunction. Circ Res 97:1342-1350.

Gupta A, Decaillot FM, Gomes I, Tkalych O, Heimann AS, Ferro ES, Devi LA (2007) Conformation state-sensitive antibodies to G-protein-coupled receptors. J Biol Chem 282:5116-5124.

Gutman GA, Chandy KG, Grissmer S, Lazdunski M, McKinnon D, Pardo LA, Robertson GA, Rudy B, Sanguinetti MC, Stuhmer W, Wang X (2005) International Union of Pharmacology. LIII. Nomenclature and molecular relationships of voltage-gated potassium channels. Pharmacol Rev 57:473-508.

Guy HR, Durell SR, Warmke J, Drysdale R, Ganetzky B (1991) Similarities in amino acid sequences of Drosophila eag and cyclic nucleotide-gated channels. Science 254:730.

Hamprecht B, Glaser T, Reiser G, Bayer E, Propst F (1985) Culture and characteristics of hormone-responsive neuroblastoma X glioma hybrid cells. Methods Enzymol 109:316-341.

Hanahan D (1983) Studies on transformation of Escherichia coli with plasmids. J Mol Biol 166:557-580.

Hemmerlein B, Weseloh RM, Mello de Queiroz F, Knotgen H, Sanchez A, Rubio ME, Martin S, Schliephacke T, Jenke M, Heinz Joachim R, Stuhmer W, Pardo LA (2006) Overexpression of Eag1 potassium channels in clinical tumours. Mol Cancer 5:41.

Hille B (2001) Ion Channels of Excitable Membranes. Sunderland, MA: Sinauer Associates Inc.

Hirdes W, Schweizer M, Schuricht KS, Guddat SS, Wulfsen I, Bauer CK, Schwarz JR (2005) Fast erg K+ currents in rat embryonic serotonergic neurones. J Physiol 564:33-49.

Hirrlinger PG, Scheller A, Braun C, Quintela-Schneider M, Fuss B, Hirrlinger J, Kirchhoff F (2005) Expression of reef coral fluorescent proteins in the central nervous system of transgenic mice. Mol Cell Neurosci 30:291-303.

Hoyer-Fender S (2010) Centriole maturation and transformation to basal body. Semin Cell Dev Biol 21:142-147.

Huang X, Dubuc AM, Hashizume R, Berg J, He Y, Wang J, Chiang C, Cooper MK, Northcott PA, Taylor MD, Barnes MJ, Tihan T, Chen J, Hackett CS, Weiss WA, James CD, Rowitch DH, Shuman MA, Jan YN, Jan LY (2012) Voltage-gated potassium channel EAG2 controls mitotic entry and tumor growth in medulloblastoma via regulating cell volume dynamics. Genes Dev 26:1780-1796.

Huang XY, Morielli AD, Peralta EG (1993) Tyrosine kinase-dependent suppression of a potassium channel by the G protein-coupled m1 muscarinic acetylcholine receptor. Cell 75:1145-1156.

Ito D, Tanaka K, Suzuki S, Dembo T, Fukuuchi Y (2001) Enhanced expression of Iba1, ionized calcium-binding adapter molecule 1, after transient focal cerebral ischemia in rat brain. Stroke 32:1208-1215.

Jan LY, Jan YN (1997) Cloned potassium channels from eukaryotes and prokaryotes. Annu Rev Neurosci 20:91-123.

Jeng CJ, Chang CC, Tang CY (2005) Differential localization of rat Eag1 and Eag2 K+ channels in hippocampal neurons. Neuroreport 16:229-233.

Jonas EA, Kaczmarek LK (1996) Regulation of potassium channels by protein kinases. Curr Opin Neurobiol 6:318-323.

Jow GM, Jeng CJ (2008) Differential localization of rat Eag1 and Eag2 potassium channels in the retina. Neurosci Lett 431:12-16.

Ju M, Wray D (2002) Molecular identification and characterisation of the human eag2 potassium channel. FEBS Lett 524:204-210.

Jung M, Kramer E, Grzenkowski M, Tang K, Blakemore W, Aguzzi A, Khazaie K, Chlichlia K, von Blankenfeld G, Kettenmann H, et al. (1995) Lines of murine oligodendroglial precursor cells immortalized by an activated neu tyrosine kinase show distinct degrees of interaction with axons in vitro and in vivo. Eur J Neurosci 7:1245-1265.

Jung S, Aliberti J, Graemmel P, Sunshine MJ, Kreutzberg GW, Sher A, Littman DR (2000) Analysis of fractalkine receptor CX(3)CR1 function by targeted deletion and green fluorescent protein reporter gene insertion. Mol Cell Biol 20:4106-4114.

Kamb A, Iverson LE, Tanouye MA (1987) Molecular characterization of Shaker, a Drosophila gene that encodes a potassium channel. Cell 50:405-413.

Kane JF, Hartley DL (1988) Formation of recombinant protein inclusion bodies in Escherichia coli. Trends in Biotechnology 6:95-101.

Kaplan WD, Trout WE, 3rd (1969) The behavior of four neurological mutants of Drosophila. Genetics 61:399-409.

Katsetos CD, Del Valle L, Geddes JF, Aldape K, Boyd JC, Legido A, Khalili K, Perentes E, Mork SJ (2002) Localization of the neuronal class III beta-tubulin in oligodendrogliomas: comparison with Ki-67 proliferative index and 1p/19q status. J Neuropathol Exp Neurol 61:307-320.

Keating MT, Sanguinetti MC (1996) Molecular genetic insights into cardiovascular disease. Science 272:681-685.

Kim J, Hoffman DA (2008) Potassium channels: newly found players in synaptic plasticity. Neuroscientist 14:276-286.

Kim J, Kato M, Beachy PA (2009) Gli2 trafficking links Hedgehog-dependent activation of Smoothened in the primary cilium to transcriptional activation in the nucleus. Proc Natl Acad Sci U S A 106:21666-21671.

Kim S, Tsiokas L (2011) Cilia and cell cycle re-entry: more than a coincidence. Cell Cycle 10:2683-2690.

Kohl T, Lorinczi E, Pardo LA, Stuhmer W (2011) Rapid internalization of the oncogenic K+ channel K(V)10.1. PLoS One 6:e26329.

Kullmann DM (2002) The neuronal channelopathies. Brain 125:1177-1195.

Larsen LA, Andersen PS, Kanters J, Svendsen IH, Jacobsen JR, Vuust J, Wettrell G, Tranebjaerg L, Bathen J, Christiansen M (2001) Screening for mutations and polymorphisms in the genes KCNH2 and KCNE2 encoding the cardiac HERG/MiRP1 ion channel: implications for acquired and congenital long Q-T syndrome. Clin Chem 47:1390-1395.

Lastraioli E, Guasti L, Crociani O, Polvani S, Hofmann G, Witchel H, Bencini L, Calistri M, Messerini L, Scatizzi M, Moretti R, Wanke E, Olivotto M, Mugnai G, Arcangeli A (2004) herg1 gene and HERG1 protein are overexpressed in colorectal cancers and regulate cell invasion of tumor cells. Cancer Res 64:606-611.

Lein ES, Hawrylycz MJ, Ao N, Ayres M, Bensinger A, Bernard A, Boe AF, Boguski MS, Brockway KS, Byrnes EJ, Chen L, Chen TM, Chin MC, Chong J, Crook BE, Czaplinska A, Dang CN, Datta S, Dee NR, Desaki AL, Desta T, Diep E, Dolbeare TA, Donelan MJ, Dong HW, Dougherty JG, Duncan BJ, Ebbert AJ, Eichele G, Estin LK, Faber C, Facer BA, Fields R, Fischer SR, Fliss TP, Frensley C, Gates SN, Glattfelder KJ, Halverson KR, Hart MR, Hohmann JG, Howell MP, Jeung DP, Johnson RA, Karr PT, Kawal R, Kidney JM, Knapik RH, Kuan CL, Lake JH, Laramee AR, Larsen KD, Lau C, Lemon TA, Liang AJ, Liu Y, Luong LT, Michaels J, Morgan JJ, Morgan RJ, Mortrud MT, Mosqueda NF, Ng LL, Ng R, Orta GJ, Overly CC, Pak TH, Parry SE, Pathak SD, Pearson OC, Puchalski RB, Riley ZL, Rockett HR, Rowland SA, Royall JJ, Ruiz MJ, Sarno NR, Schaffnit K, Shapovalova NV, Sivisay T, Slaughterbeck CR, Smith SC, Smith KA, Smith BI, Sodt AJ, Stewart NN, Stumpf KR, Sunkin SM, Sutram M, Tam A, Teemer CD, Thaller C, Thompson CL, Varnam LR, Visel A, Whitlock RM, Wohnoutka PE, Wolkey CK, Wong VY, Wood M, Yaylaoglu MB, Young RC, Youngstrom BL, Yuan XF, Zhang B, Zwingman TA, Jones AR (2007) Genome-wide atlas of gene expression in the adult mouse brain. Nature 445:168-176.

Li M, Jan YN, Jan LY (1992) Specification of subunit assembly by the hydrophilic amino-terminal domain of the Shaker potassium channel. Science 257:1225-1230.

Lienkamp S, Ganner A, Walz G (2012) Inversin, Wnt signaling and primary cilia. Differentiation 83:S49-55.

Lindskog M, Rockberg J, Uhlen M, Sterky F (2005) Selection of protein epitopes for antibody production. Biotechniques 38:723-727.

Livak KJ, Schmittgen TD (2001) Analysis of relative gene expression data using real-time quantitative PCR and the 2(-Delta Delta C(T)) Method. Methods 25:402-408.

Logothetis DE, Movahedi S, Satler C, Lindpaintner K, Nadal-Ginard B (1992) Incremental reductions of positive charge within the S4 region of a voltage-gated K+ channel result in corresponding decreases in gating charge. Neuron 8:531-540.

Ludwig J, Owen D, Pongs O (1997) Carboxy-terminal domain mediates assembly of the voltage-gated rat ether-a-go-go potassium channel. Embo J 16:6337-6345.

Ludwig J, Terlau H, Wunder F, Bruggemann A, Pardo LA, Marquardt A, Stuhmer W, Pongs O (1994) Functional expression of a rat homologue of the voltage gated either a go-go

potassium channel reveals differences in selectivity and activation kinetics between the Drosophila channel and its mammalian counterpart. Embo J 13:4451-4458.

Ludwig J, Weseloh R, Karschin C, Liu Q, Netzer R, Engeland B, Stansfeld C, Pongs O (2000) Cloning and functional expression of rat eag2, a new member of the ether-a-go-go family of potassium channels and comparison of its distribution with that of eag1. Mol Cell Neurosci 16:59-70.

Martin S, Lino-de-Oliveira C, Joca SR, Weffort de Oliveira R, Echeverry MB, Da Silva CA, Pardo L, Stuhmer W, Bel ED (2010) Eag 1, Eag 2 and Kcnn3 gene brain expression of isolated reared rats. Genes Brain Behav 9:918-924.

Martin S, Lino de Oliveira C, Mello de Queiroz F, Pardo LA, Stuhmer W, Del Bel E (2008) Eag1 potassium channel immunohistochemistry in the CNS of adult rat and selected regions of human brain. Neuroscience 155:833-844.

Maruyama Y, Shimada H, Taniguchi J (1995) Ca(2+)-activated K(+)-channels in the nuclear envelope isolated from single pancreatic acinar cells. Pflugers Arch 430:148-150.

Mazzanti M, DeFelice LJ, Cohn J, Malter H (1990) Ion channels in the nuclear envelope. Nature 343:764-767.

Menco BP (1994) Ultrastructural aspects of olfactory transduction and perireceptor events. Semin Cell Biol 5:11-24.

Morris GE (2007) Epitope Mapping: B-cell Epitopes. eLS John Wiley & Sons, Ltd: Chichester.

Murray KF, Larson AM (2010) Fibrocystic Diseases of the Liver (Clinical Gastroenterology). Heidelberg: Springer-Verlag GmbH.

Nagy A (2000) Cre recombinase: the universal reagent for genome tailoring. Genesis 26:99-109.

Nakazawa M, Mukumoto M, Miyatake K (2010) Production and purification of polyclonal antibodies. Methods Mol Biol 657:63-74.

Napp J, Monje F, Stuhmer W, Pardo LA (2005) Glycosylation of Eag1 (Kv10.1) potassium channels: intracellular trafficking and functional consequences. J Biol Chem 280:29506-29512.

Nerbonne JM, Gerber BR, Norris A, Burkhalter A (2008) Electrical remodelling maintains firing properties in cortical pyramidal neurons lacking KCND2-encoded A-type K+ currents. J Physiol 586:1565-1579.

Nilsson P, Paavilainen L, Larsson K, Odling J, Sundberg M, Andersson AC, Kampf C, Persson A, Al-Khalili Szigyarto C, Ottosson J, Bjorling E, Hober S, Wernerus H, Wester K, Ponten F, Uhlen M (2005) Towards a human proteome atlas: high-throughput generation of mono-specific antibodies for tissue profiling. Proteomics 5:4327-4337.

Nolte C, Matyash M, Pivneva T, Schipke CG, Ohlemeyer C, Hanisch UK, Kirchhoff F, Kettenmann H (2001) GFAP promoter-controlled EGFP-expressing transgenic mice: a tool to visualize astrocytes and astrogliosis in living brain tissue. Glia 33:72-86.

Notredame C, Higgins DG, Heringa J (2000) T-Coffee: A novel method for fast and accurate multiple sequence alignment. J Mol Biol 302:205-217.

Okada Y (2004) Ion channels and transporters involved in cell volume regulation and sensor mechanisms. Cell Biochem Biophys 41:233-258.

Packer J, Conley E, Castle N, Wray D, January C, Patmore L (2000) Internet resources for exploring gene family diversity. Trends Pharmacol Sci 21:327-329.

Papazian DM, Schwarz TL, Tempel BL, Jan YN, Jan LY (1987) Cloning of genomic and complementary DNA from Shaker, a putative potassium channel gene from Drosophila. Science 237:749-753.

Papazian DM, Schwarz TL, Tempel BL, Timpe LC, Jan LY (1988) Ion channels in Drosophila. Annu Rev Physiol 50:379-394.

Papazian DM, Timpe LC, Jan YN, Jan LY (1991) Alteration of voltage-dependence of Shaker potassium channel by mutations in the S4 sequence. Nature 349:305-310.

Pardo LA, Contreras-Jurado C, Zientkowska M, Alves F, Stuhmer W (2005) Role of voltage-gated potassium channels in cancer. J Membr Biol 205:115-124.

Pardo LA, del Camino D, Sanchez A, Alves F, Bruggemann A, Beckh S, Stuhmer W (1999) Oncogenic potential of EAG K(+) channels. Embo J 18:5540-5547.

Peden DR, Petitjean CM, Herd MB, Durakoglugil MS, Rosahl TW, Wafford K, Homanics GE, Belelli D, Fritschy JM, Lambert JJ (2008) Developmental maturation of synaptic and extrasynaptic GABAA receptors in mouse thalamic ventrobasal neurones. J Physiol 586:965-987.

Pereira DS, Kushner DB, Ricciardi RP, Graham FL (1996) Testing NF-kappa B1-p50 antibody specificity using knockout mice. Oncogene 13:445-446.

Pinching AJ, Powell TP (1971) The neuropil of the glomeruli of the olfactory bulb. J Cell Sci 9:347-377.

Pongs O, Kecskemethy N, Muller R, Krah-Jentgens I, Baumann A, Kiltz HH, Canal I, Llamazares S, Ferrus A (1988) Shaker encodes a family of putative potassium channel proteins in the nervous system of Drosophila. Embo J 7:1087-1096.

Pradidarcheep W, Labruyere WT, Dabhoiwala NF, Lamers WH (2008) Lack of specificity of commercially available antisera: better specifications needed. J Histochem Cytochem 56:1099-1111.

Praetorius HA, Spring KR (2001) Bending the MDCK cell primary cilium increases intracellular calcium. J Membr Biol 184:71-79.

Praetorius HA, Spring KR (2003) The renal cell primary cilium functions as a flow sensor. Curr Opin Nephrol Hypertens 12:517-520.

Quarmby LM, Parker JD (2005) Cilia and the cell cycle? J Cell Biol 169:707-710.

Ren D, Pipes GD, Liu D, Shih LY, Nichols AC, Treuheit MJ, Brems DN, Bondarenko PV (2009) An improved trypsin digestion method minimizes digestion-induced modifications on proteins. Anal Biochem 392:12-21.

Rohatgi R, Scott MP (2008) Cell biology. Arrestin' movement in cilia. Science 320:1726-1727.

Rowell JJ, Mallik AK, Dugas-Ford J, Ragsdale CW (2010) Molecular analysis of neocortical layer structure in the ferret. J Comp Neurol 518:3272-3289.

Rozen S, Skaletsky H (2000) Primer3 on the WWW for general users and for biologist programmers. Methods Mol Biol 132:365-386.

Rudy B (1988) Diversity and Ubiquity of K-Channels. Neuroscience 25:729-749.

Saganich MJ, Machado E, Rudy B (2001) Differential expression of genes encoding subthreshold-operating voltage-gated K+ channels in brain. J Neurosci 21:4609-4624.

Saganich MJ, Vega-Saenz de Miera E, Nadal MS, Baker H, Coetzee WA, Rudy B (1999) Cloning of components of a novel subthreshold-activating K(+) channel with a unique pattern of expression in the cerebral cortex. J Neurosci 19:10789-10802.

Salkoff L, Jegla T (1995) Surfing the DNA databases for K+ channels nets yet more diversity. Neuron 15:489-492.

Sanguinetti MC (2010) HERG1 channelopathies. Pflugers Arch 460:265-276.

Sanguinetti MC, Curran ME, Zou A, Shen J, Spector PS, Atkinson DL, Keating MT (1996) Coassembly of K(V)LQT1 and minK (IsK) proteins to form cardiac I(Ks) potassium channel. Nature 384:80-83.

Sanguinetti MC, Spector PS (1997) Potassium channelopathies. Neuropharmacology 36:755-762.

Schindelin J, Arganda-Carreras I, Frise E, Kaynig V, Longair M, Pietzsch T, Preibisch S, Rueden C, Saalfeld S, Schmid B, Tinevez JY, White DJ, Hartenstein V, Eliceiri K, Tomancak P, Cardona A (2012) Fiji: an open-source platform for biological-image analysis. Nat Methods 9:676-682.

Schneider L, Cammer M, Lehman J, Nielsen SK, Guerra CF, Veland IR, Stock C, Hoffmann EK, Yoder BK, Schwab A, Satir P, Christensen ST (2010) Directional cell migration and chemotaxis in wound healing response to PDGF-AA are coordinated by the primary cilium in fibroblasts. Cell Physiol Biochem 25:279-292.

Shen NV, Chen X, Boyer MM, Pfaffinger PJ (1993) Deletion analysis of K+ channel assembly. Neuron 11:67-76.

Siemen D, Loupatatzis C, Borecky J, Gulbins E, Lang F (1999) Ca2+-activated K channel of the BK-type in the inner mitochondrial membrane of a human glioma cell line. Biochem Biophys Res Commun 257:549-554.

Singla V, Reiter JF (2006) The primary cilium as the cell's antenna: signaling at a sensory organelle. Science 313:629-633.

Skarnes WC, Rosen B, West AP, Koutsourakis M, Bushell W, Iyer V, Mujica AO, Thomas M, Harrow J, Cox T, Jackson D, Severin J, Biggs P, Fu J, Nefedov M, de Jong PJ, Stewart AF, Bradley A (2011) A conditional knockout resource for the genome-wide study of mouse gene function. Nature 474:337-342.

Sofroniew MV, Vinters HV (2010) Astrocytes: biology and pathology. Acta Neuropathol 119:7-35.

Sorokin S (1962) Centrioles and the formation of rudimentary cilia by fibroblasts and smooth muscle cells. J Cell Biol 15:363-377.

Stansfeld CE, Roper J, Ludwig J, Weseloh RM, Marsh SJ, Brown DA, Pongs O (1996) Elevation of intracellular calcium by muscarinic receptor activation induces a block of voltage-activated rat ether-a-go-go channels in a stably transfected cell line. Proc Natl Acad Sci U S A 93:9910-9914.

Stein WD, Lieb WR (1986) Transport and diffusion across cell membranes. Orlando: Academic Press.

Sugiyama H, Nakamura K, Morita H, Akagi S, Tani Y, Katayama Y, Nishii N, Miyoshi T, Nagase S, Kohno K, Kusano KF, Ohe T, Kurokawa J, Furukawa T, Ito H (2011) Circulating KCNH2 current-activating factor in patients with heart failure and ventricular tachyarrhythmia. PLoS One 6:e19897.

Sulik K, Dehart DB, Iangaki T, Carson JL, Vrablic T, Gesteland K, Schoenwolf GC (1994) Morphogenesis of the murine node and notochordal plate. Dev Dyn 201:260-278.

Szabo I, Bock J, Jekle A, Soddemann M, Adams C, Lang F, Zoratti M, Gulbins E (2005) A novel potassium channel in lymphocyte mitochondria. J Biol Chem 280:12790-12798.

Szewczyk A, Czyz A, Wojcik G, Wojtczak L, Nalecz MJ (1996) ATP-regulated K+ channel in mitochondria: pharmacology and function. J Bioenerg Biomembr 28:147-152.

Takahashi T, Imai K, Hashizume K (2004) Generation and characterization of anti-leptin antisera against synthetic peptides and recombinant protein. J Reprod Dev 50:717-724.

Tanaka T, Slamon DJ, Cline MJ (1985) Efficient generation of antibodies to oncoproteins by using synthetic peptide antigens. Proc Natl Acad Sci U S A 82:3400-3404.

Terlau H, Ludwig J, Steffan R, Pongs O, Stuhmer W, Heinemann SH (1996) Extracellular Mg2+ regulates activation of rat eag potassium channel. Pflugers Arch 432:301-312.

Titus SA, Warmke JW, Ganetzky B (1997) The Drosophila erg K+ channel polypeptide is encoded by the seizure locus. J Neurosci 17:875-881.

Trudeau MC, Warmke JW, Ganetzky B, Robertson GA (1995) HERG, a human inward rectifier in the voltage-gated potassium channel family. Science 269:92-95.

Ufartes R, Schneider T, Mortensen LS, de Juan Romero C, Hentrich K, Knoetgen H, Beilinson V, Moebius W, Tarabykin V, Alves F, Pardo LA, Rawlins JN, Stuehmer W (2013) Behavioural and functional characterization of Kv10.1 (Eag1) knockout mice. Hum Mol Genet.

Uhlen M, Bjorling E, Agaton C, Szigyarto CA, Amini B, Andersen E, Andersson AC, Angelidou P, Asplund A, Asplund C, Berglund L, Bergstrom K, Brumer H, Cerjan D, Ekstrom M, Elobeid A, Eriksson C, Fagerberg L, Falk R, Fall J, Forsberg M, Bjorklund MG, Gumbel K, Halimi A, Hallin I, Hamsten C, Hansson M, Hedhammar M, Hercules G, Kampf C, Larsson K, Lindskog M, Lodewyckx W, Lund J, Lundeberg J, Magnusson K, Malm E, Nilsson P, Odling J, Oksvold P, Olsson I, Oster E, Ottosson J, Paavilainen L, Persson A, Rimini R, Rockberg J, Runeson M, Sivertsson A, Skollermo A, Steen J, Stenvall M, Sterky F, Stromberg S, Sundberg M, Tegel H, Tourle S, Wahlund E, Walden A, Wan J, Wernerus H, Westberg J, Wester K, Wrethagen U, Xu LL, Hober S, Ponten F (2005) A human protein atlas for normal and cancer tissues based on antibody proteomics. Mol Cell Proteomics 4:1920-1932.

Uhlen M, Oksvold P, Fagerberg L, Lundberg E, Jonasson K, Forsberg M, Zwahlen M, Kampf C, Wester K, Hober S, Wernerus H, Bjorling L, Ponten F (2010) Towards a knowledge-based Human Protein Atlas. Nat Biotechnol 28:1248-1250.

Wadhwa S, Wadhwa P, Dinda AK, Gupta NP (2009) Differential expression of potassium ion channels in human renal cell carcinoma. Int Urol Nephrol 41:251-257.

Warmke J, Drysdale R, Ganetzky B (1991) A distinct potassium channel polypeptide encoded by the Drosophila eag locus. Science 252:1560-1562.

Warmke JW, Ganetzky B (1994) A family of potassium channel genes related to eag in Drosophila and mammals. Proc Natl Acad Sci U S A 91:3438-3442.

Wei A, Jegla T, Salkoff L (1996) Eight potassium channel families revealed by the C. elegans genome project. Neuropharmacology 35:805-829.

West SM, Guise AD, Chaudhuri JB (1997) A Comparison of the Denaturants Urea and Guanidine Hydrochloride on Protein Refolding. Food and Bioproducts Processing 75:50-56.

Wimmers S, Bauer CK, Schwarz JR (2002) Biophysical properties of heteromultimeric erg K+ channels. Pflugers Arch 445:423-430.

Wimmers S, Wulfsen I, Bauer CK, Schwarz JR (2001) Erg1, erg2 and erg3 K channel subunits are able to form heteromultimers. Pflugers Arch 441:450-455.

Wojciechowski K, Chang CH, Hocking DC (2004) Expression, production, and characterization of full-length vitronectin in Escherichia coli. Protein Expr Purif 36:131-138.

Wray D (2004) The roles of intracellular regions in the activation of voltage-dependent potassium channels. Eur Biophys J 33:194-200.

Yellen G (2002) The voltage-gated potassium channels and their relatives. Nature 419:35-42.

Yokoo H, Nobusawa S, Takebayashi H, Ikenaka K, Isoda K, Kamiya M, Sasaki A, Hirato J, Nakazato Y (2004) Anti-human Olig2 antibody as a useful immunohistochemical marker of normal oligodendrocytes and gliomas. Am J Pathol 164:1717-1725.

Yoshimura K, Kawate T, Takeda S (2011) Signaling through the primary cilium affects glial cell survival under a stressed environment. Glia 59:333-344.